Supporting Information

Insights into Thiol-Aromatic Interactions:
A Stereoelectronic Basis for S–H/π Interactions

Christina R. Forbes, Sudipta K. Sinha[‡], Himal K. Ganguly[‡], Shi Bai*, Glenn P. A. Yap*, Sandeep Patel*, and Neal J. Zondlo*

Department of Chemistry and Biochemistry
University of Delaware
Newark, DE 19716
United States

[‡] These authors contributed equally.

Contents

Materials

Boc-L-4-thiolphenylalanine *tert*-butyl ester (**1**) was synthesized as previously described.[1] *p*-Thiocresol was purchased from Sigma and was used without further purification. Solution NMR spectra were recorded on a Brüker 400 MHz NMR spectrometer equipped with a cryogenic QNP probe or a Brüker 600 MHz NMR spectrometer equipped with a 5-mm Brüker SMART probe.

FT-IR Spectroscopy

All spectra (64 scans) were recorded on a Nicolet Magna-IR 750 FT-IR spectrometer equipped with a liquid nitrogen-cooled MCT/A detector at a spectral resolution of 1 cm^{-1}. Solution samples were filled in a gas-tight IR cell (100 μL volume) equipped with quartz windows, and contained 200 mM of **1** or *p*-thiocresol. *p*-Thiocresol was used as purchased without further purification (Sigma-Aldrich). Solvent spectra were subtracted from the sample spectra. The baseline was manually corrected using the OMNIC FT-IR Software (Nicolet). Crystalline samples were measured using the pressed pellet method with anhydrous KBr (Sigma-Aldrich).

Table S8. IR data for the S–H stretching frequency of **1** and *p*-thiocresol: ν_{max} of the S–H stretching frequency (cm^{-1}), signal intensity (absorbance), and the full-width at half-maximum (FWHM). Standard errors for absorbance intensity at the indicated ν_{max} were less than 10%, unless otherwise indicated (in parentheses as ± standard error).

	1			*p*-thiocresol		
	ν_{max}, cm^{-1}	Intensity, Absorbance	FWHM, cm^{-1}	ν_{max}, cm^{-1}	Intensity, Absorbance	FWHM, cm^{-1}
Crystalline	2538	0.2315[a] [0.0956]	18	2563	0.0235[a] [0.0264]	18
CCl$_4$	n.d[b]	n.d.[b]	n.d.[b]	2586	0.0022	25
CHCl$_3$	2585	0.0037	21	2585	0.0051	21
Ethyl Acetate	2566	0.0195	33	2567	0.0211	33
25% Ethyl Acetate in CCl$_4$	2567	0.0084	37	2569	0.0093	35
10% Ethyl Acetate in CCl$_4$	2569	0.0033 (±0.0009)	52	2571	0.0046	39
Acetone	2558	0.0200	55	2558	0.0267	55
25% Acetone in CCl$_4$	2559	0.0088 (±0.0010)	49	2561	0.0105	52
10% Acetone in CCl$_4$	2559	0.0052 (±0.0009)	57	2565	0.0055	55
25% MeOH in CCl$_4$	2541 2497	0.0045 0.0050	br[c]	2521	0.0062	br[c]
10% MeOH in CCl$_4$	2554 2499	0.0025 0.0026	br[c]	2584 2548 2518	0.0027 0.0023 0.0021	br[c]
25% THF in CCl$_4$	2534	0.0057	75	2530	0.0082	69
10% THF in CCl$_4$	2541	0.0034	br[c]	2531	0.0036	br[c]

[a] Absolute intensity was normalized with respect to the ν_{max} at 2925-2935 cm^{-1} in 25% acetone/CCl$_4$. This approach was employed because the signal in crystalline material is based on an arbitrary amount of solid. In contrast, all solution data were collected with 200 mM of compound in the indicated solvents. The normalization of the S–H stretching frequency for crystalline samples was based on the C–H stretching frequency due to its relatively constant relative intensity in all solution samples. This normalization allows for direct comparison of the relative intensities of the S–H stretching frequencies in solution versus in solid state. The absolute absorbance for the crystalline sample is shown in brackets.

[b] n.d. not determined due to low solubility.

[c] broad signal (FWHM > 80 cm^{-1} or apparently overlapping signals)

Table S9. Relative absorbance intensities for **1**. The intensity of the S–H stretching frequency (2534-2586 cm^{-1}) was compared to the intensity of the aromatic C–C frequency (1494-1497 cm^{-1}). Standard errors for intensity at the indicated ν_{max} were less than 10%.

|	ν_{max}, cm^{-1}		Absorbance Intensity		$\dfrac{\text{S–H Intensity}}{\text{C–C Intensity}}$
	S–H	C–C	S–H	C–C	
Crystalline	2538	1496	0.0956	0.0886	1.08
CCl$_4$	n.d.^{a}	n.d.^{a}	n.d^a	n.d.^{a}	n.d.^{a}
CHCl$_3$	2585	1495	0.0038	0.4859	0.01
Ethyl Acetate	2566	1497	0.0195	0.2908	0.07
25% Ethyl Acetate in CCl$_4$	2567	1495	0.0084	0.4079	0.02
10% Ethyl Acetate in CCl$_4$	2569	1494	0.0037	0.3775	0.01
Acetone	2558	1497	0.0200	0.2588	0.08
25% Acetone in CCl$_4$	2559	1495	0.0088	0.3813	0.02
10% Acetone in CCl$_4$	2559	1495	0.0052	0.4397	0.01
25% MeOH in CCl$_4$	2541 / 2497	1496	0.0045 / 0.0050	0.2845	0.02 / 0.02
10% MeOH in CCl$_4$	2554 / 2499	1495	0.0025 / 0.0026	0.3209	0.01 / 0.01
25% THF in CCl$_4$	2534	1495	0.0057	0.3694	0.02
10% THF in CCl$_4$	2541	1494	0.0034	0.4044	0.01

^{a}n.d. not determined due to low solubility.

Table S10. Relative absorbance intensities for *p*-thiocresol. The intensity of the S–H stretching frequency (2530-2586 cm^{-1}) was compared to the intensity of the aromatic C–C frequency (1493-1496 cm^{-1}). Standard errors for intensity at the indicated ν_{max} were less than 10%.

	ν_{max}, cm^{-1}		Absorbance Intensity		$\dfrac{\text{S–H Intensity}}{\text{C–C Intensity}}$
	S–H	C–C	S–H	C–C	
Crystalline	2563	1493	0.0264	0.1057	0.25
CCl$_4$	2586	1496	0.0022	0.1343	0.02
CHCl$_3$	2585	1495	0.0051	0.1767	0.03
Ethyl Acetate	2567	1496	0.0211	0.1368	0.15
25% Ethyl Acetate in CCl$_4$	2569	1496	0.0093	0.1488	0.06
10% Ethyl Acetate in CCl$_4$	2571	1496	0.0046	0.1448	0.03
Acetone	2558	1496	0.0267	0.1713	0.16
25% Acetone in CCl$_4$	2561	1496	0.0105	0.1465	0.07
10% Acetone in CCl$_4$	2565	1496	0.0055	0.1500	0.04
25% MeOH in CCl$_4$	2521	1496	0.0062	0.1402	0.04
	2584		0.0027		0.02
10% MeOH in CCl$_4$	2548	1496	0.0023	0.1496	0.02
	2518		0.0021		0.01
25% THF in CCl$_4$	2530	1495	0.0082	0.1407	0.06
10% THF in CCl$_4$	2531	1496	0.0036	0.1349	0.03
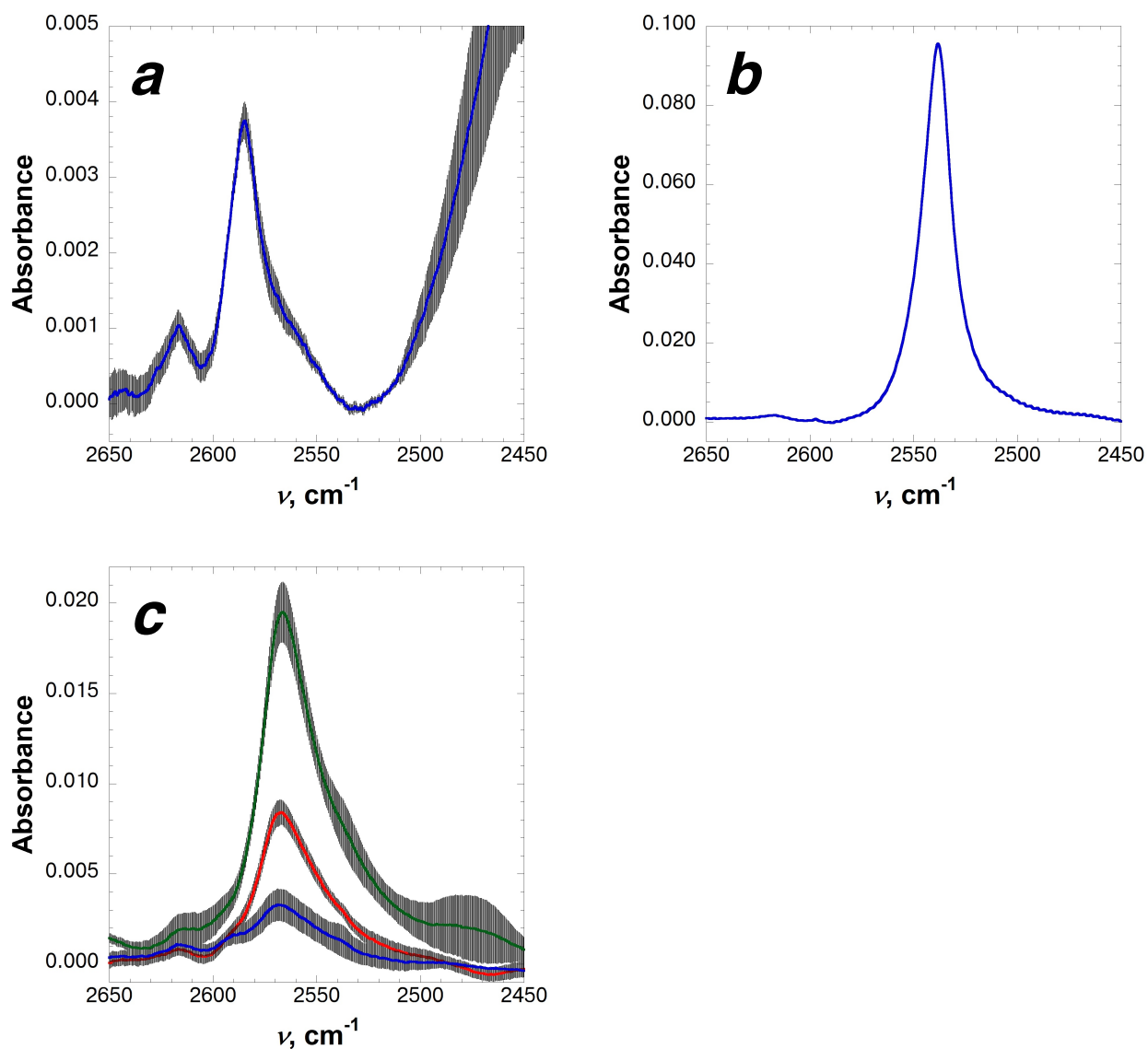
Figure S1. FT-IR spectrum of the S–H stretching region of **1**, Boc-L-4-thiolphenylalanine *tert*-butyl ester (200 mM) in (a) CHCl$_3$, (b) crystalline form, or (c) ethyl acetate in CCl$_4$ (green, 100% ethyl acetate; red, 25% ethyl acetate; blue, 10% ethyl acetate). Error bars indicate standard error. ν_{max} and signal intensity are reported in Table S8.
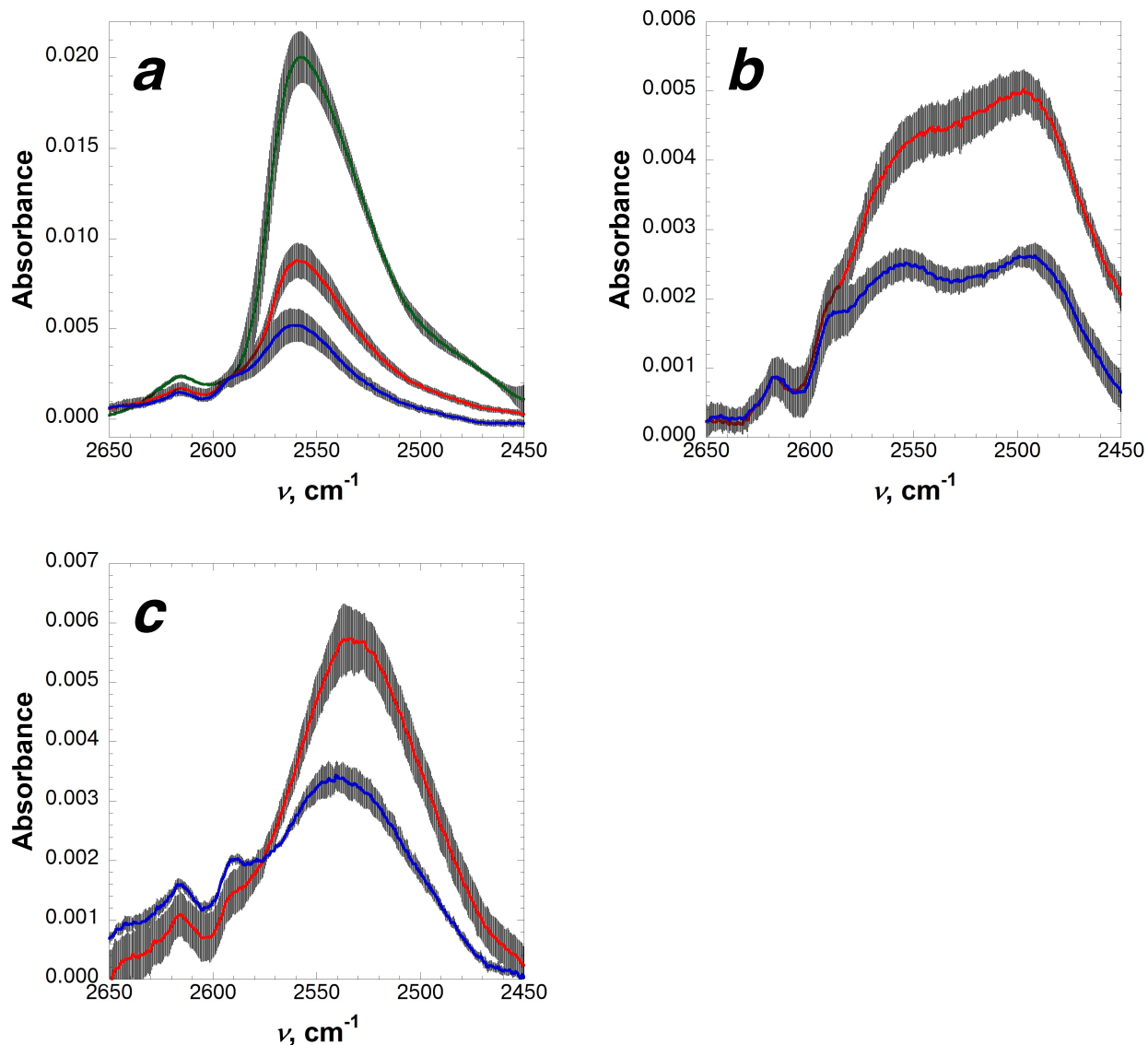
Figure S2. FT-IR spectrum of the S–H stretching region of **1**, Boc-L-4-thiolphenylalanine *tert*-butyl ester (200 mM) in solutions of (a) acetone in CCl$_4$ (green, 100% acetone; red, 25% acetone; blue, 10% acetone); (b) methanol in CCl$_4$ (red, 25% methanol; blue, 10% methanol); or (c) THF in CCl$_4$ (red, 25% THF; blue, 10% THF). Error bars indicate standard error. ν_{max} and signal intensity are reported in Table S8.
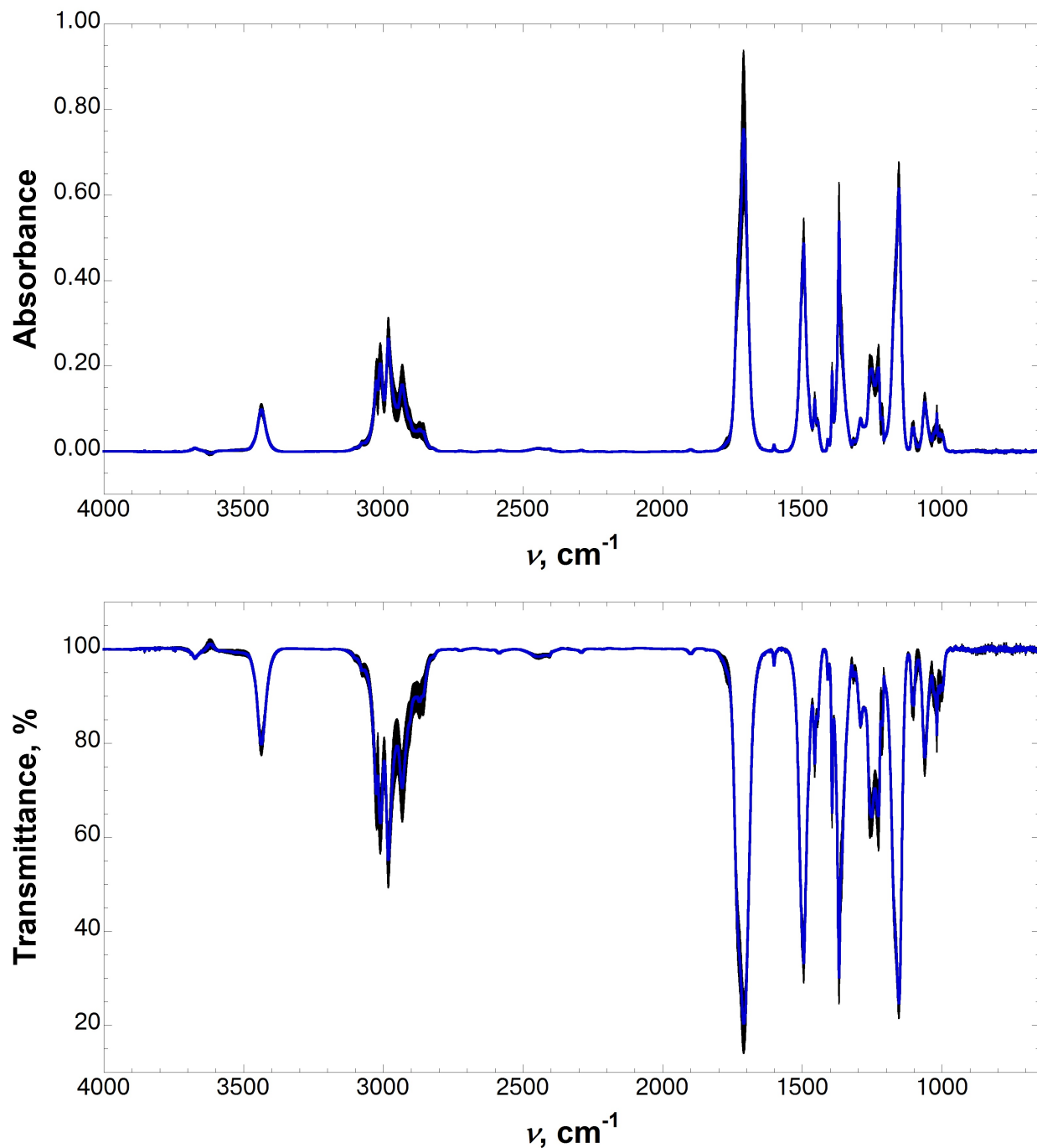
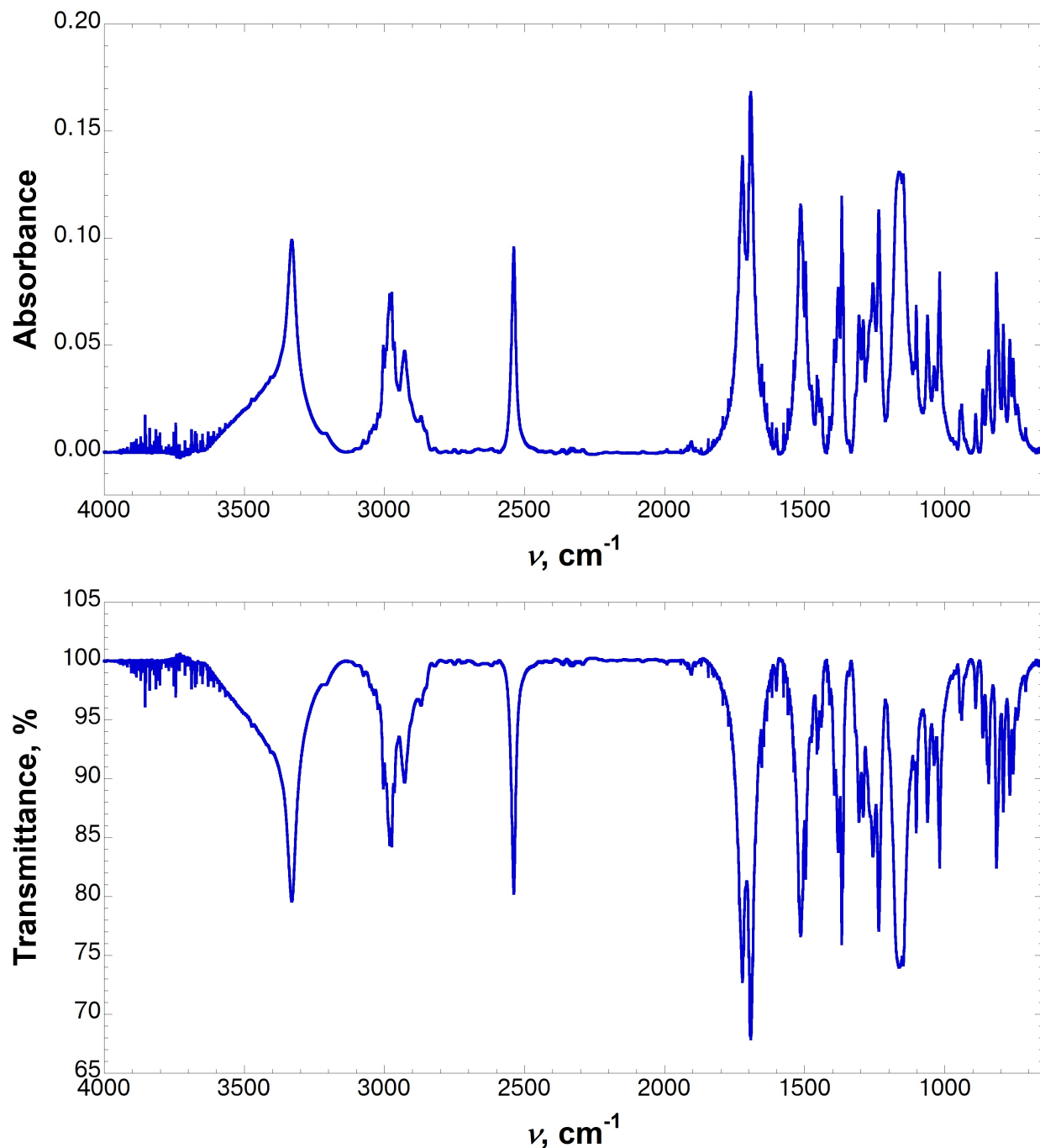**Figure S3**. FT-IR spectrum of **1**, Boc-ʟ-4-thiolphenylalanine *tert*-butyl ester (200 mM) in CHCl₃. Three independent spectra were solvent subtracted, baseline corrected, and averaged. Error bars indicate standard error. Top: full IR absorbance spectrum; bottom: full IR transmittance spectrum. ν_{max} of the S–H stretching frequency is 2585 cm^{-1}.

Figure S4. FT-IR spectrum of crystalline **1**, Boc-L-4-thiolphenylalanine *tert*-butyl ester in a pressed KBr pellet. **1** crystallized from 25% ethyl acetate in hexanes (v/v) via slow evaporation at room temperature. The spectrum was baseline corrected. Top: full IR absorbance spectrum; bottom: full IR transmittance spectrum. ν_{max} of the S–H stretching frequency is 2538 cm^{-1}.
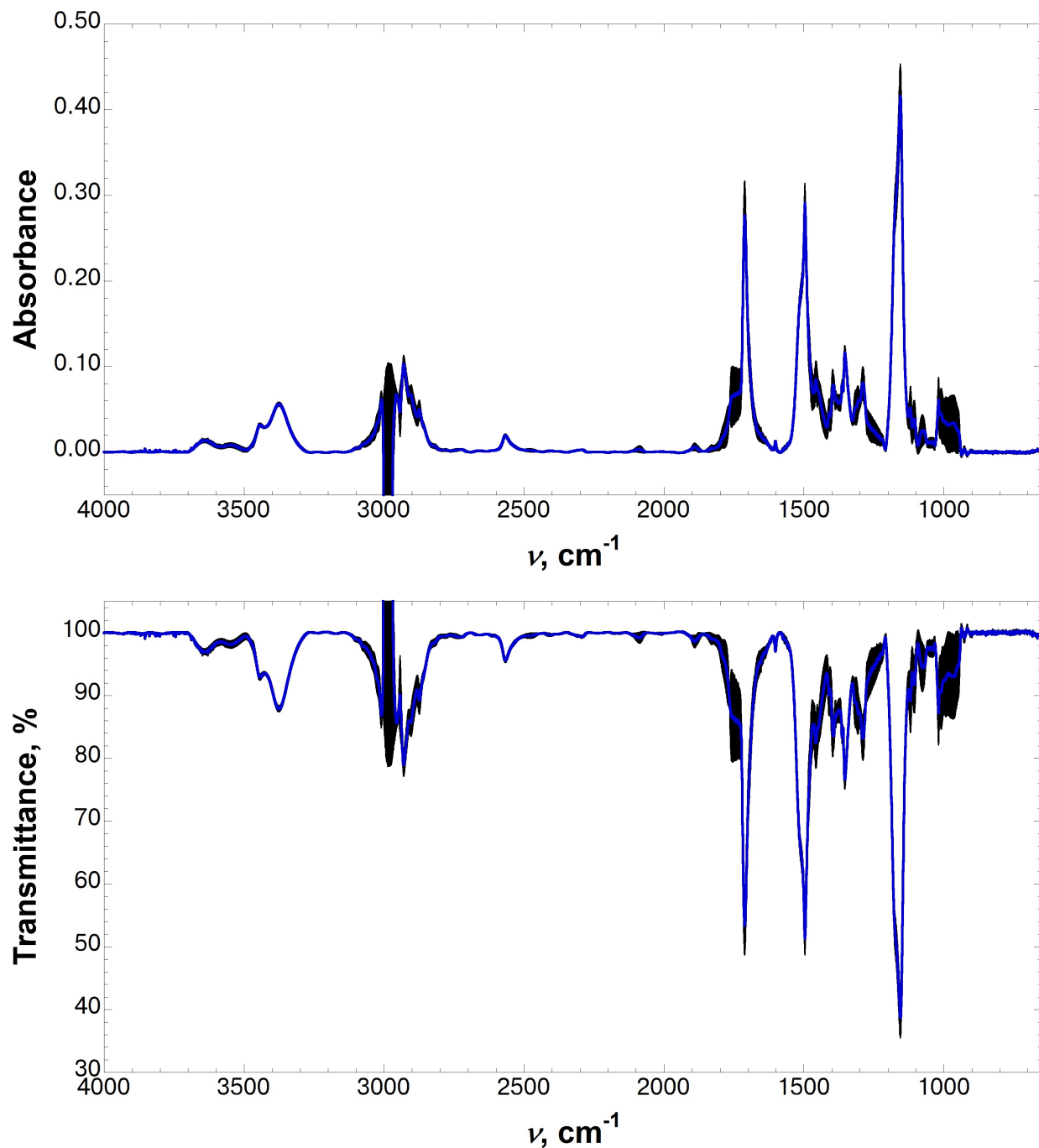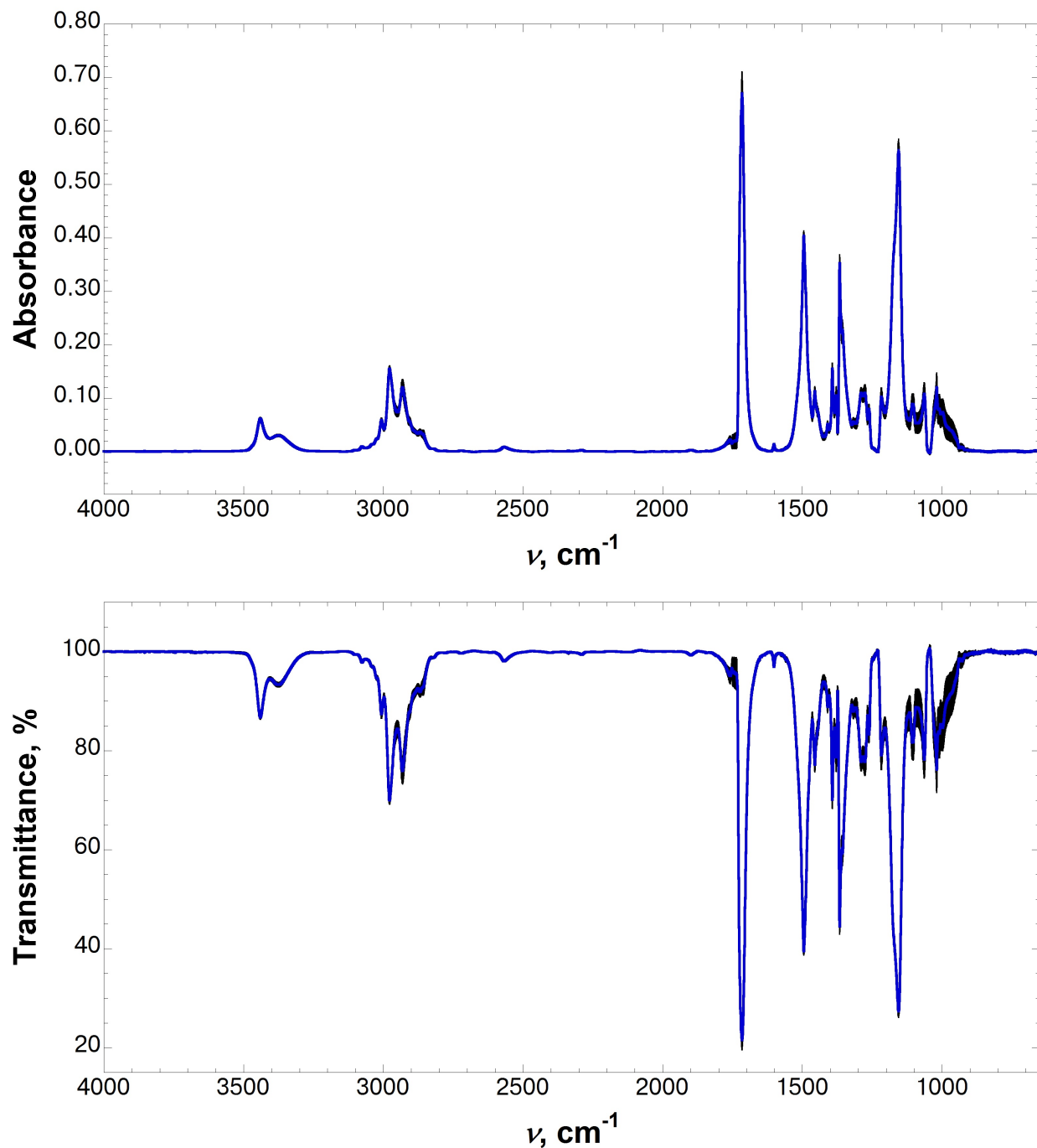
Figure S5. FT-IR spectrum of **1**, Boc-ʟ-4-thiolphenylalanine *tert*-butyl ester (200 mM) in ethyl acetate. Three independent spectra were solvent subtracted, baseline corrected, and averaged. Error bars indicate standard error. Top: full IR absorbance spectrum; bottom: full IR transmittance spectrum. ν_{max} of the S–H stretching frequency is 2566 cm^{-1}.

Figure S6. FT-IR spectrum of **1**, Boc-ʟ-4-thiolphenylalanine *tert*-butyl ester (200 mM) in 25% ethyl acetate in CCl₄. Three independent spectra were solvent subtracted, baseline corrected, and averaged. Error bars indicate standard error. Top: full IR absorbance spectrum; bottom: full IR transmittance spectrum. ν_{max} of the S–H stretching frequency is 2567 cm^{-1}.
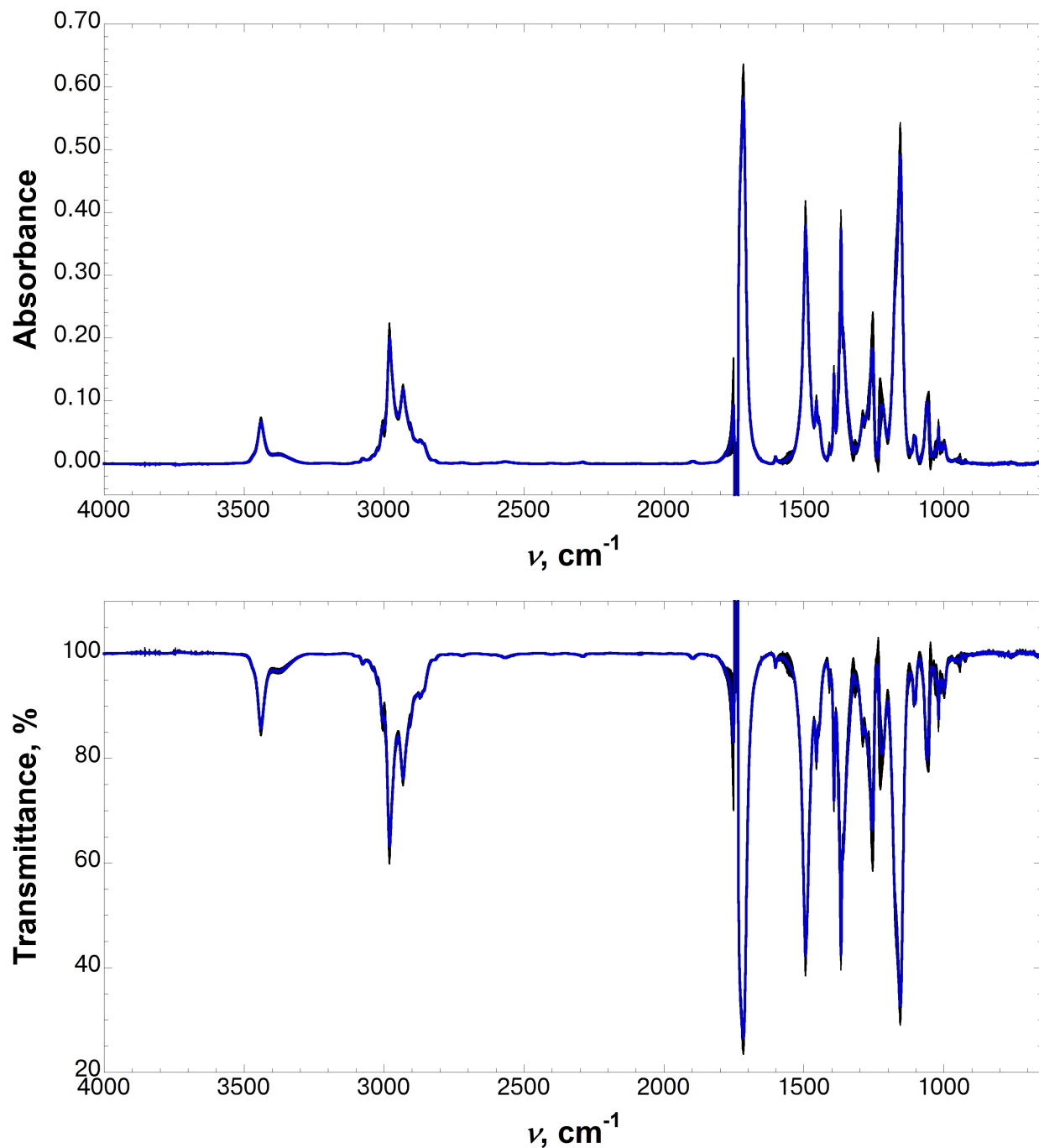
Figure S7. FT-IR spectrum of **1**, Boc-ʟ-4-thiolphenylalanine *tert*-butyl ester (200 mM) in 10% ethyl acetate in CCl$_4$. Three independent spectra were solvent subtracted, baseline corrected, and averaged. Error bars indicate standard error. Top: full IR absorbance spectrum; bottom: full IR transmittance spectrum. ν_{max} of the S–H stretching frequency is 2569 cm^{-1}.
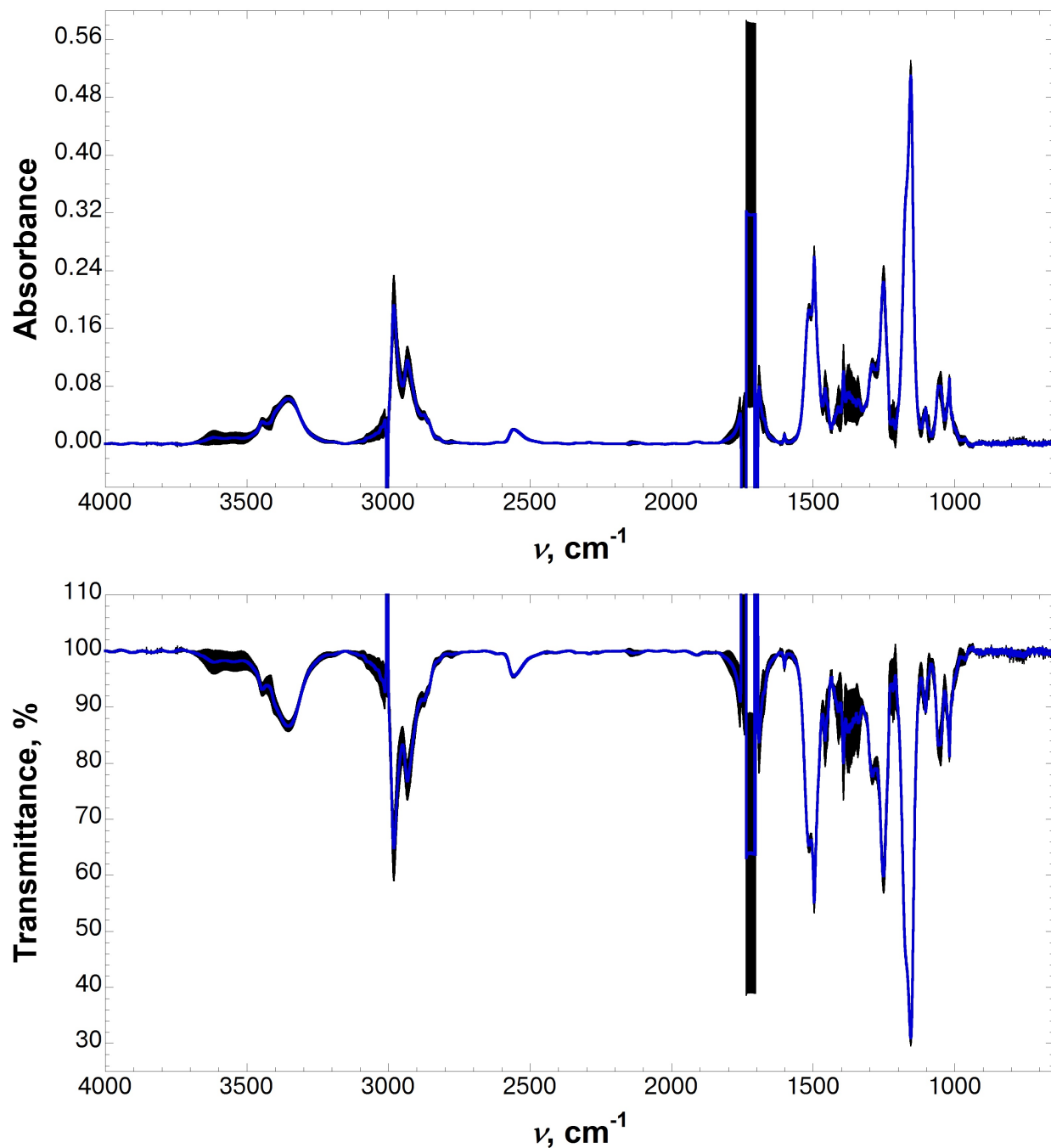
Figure S8. FT-IR spectrum of **1**, Boc-ʟ-4-thiolphenylalanine *tert*-butyl ester (200 mM) in acetone. Three independent spectra were solvent subtracted, baseline corrected, and averaged. Error bars indicate standard error. Top: full IR absorbance spectrum; bottom: full IR transmittance spectrum. ν_{max} of the S–H stretching frequency is 2558 cm^{-1}.

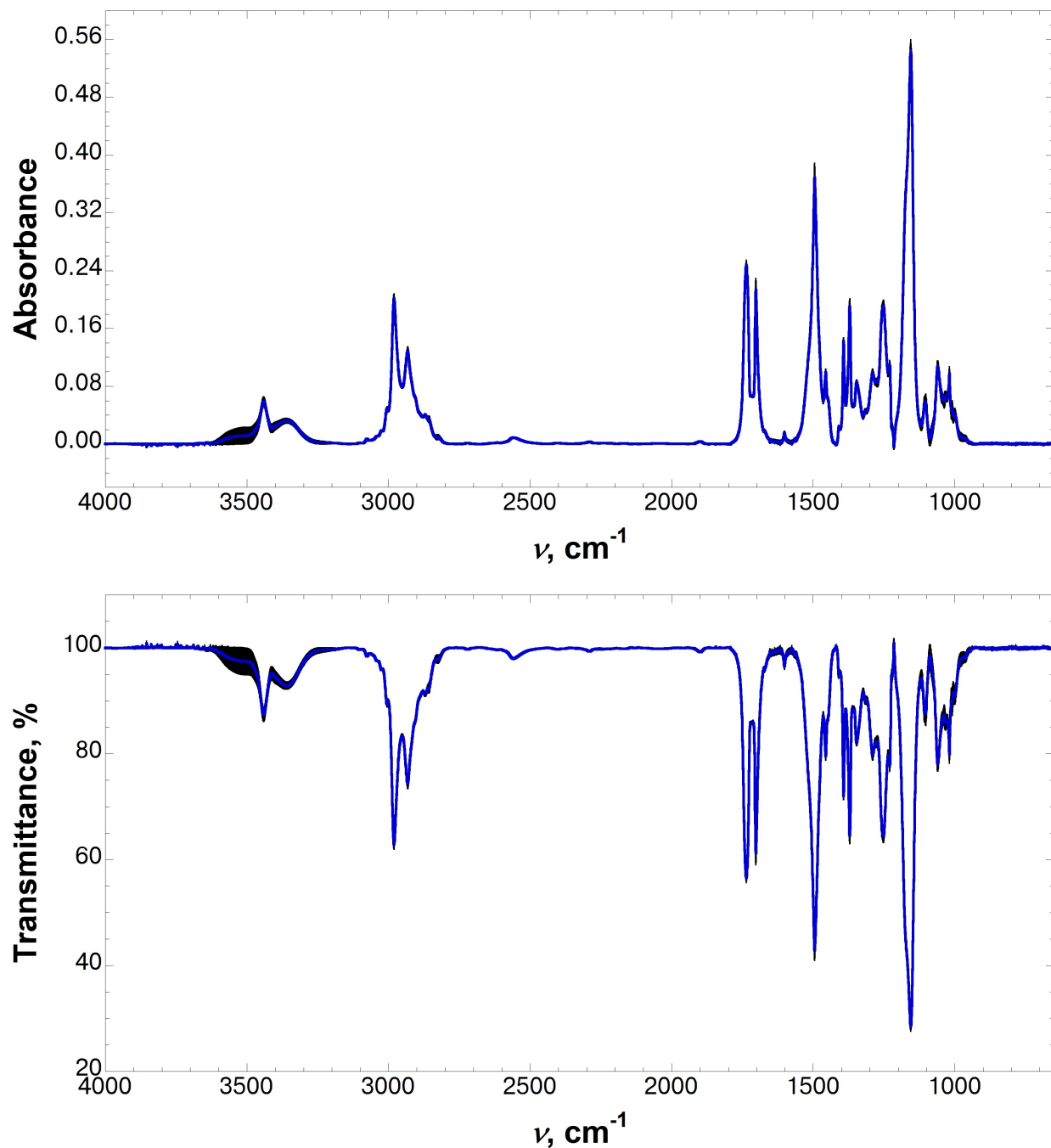**Figure S9**. FT-IR spectrum of **1**, Boc-ʟ-4-thiolphenylalanine *tert*-butyl ester (200 mM) in 25% acetone in CCl₄. Three independent spectra were solvent subtracted, baseline corrected, and averaged. Error bars indicate standard error. Top: full IR absorbance spectrum; bottom: full IR transmittance spectrum. v_{max} of the S–H stretching frequency is 2559 cm⁻¹.

Figure S10. FT-IR spectrum of **1**, Boc-ʟ-4-thiolphenylalanine *tert*-butyl ester (200 mM) in 10% acetone in CCl₄. Three independent spectra were solvent subtracted, baseline corrected, and averaged. Error bars indicate standard error. Top: full IR absorbance spectrum; bottom: full IR transmittance spectrum. ν_{max} of the S–H stretching frequency is 2559 cm^{-1}.
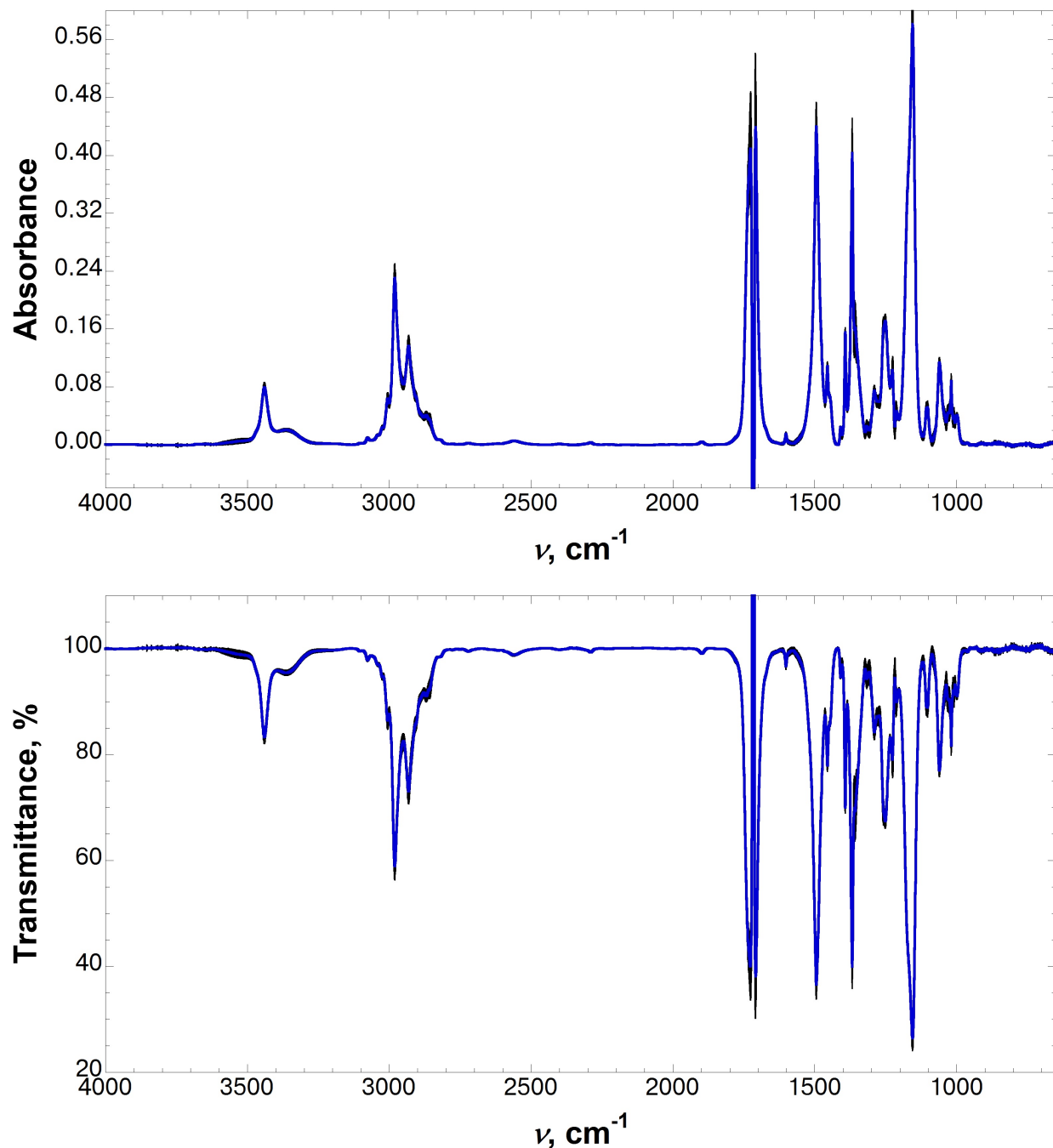
Figure S11. FT-IR spectrum of **1**, Boc-ʟ-4-thiolphenylalanine *tert*-butyl ester (200 mM) in 25% methanol in CCl$_4$. Three independent spectra were solvent subtracted, baseline corrected, and averaged. Error bars indicate standard error. Top: full IR absorbance spectrum; bottom: full IR transmittance spectrum. ν_{max} of the S–H stretching frequency is 2497 cm^{-1}.
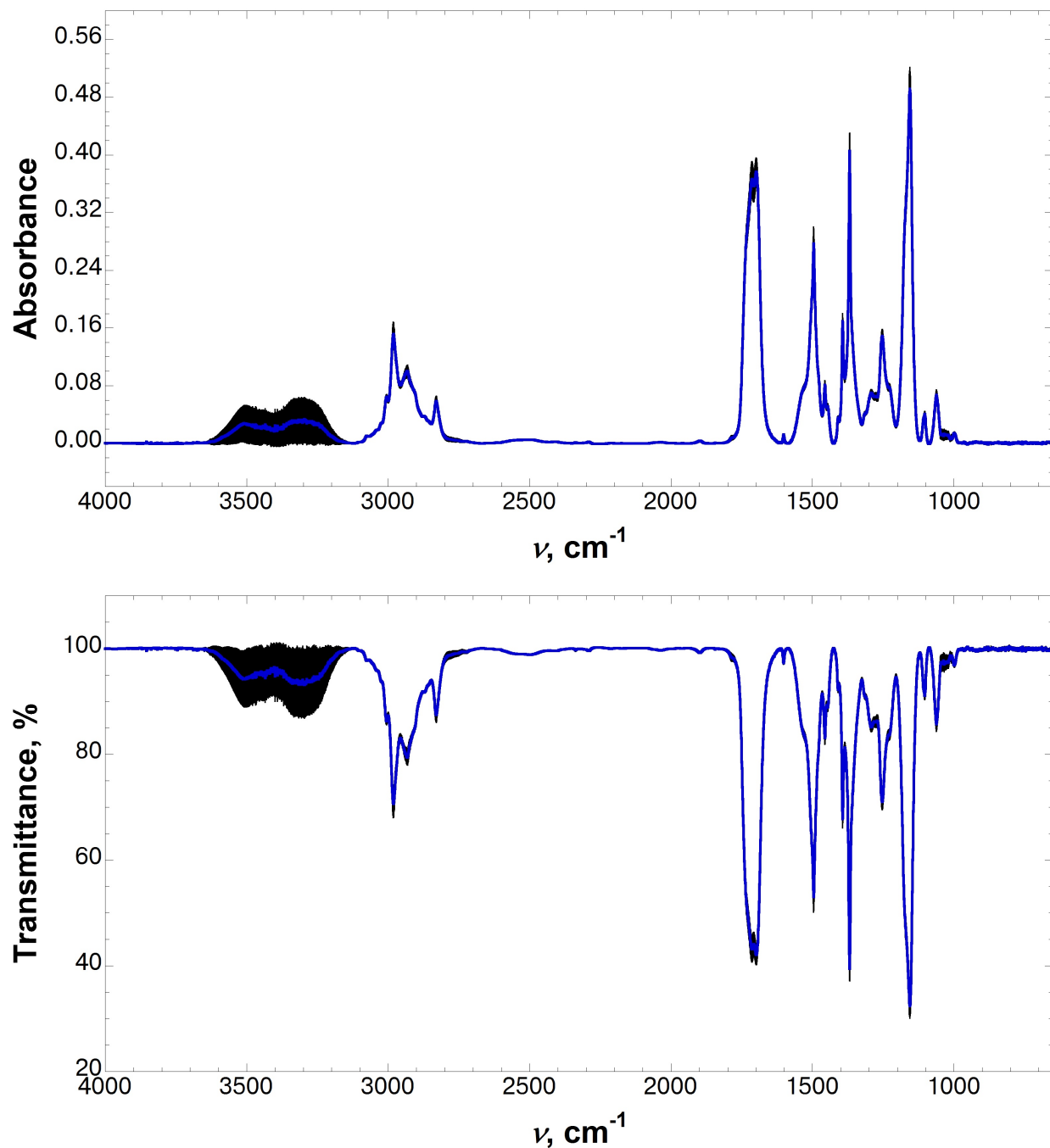
Figure S12. FT-IR spectrum of **1**, Boc-L-4-thiolphenylalanine *tert*-butyl ester (200 mM) in 10% methanol in CCl$_4$. Three independent spectra were solvent subtracted, baseline corrected, and averaged. Error bars indicate standard error. Top: full IR absorbance spectrum; bottom: full IR transmittance spectrum. Values for ν_{max} which are consistent with the S–H stretching frequency are 2554 cm^{-1} and 2499 cm^{-1}.
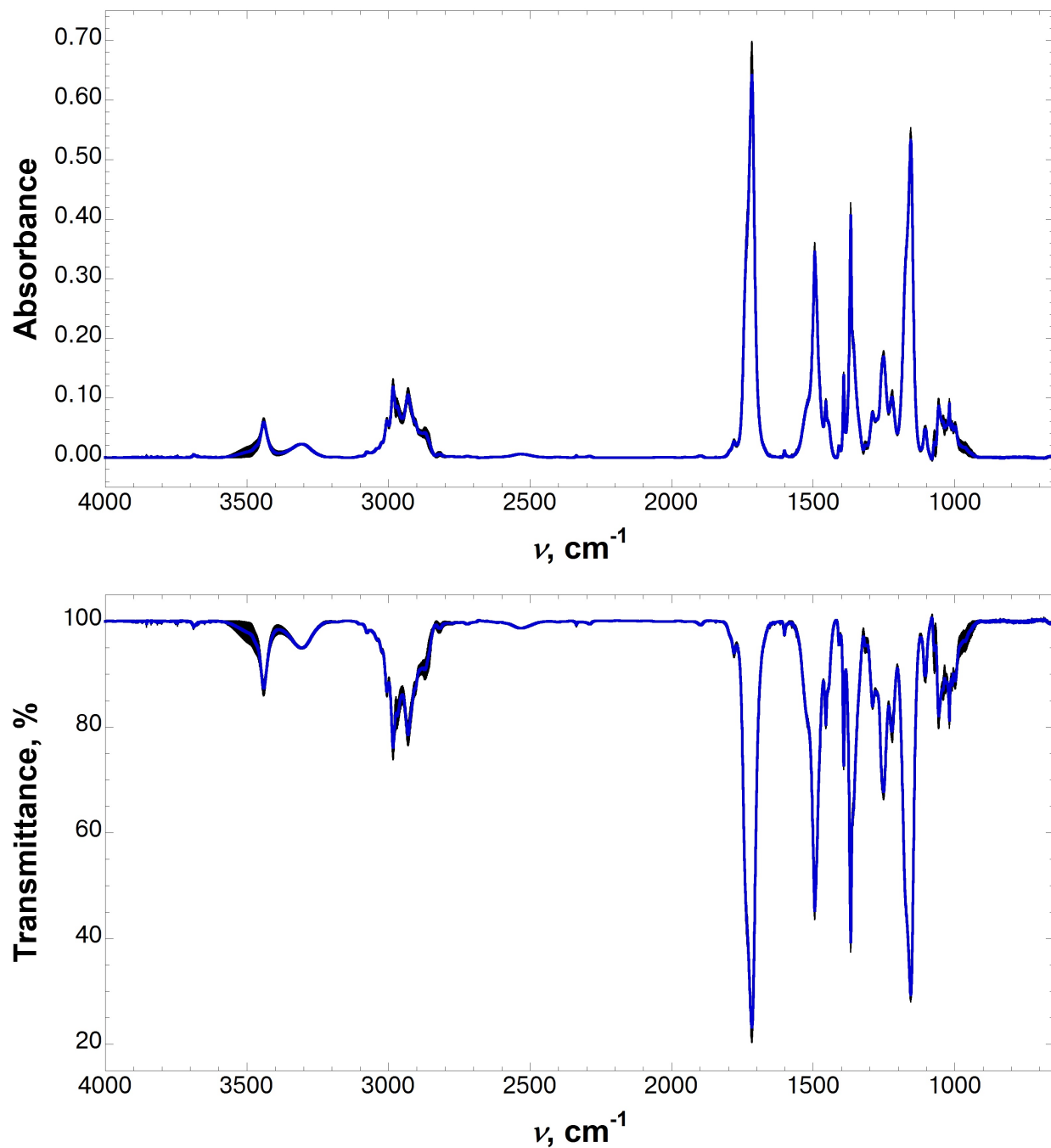
Figure S13. FT-IR spectrum of **1**, Boc-ʟ-4-thiolphenylalanine *tert*-butyl ester (200 mM) in 25% THF in CCl$_4$. Three independent spectra were solvent subtracted, baseline corrected, and averaged. Error bars indicate standard error. Top: full IR absorbance spectrum; bottom: full IR transmittance spectrum. ν_{max} of the S–H stretching frequency is 2534 cm^{-1}.
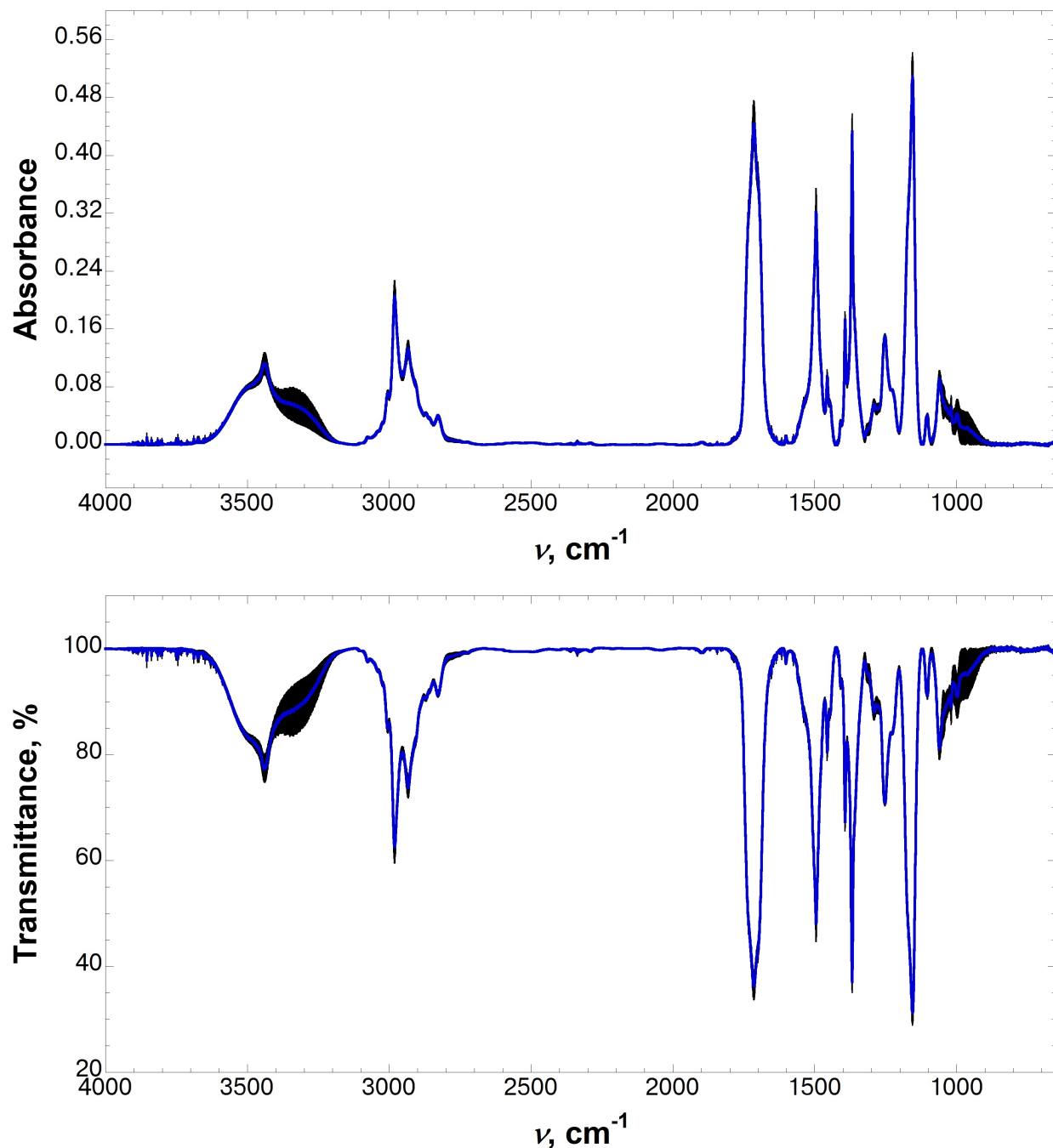
Figure S14. FT-IR spectrum of **1**, Boc-ʟ-4-thiolphenylalanine *tert*-butyl ester (200 mM) in 10% THF in CCl$_4$. Three independent spectra were solvent subtracted, baseline corrected, and averaged. Error bars indicate standard error. Top: full IR absorbance spectrum; bottom: full IR transmittance spectrum. ν_{max} of the S–H stretching frequency is 2541 cm^{-1}.

Figure S15. FT-IR spectrum of the S–H stretching region of *p*-thiocresol (200 mM) in (a) CCl$_4$, (b) CHCl$_3$, (c) crystalline form, or (d) ethyl acetate in CCl$_4$ (green, 100% ethyl acetate; red, 25% ethyl acetate; blue, 10% ethyl acetate). Error bars indicate standard error. ν_{max} and signal intensity are reported in Table S8.
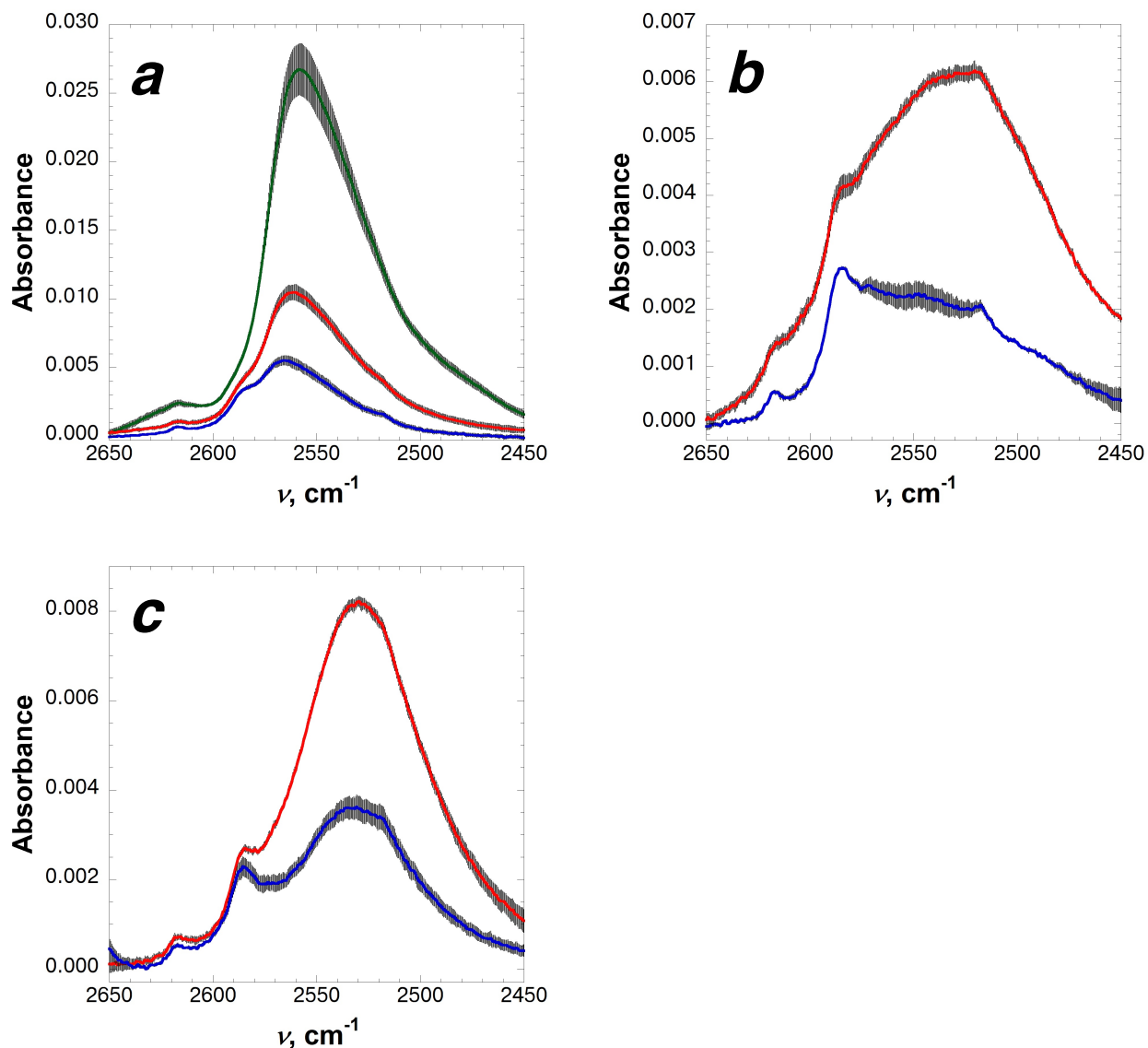
Figure S16. FT-IR spectrum of the S–H stretching region of *p*-thiocresol (200 mM). Right: *p*-thiocresol in solutions of acetone in CCl₄ (green, 100% acetone; red, 25% acetone; blue, 10% acetone); (b) methanol in CCl₄ (red, 25% methanol; blue, 10% methanol); or (c) THF in CCl₄ (red, 25% THF; blue, 10% THF). Error bars indicate standard error. ν_{max} and signal intensity are reported in Table S8.

Figure S17. FT-IR spectra of *p*-thiocresol (200 mM) in CCl$_4$. Four independent spectra were solvent subtracted, baseline corrected, and averaged. Error bars indicate standard error. Top: full IR absorbance spectrum; bottom: full IR transmittance spectrum. ν_{max} of the S–H stretching frequency is 2586 cm^{-1}.
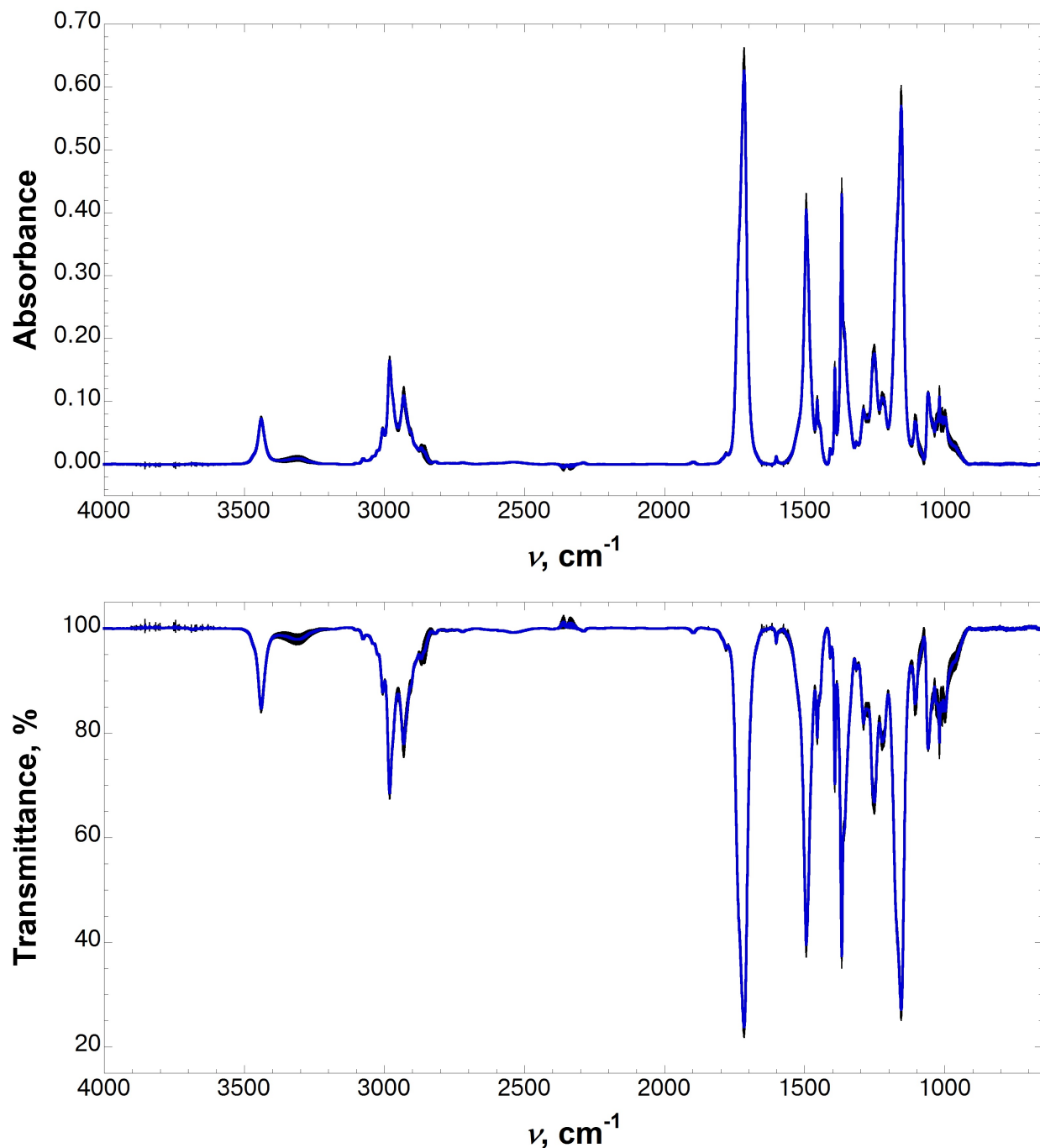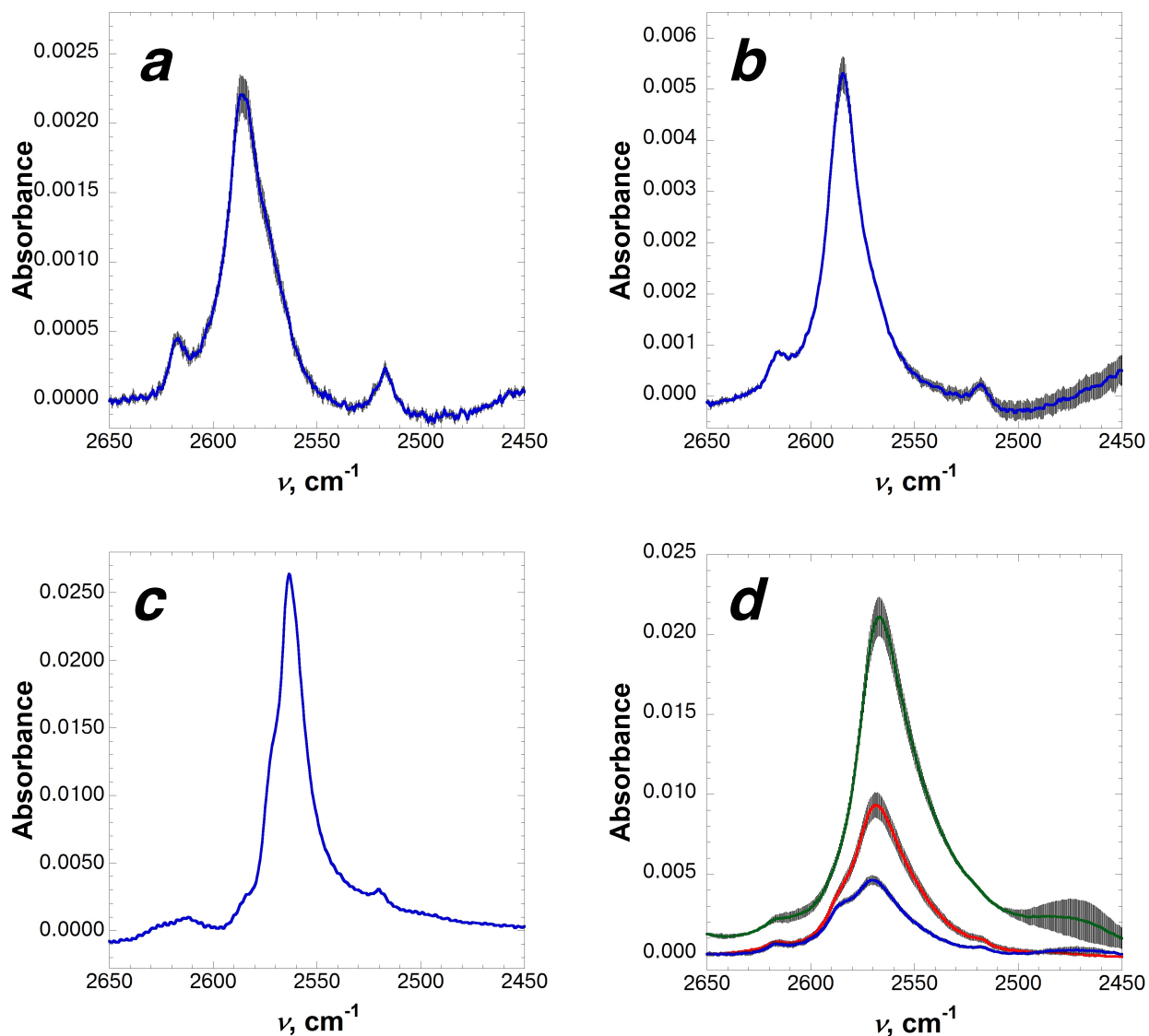
Figure S18. FT-IR spectrum of *p*-thiocresol (200 mM) in CHCl$_3$. Three independent spectra were solvent subtracted, baseline corrected, and averaged. Error bars indicate standard error. Top: full IR absorbance spectrum; bottom: full IR transmittance spectrum. ν_{max} of the S–H stretching frequency is 2585 cm^{-1}.
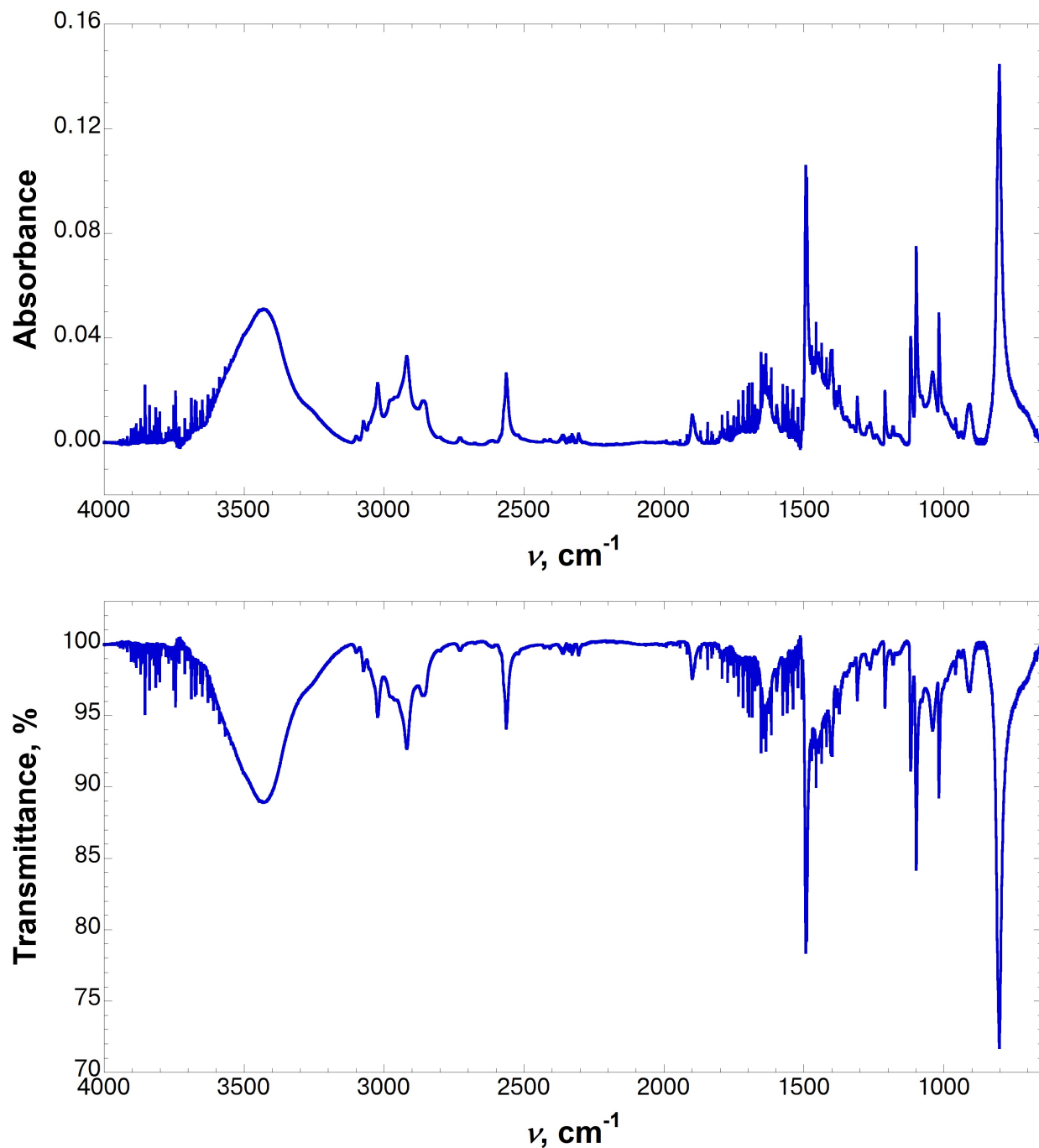
Figure S19. FT-IR spectrum of crystalline *p*-thiocresol in a pressed KBr pellet. Crystalline *p*-thiocresol was not recrystallized, and was used as purchased. The spectrum was baseline corrected. Top: full IR absorbance spectrum; bottom: full IR transmittance spectrum. ν_{max} of the S–H stretching frequency is 2563 cm^{-1}.

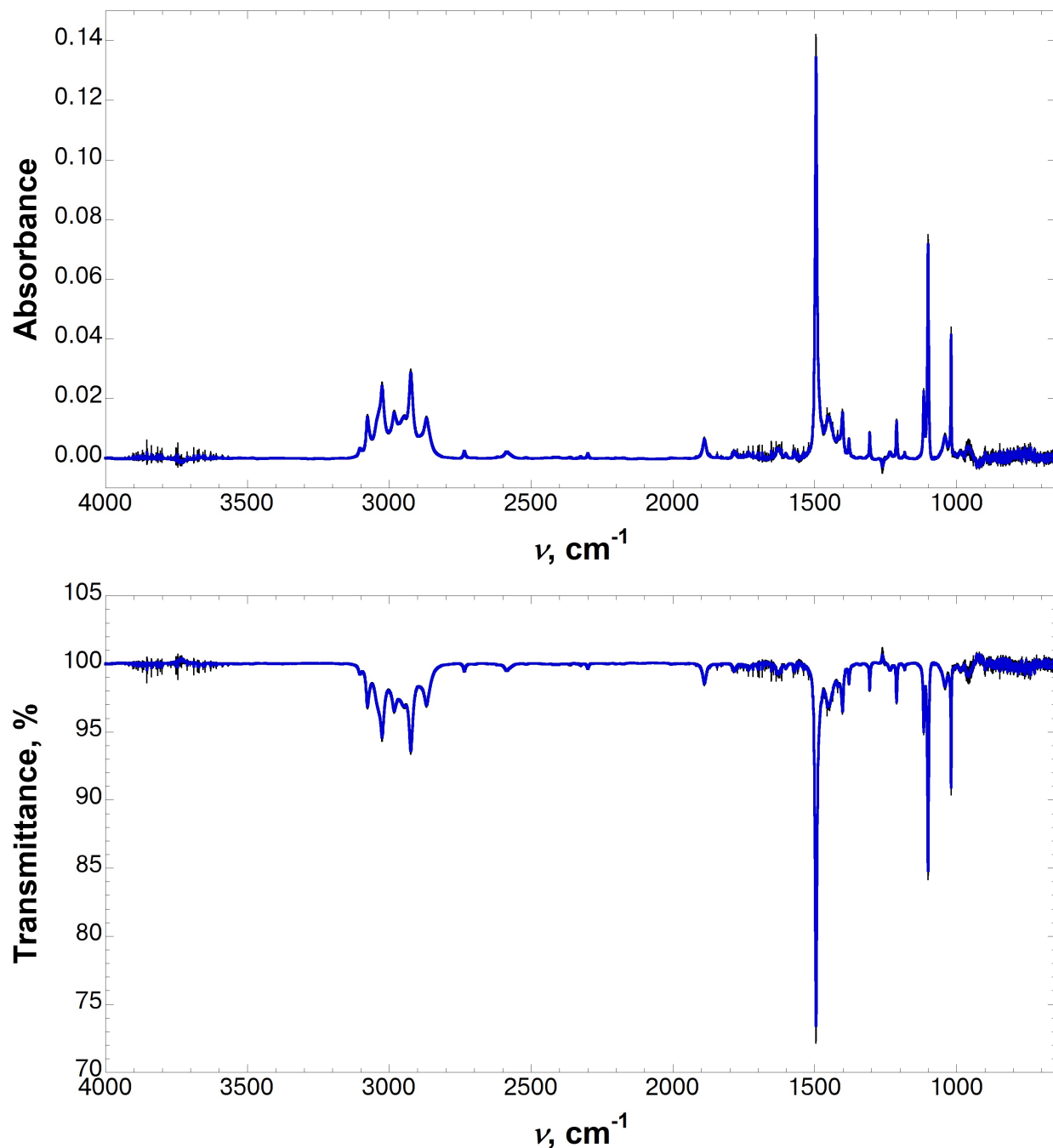**Figure S20**. FT-IR spectrum of *p*-thiocresol (200 mM) in ethyl acetate. Three independent spectra were solvent subtracted, baseline corrected, and averaged. Error bars indicate standard error. Top: full IR absorbance spectrum; bottom: full IR transmittance spectrum. ν_{max} of the S–H stretching frequency is 2567 cm^{-1}.

Figure S21. FT-IR spectrum of *p*-thiocresol (200 mM) in 25% ethyl acetate in CCl_4. Three independent spectra were solvent subtracted, baseline corrected, and averaged. Error bars indicate standard error. Top: full IR absorbance spectrum; bottom: full IR transmittance spectrum. ν_{max} of the S–H stretching frequency is 2569 cm^{-1}.
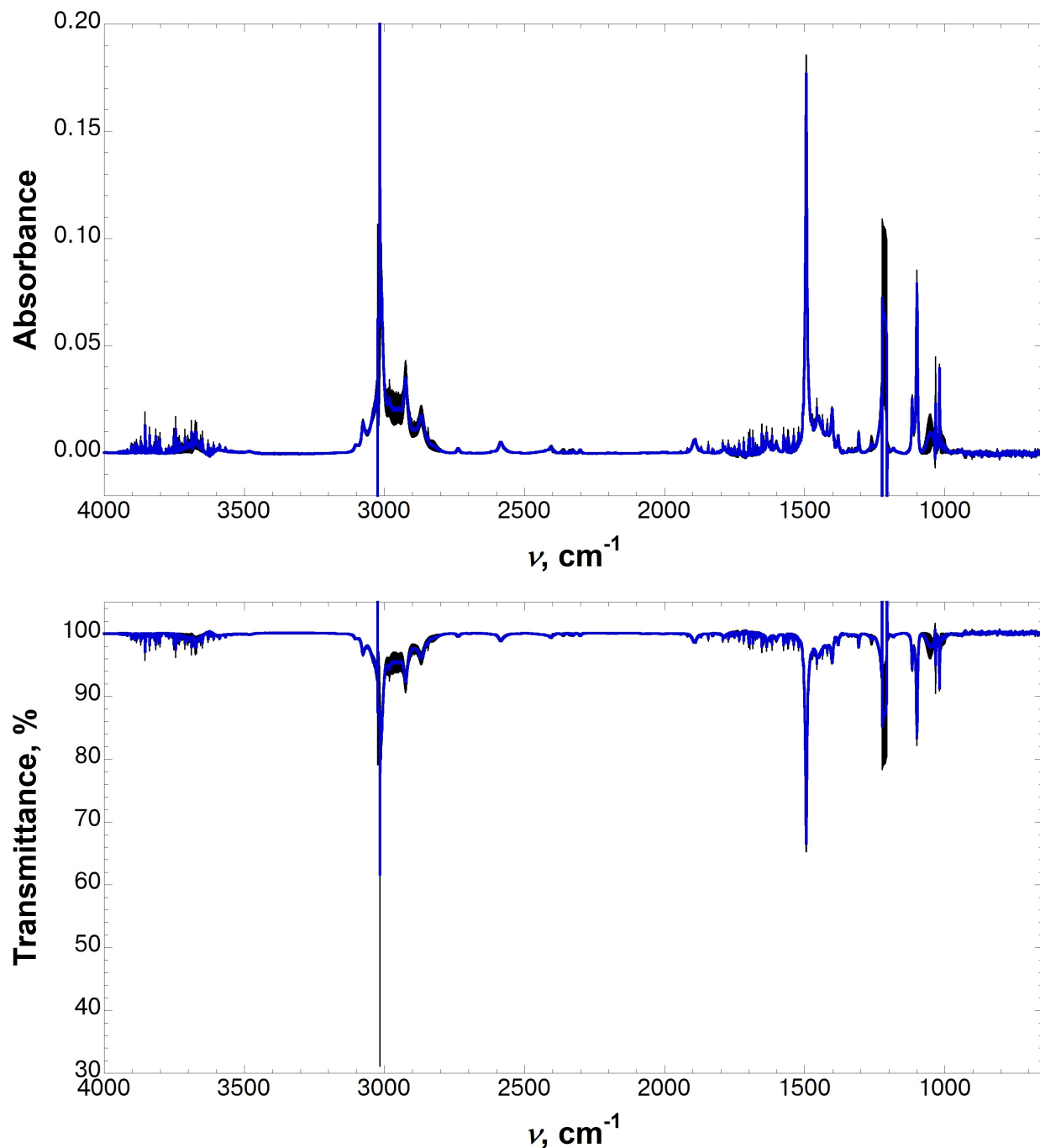
Figure S22. FT-IR spectrum of *p*-thiocresol (200 mM) in 10% ethyl acetate in CCl_4. Three independent spectra were solvent subtracted, baseline corrected, and averaged. Error bars indicate standard error. Top: full IR absorbance spectrum; bottom: full IR transmittance spectrum. ν_{max} of the S–H stretching frequency is 2571 cm^{-1}.

Figure S23. FT-IR spectrum of *p*-thiocresol (200 mM) in acetone. Three independent spectra were solvent subtracted, baseline corrected, and averaged. Error bars indicate standard error. Top: full IR absorbance spectrum; bottom: full IR transmittance spectrum. ν_{max} of the S–H stretching frequency is 2558 cm^{-1}.
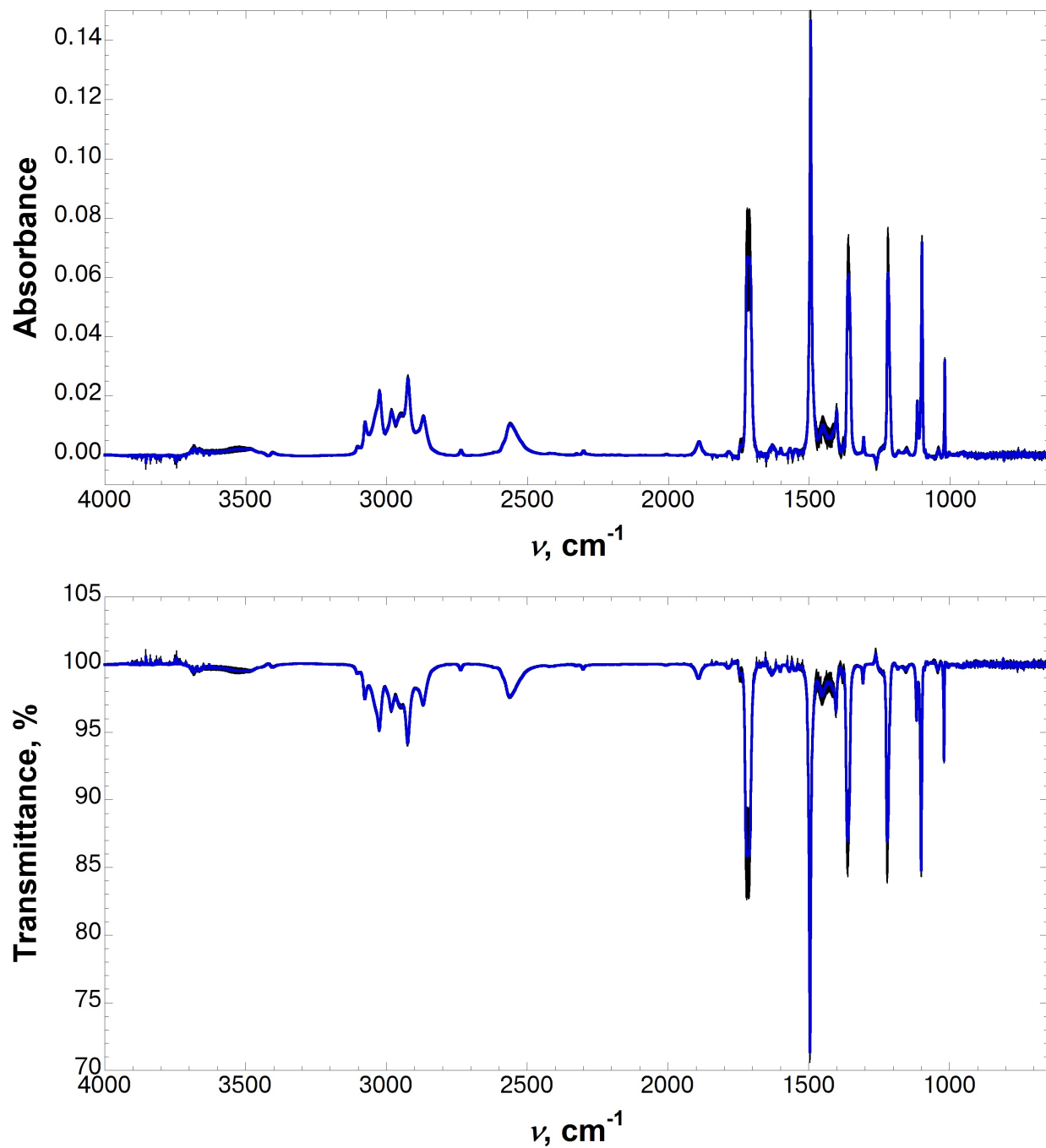
Figure S24. FT-IR spectrum of *p*-thiocresol (200 mM) in 25% acetone in CCl$_4$. Three independent spectra were solvent subtracted, baseline corrected, and averaged. Error bars indicate standard error. Top: full IR absorbance spectrum; bottom: full IR transmittance spectrum. ν_{max} of the S–H stretching frequency is 2561 cm^{-1}.
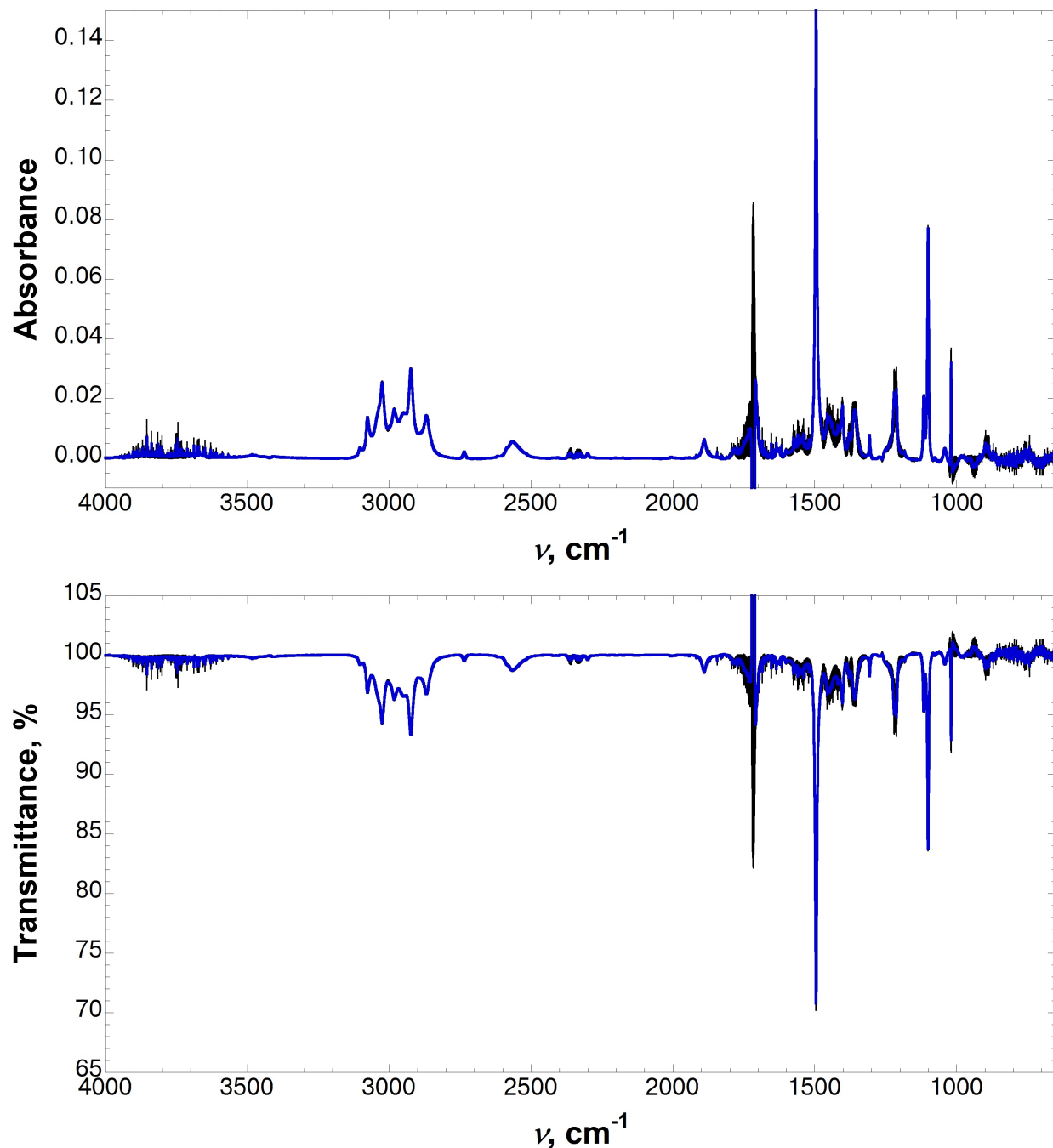
Figure S25. FT-IR spectrum of *p*-thiocresol (200 mM) in 10% acetone in CCl$_4$. Three independent spectra were solvent subtracted, baseline corrected, and averaged. Error bars indicate standard error. Top: full IR absorbance spectrum; bottom: full IR transmittance spectrum. ν_{max} of the S–H stretching frequency is 2565 cm^{-1}.
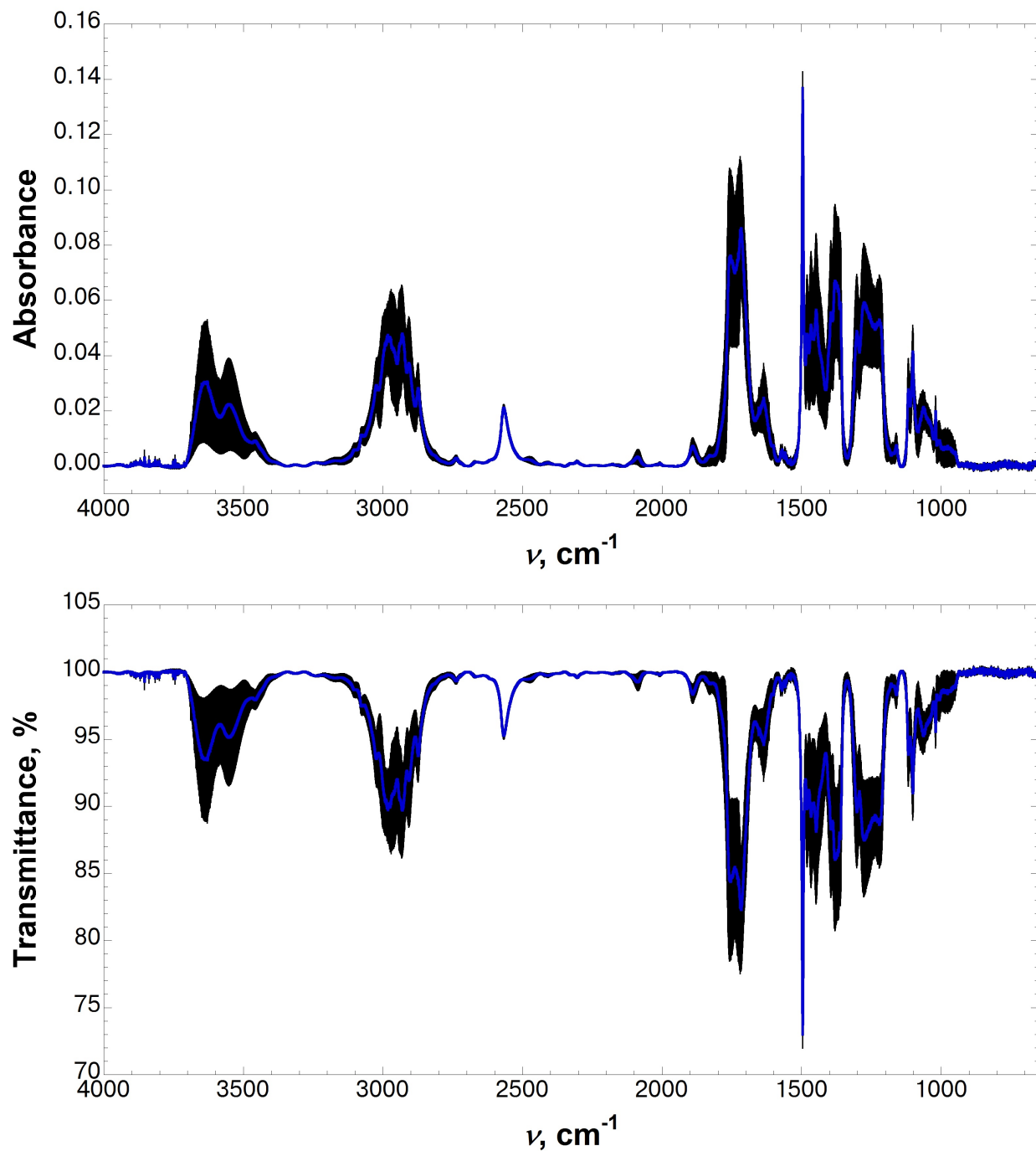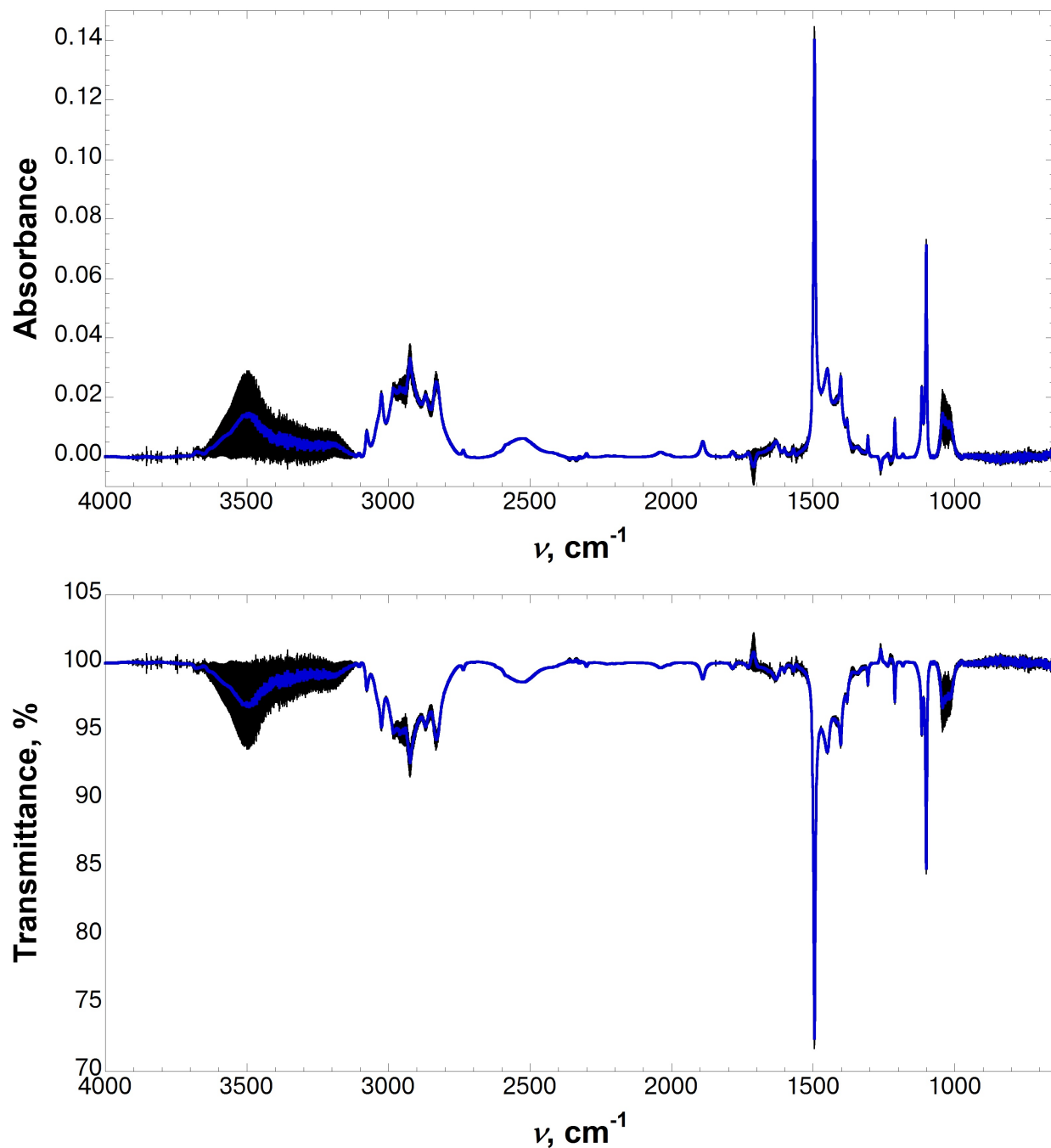
Figure S26. FT-IR spectrum of *p*-thiocresol (200 mM) in 25% methanol in CCl$_4$. Three independent spectra were solvent subtracted, baseline corrected, and averaged. Error bars indicate standard error. Top: full IR absorbance spectrum; bottom: full IR transmittance spectrum. ν_{max} of the S–H stretching frequency is 2521 cm^{-1}.
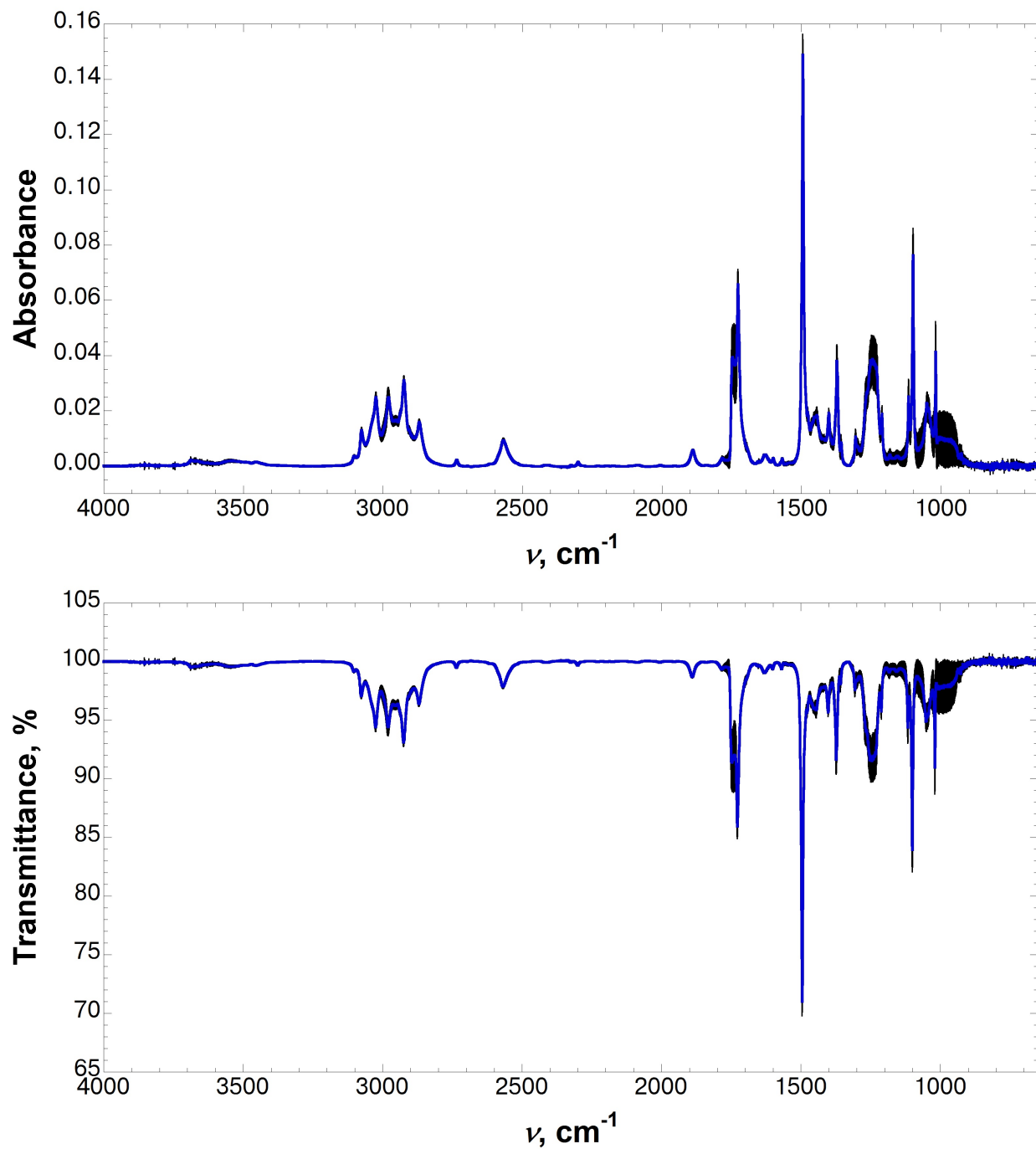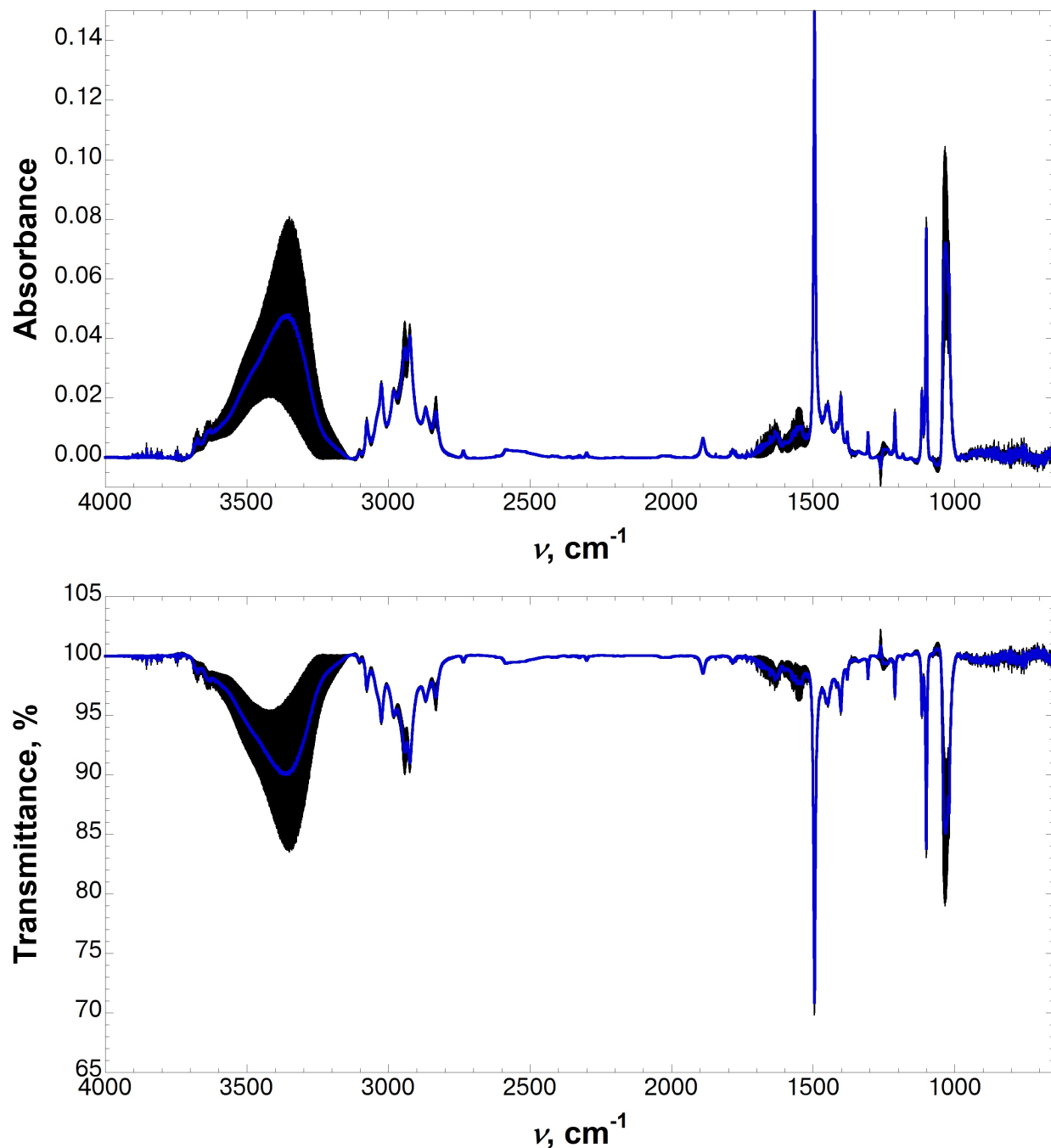
Figure S27. FT-IR spectrum of *p*-thiocresol (200 mM) in 10% methanol in CCl$_4$. Three independent spectra were solvent subtracted, baseline corrected, and averaged. Error bars indicate standard error. Top: full IR absorbance spectrum; bottom: full IR transmittance spectrum. Values for ν_{max} which are consistent with the S–H stretching frequency are 2584 cm^{-1}, 2548 cm^{-1}, and 2518 cm^{-1}.
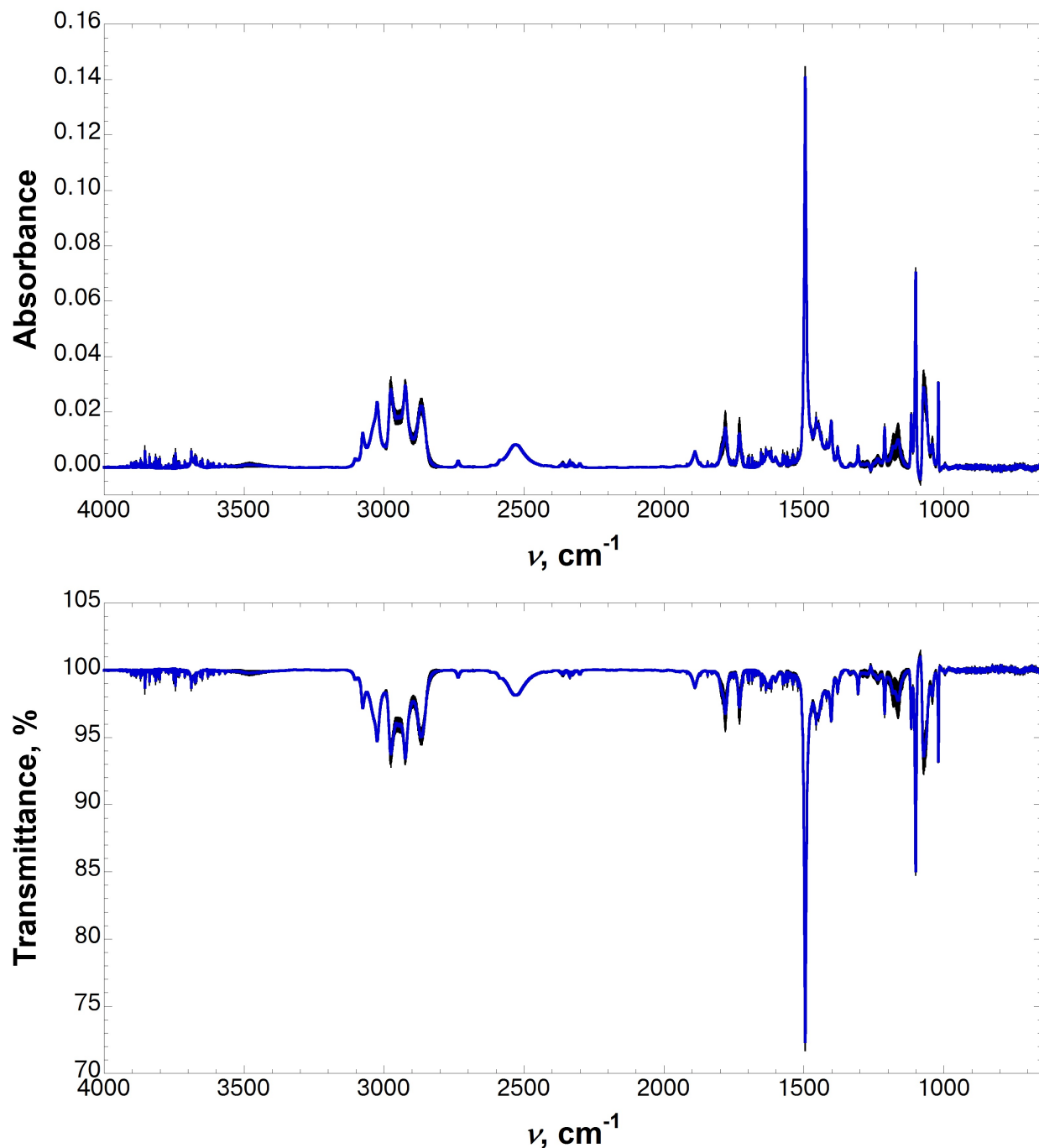
Figure S28. FT-IR spectrum of *p*-thiocresol (200 mM) in 25% THF in CCl$_4$. Three independent spectra were solvent subtracted, baseline corrected, and averaged. Error bars indicate standard error. Top: full IR absorbance spectrum; bottom: full IR transmittance spectrum. ν_{max} of the S–H stretching frequency is 2530 cm^{-1}.
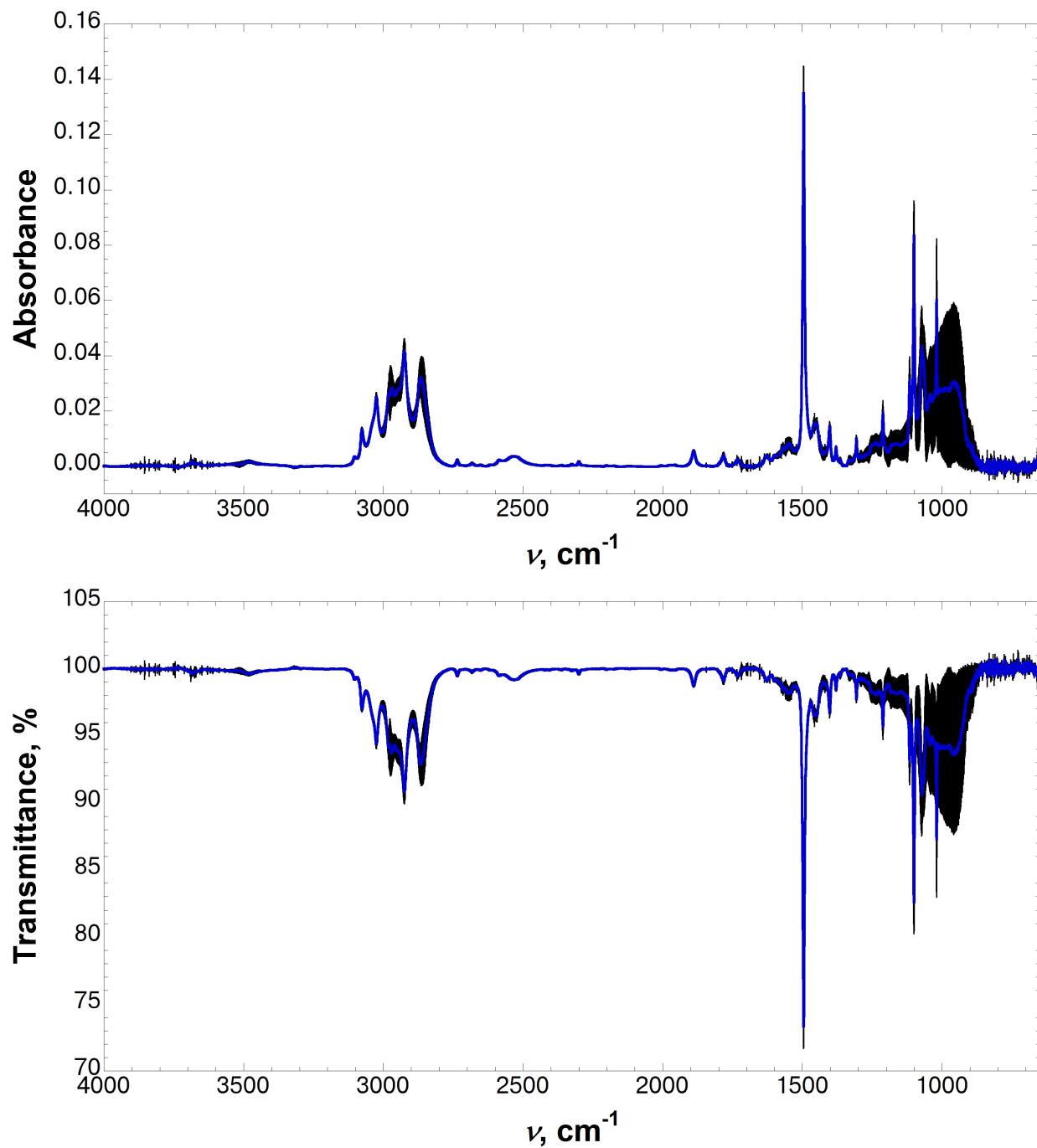
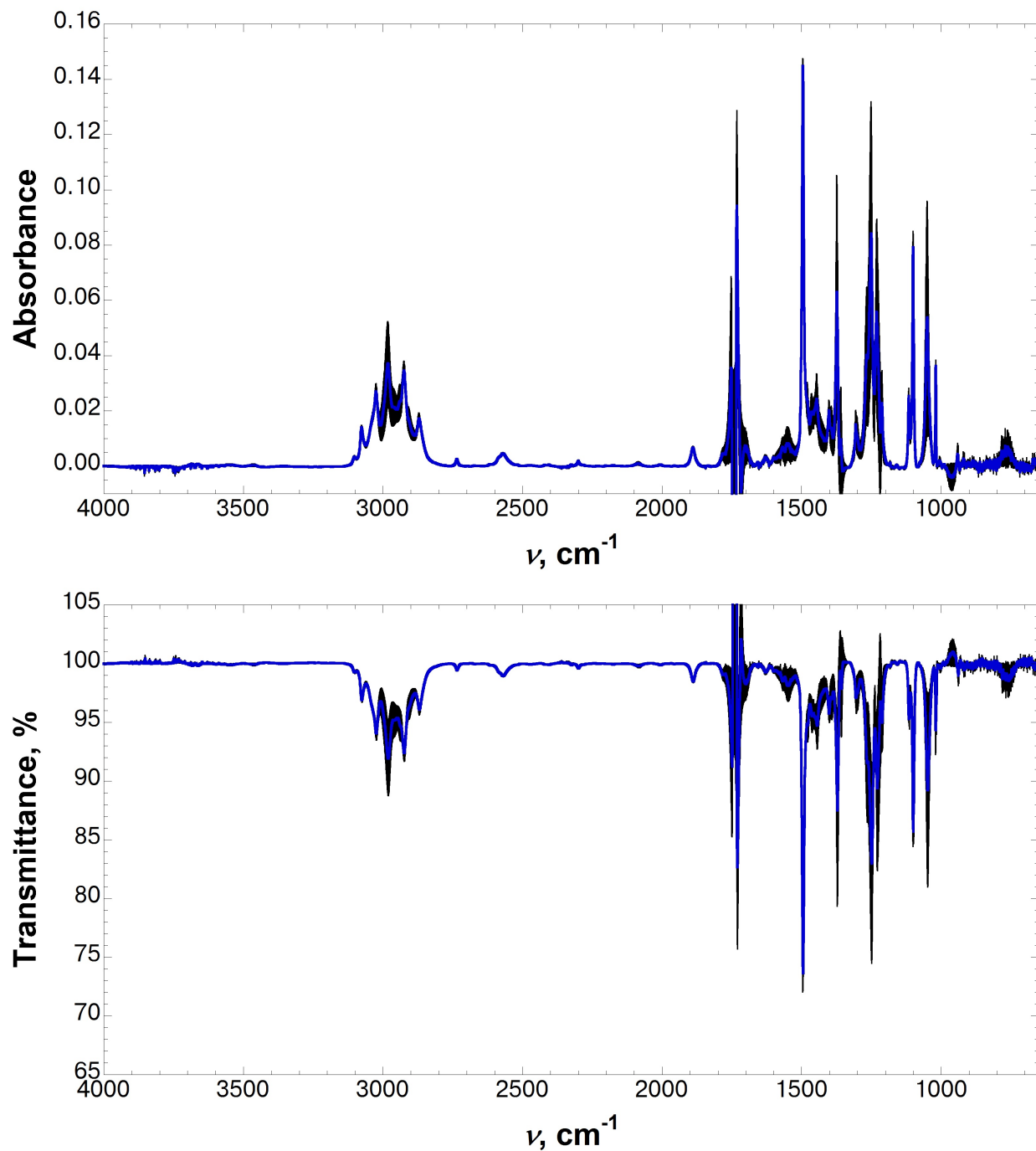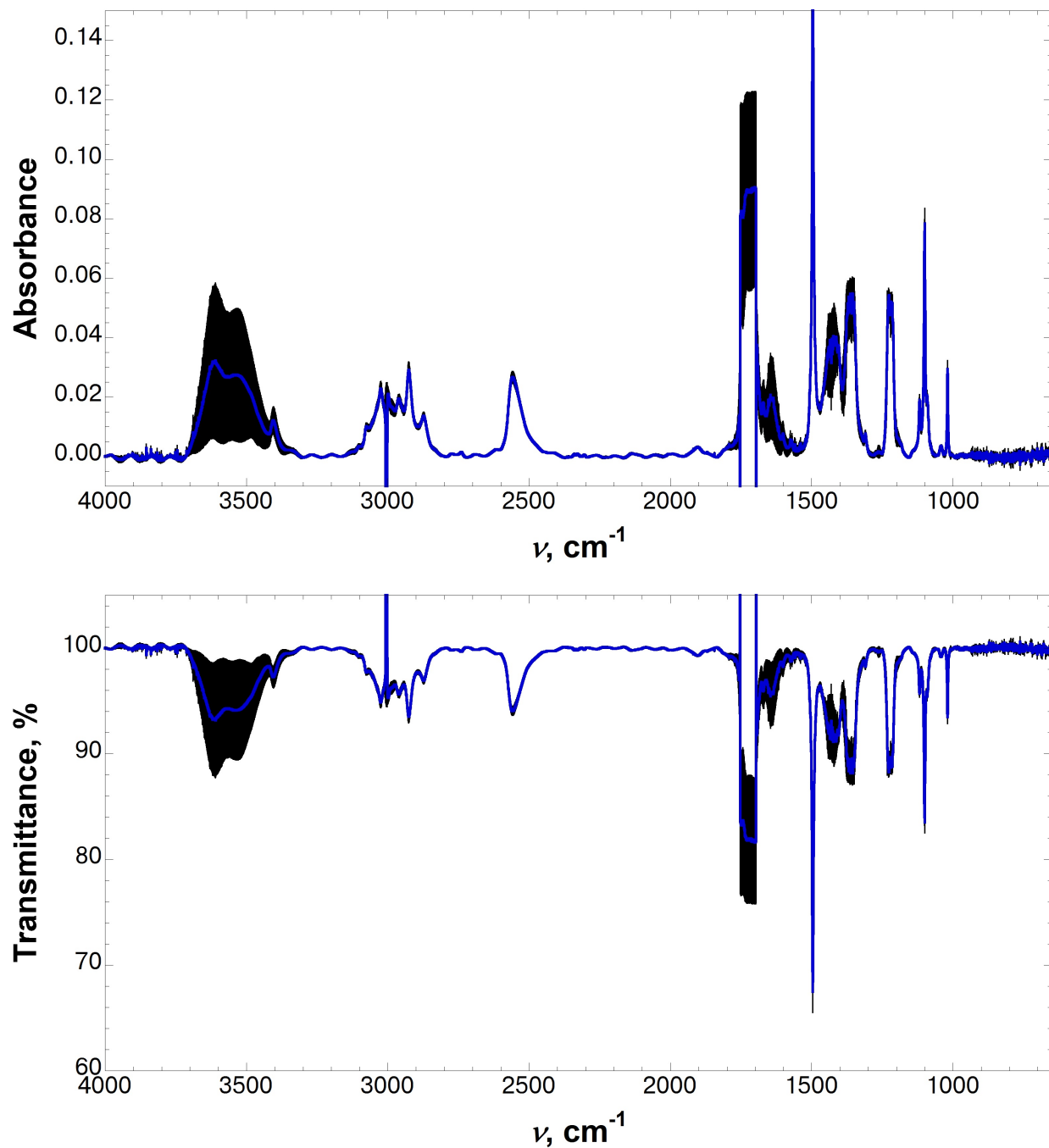**Figure S29**. FT-IR spectrum of *p*-thiocresol (200 mM) in 10% THF in CCl$_4$. Three independent spectra were solvent subtracted, baseline corrected, and averaged. Error bars indicate standard error. Top: full IR absorbance spectrum; bottom: full IR transmittance spectrum. ν_{max} of the S–H stretching frequency is 2531 cm^{-1}.

**Comparison of the S–H stretching frequency of *p*-thiocresol in the presence of different aromatic donors**
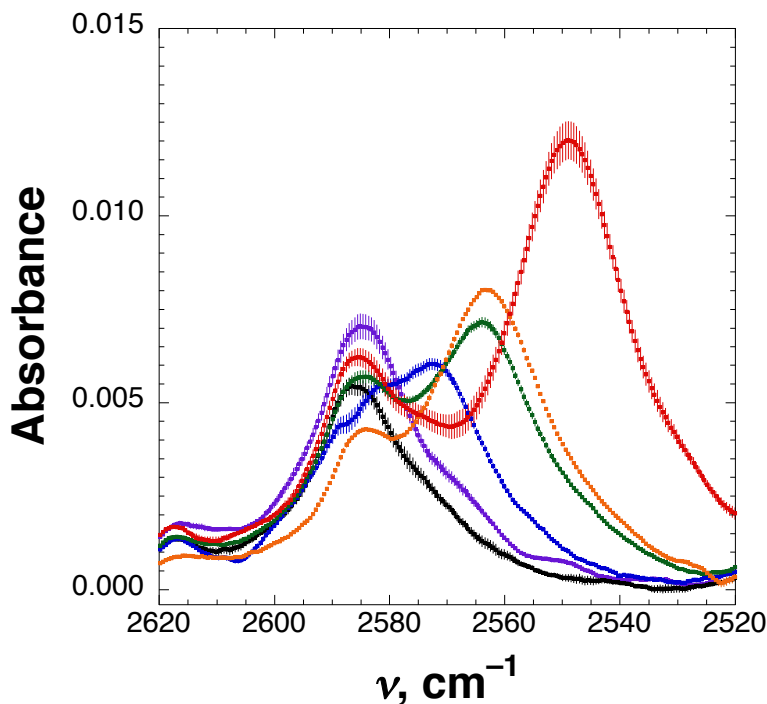
Figure S30. Infrared spectroscopy for the S–H stretching of *p*-thiocresol (55 mM) in CCl$_4$ in the absence of additional aromatic compounds (black) and in the presence of 800 mM hexamethylbenzene (red), 1-methylindole (orange), mesitylene (green), toluene (blue), *m*-dichlorobenzene (purple). Error bars indicate standard error.

Table S11. S–H stretching frequencies of *p*-thiocresol in the presence of added aromatic compounds in CCl$_4$. The changes in S–H stretching frequencies indicate the magnitude of interaction of the aromatic compounds with the thiol hydrogen. More electron-rich aromatic compounds result in larger red shifts in the S–H stretching frequency.

aromatic additive in CCl$_4$	ν_{S-H}, cm^{-1}	
	interacting thiol	non-interacting thiol
m–Dichlorobenzene	2586	2581
Toluene	2586	2571
Mesitylene	2586	2563
1-Methylindole	2586	2561
Hexamethylbenzene	2586	2549

Comparison of the S–H stretching frequency of *p*-thiocresol in the presence of different aromatic donors at low concentrations
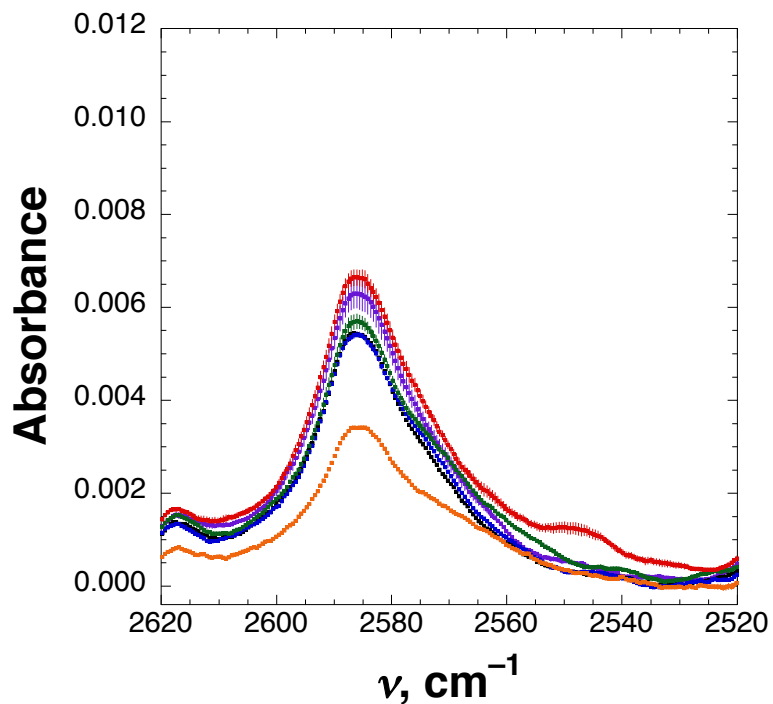
Figure S31. Infrared spectroscopy (S–H stretching frequency) of *p*-thiocresol (55 mM) in CCl$_4$ in the absence of additional aromatic compound (black) and in the presence of 50 mM hexamethylbenzene (red), 1-methylindole (orange), mesitylene (green), toluene (blue), *m*-dichlorobenzene (purple). Error bars indicate the standard error.

Self-association of *p*-thiocresol in solution
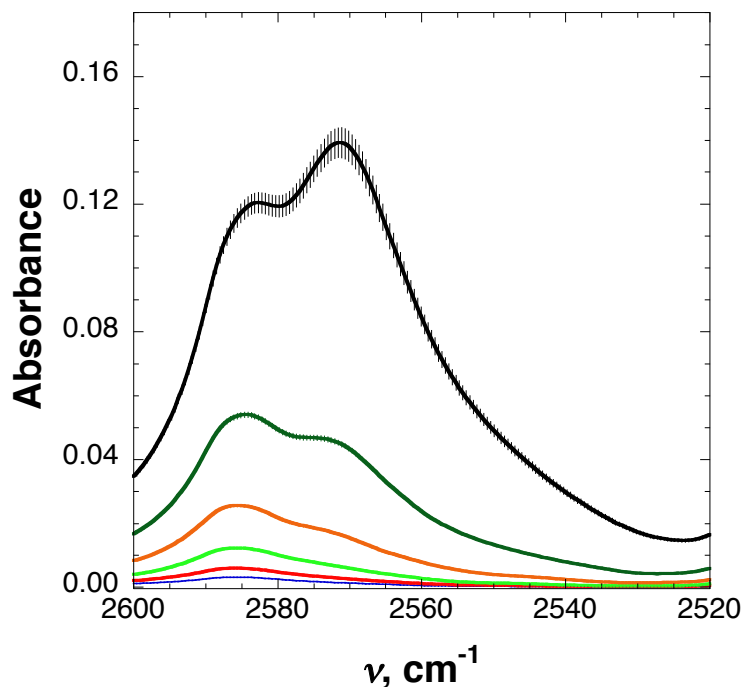
Figure S32. Infrared spectroscopy (S–H stretching frequency) of *p*-thiocresol as a function of concentration in CCl_4: 34.2 mM (blue), 68.5 mM (red), 137 mM (green), 274 mM (orange) 548 mM (dark green), and 1096 mM (black). With increasing concentration of *p*-thiocresol, the peak at 2572 cm^{-1} increases in magnitude relative to that of the non-interacting peak (2586 cm^{-1}). The peak or shoulder at 2572 cm^{-1} is attributed to ν_{S-H} of self-associated of *p*-thiocresol, either via an S–H/π interaction or hydrogen bonding.
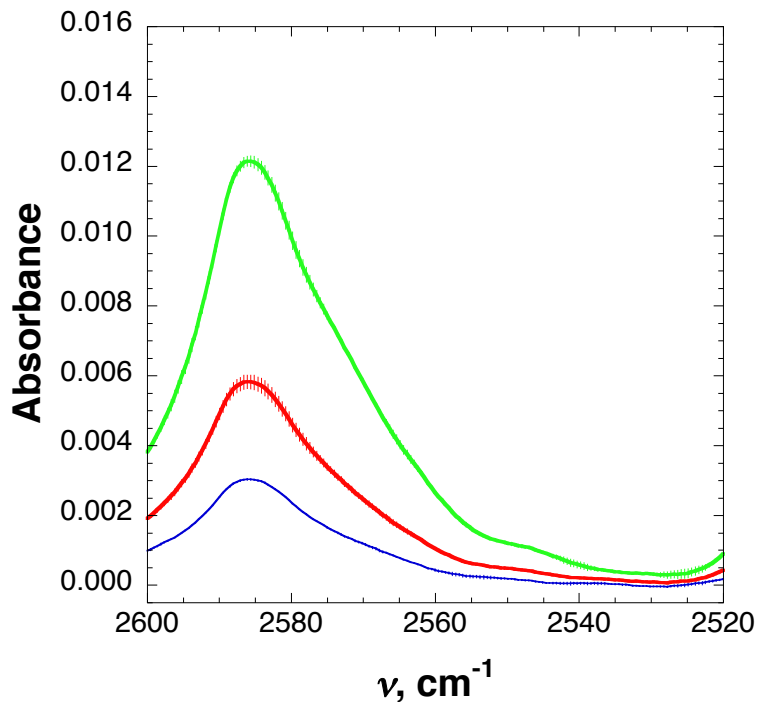
Figure S33. Infrared spectroscopy (S–H stretching frequency) of *p*-thiocresol at lower concentrations: 34.2 mM (blue), 68.5 mM (red), and 137 mM (green). Note that with increasing concentration of *p*-thiocresol, the shoulder at 2572 cm^{-1} contributes significantly to the intensity of the non-interacting peak (2586 cm^{-1}).

The normalized area of ν_{S-H} at 2571 cm^{-1} due to self-association of *p*-thiocresol follows a 1:1 binding equation:

$$Y = (Y_{max} - Y_0) \left[1 + \left\{ \frac{-1 + \sqrt{8L + 1}}{4L} \right\} \right]$$

[Equation S1]

where L = $K_{self} \times [SH_{total}]$, $[SH]_{total}$ = total concentration of *p*-thiocresol.
Y_0 and Y_{max} represent the maximum and minimum signal (area under the curve divided by the concentration of *p*-thiocresol) at 2572 cm^{-1}.
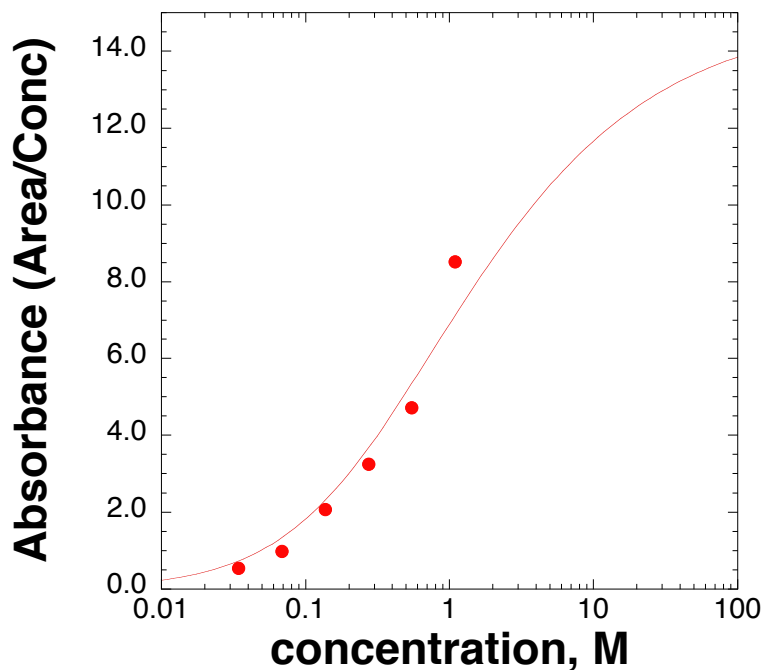
Figure S34. Binding curve for the self-association of *p*-thiocresol in solutions in CCl_4. The y-axis represents the area under the curve divided by the *p*-thiocresol concentration for the peak at 2572 cm^{-1}.

The fit of the binding curve (from equation S1) indicates K_d = 786 ($\pm$ 123) mM for self-association of *p*-thiocresol. These data do not indicate whether the "interacting" frequency is due to an S–H/π interaction or a conventional hydrogen bond. These data are consistent with a free thiol (non-interacting frequency, 2586 cm^{-1}) and thiol dimer (termed "interacting" frequency, 2572 cm^{-1}).

Titration of *p*-thiocresol with different aromatic donors

Five aromatic compounds (hexamethylbenzene, 1-methylindole, mesitylene, toluene, and *m*-dichlorobenzene) were selected for titration with *p*-thiocresol, based on differing π-electron donation capabilities. All of the selected aromatic compounds (except for 1-methylindole) have a benzene ring as the donor π system. The extent of π electron donation could be controlled via variable substitution on the aromatic ring. Hexamethylbenzene, with six electron-donating methyl groups, was expected to have highest electron donation, followed by mesitylene and toluene. The *m*-dichlorobenzene was expected to be the weakest donor, with two electron-withdrawing chlorine atoms directly attached to the aromatic π system. 1-Methylindole and toluene were used as model compounds representing the electronic properties of tryptophan and phenylalanine respectively, which are relevant to S–H/π interactions involving aromatic donors in biological systems. 1-Methylindole was used in place of the direct tryptophan analogue, 3-methylindole, in order to avoid compounding effects of N–H/π interaction via the hydrogen-bond donor capabilities of the indole NH.

hexamethylbenzene   1-methylindole   mesitylene   toluene   *m*-dichlorobenzene

Phenylalanine   *Tryptophan*
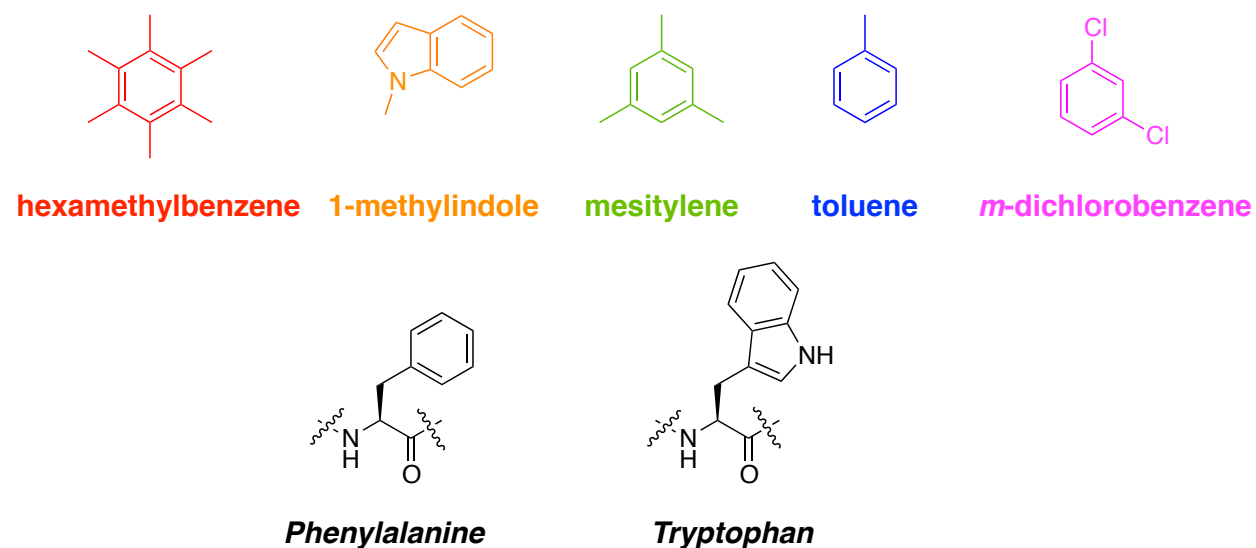
Figure S35. Comparison of aromatic compounds used to investigate the strength of the S–H/π interaction as a function of π–electron donating capabilities. Toluene and 1-methylindole were used as model compounds representing the electronic properties of phenylalanine and tryptophan, respectively.

Concentration-dependent IR spectroscopy
The nature of S–H/π interaction was examined using 55 mM *p*-thiocresol in CCl$_4$ via titration with five aromatic compounds: hexamethylbenzene, 1-methylindole, mesitylene, toluene, and *m*-dichlorobenzene. All IR spectra were collected in a Nicolet Magna-IR 750 FT-IR spectrometer equipped with a liquid nitrogen-cooled MCT/A detector at a spectral resolution of 1 cm^{-1}. The samples were filled in a gas-tight liquid IR cell fitted with quartz windows. All IR spectra (512 or 1024 scans) were individually background corrected and were baseline corrected using the OMNIC FT-IR Software (Nicolet). Each titration was averaged over at least three independent trials.

Titration of *p*-thiocresol with hexamethylbenzene
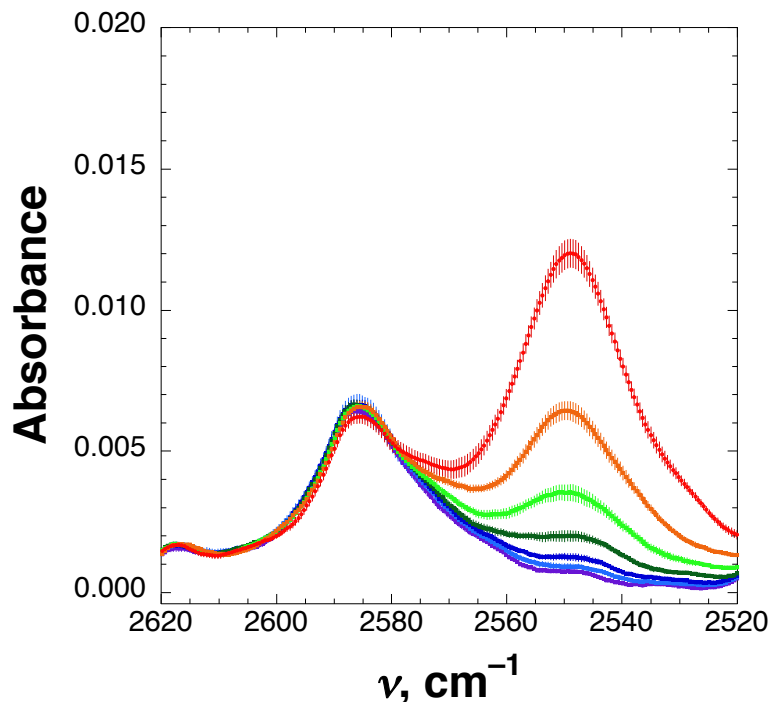
Figure S36. Infrared spectroscopy of the S–H stretching frequency of *p*-thiocresol (55 mM) in the presence of different concentrations of hexamethylbenzene in CCl_4 (12.5 mM (orange), 25 mM (cyan), 50 mM (brick red), 100 mM (green), 200 mM (blue), 400 mM (purple), and 800 mM (red)). The peak at 2586 cm^{-1} corresponds to the non-interacting S–H stretching frequency of *p*-thiocresol. The peak at 2549 cm^{-1} corresponds to the S–H stretching frequency for the thiol hydrogen interacting with hexamethylbenzene via an S–H/π interaction. The intensity of the peak at 2549 cm^{-1} increases with increasing hexamethylbenzene concentration, consistent with increased binding of the aromatic donor to the thiol hydrogen via an S–H/π interaction. The shoulder at 2572 cm^{-1} is due to the self-association *p*-thiocresol. At concentrations above 800 mM, hexamethylbenzene was observed to precipitate during the experiment. Error bars indicate standard error.

Each of the IR spectra was fit with a three-component Lorentzian distribution function with the general formula

$$Y = Y_0 + \sum_{n=1}^{3} \frac{A_n}{(x - x_n)^2 + B_n}$$

where Y_0 is the offset in y-axis, A_n and B_n are maximum intensity and width of the distribution around the peak position at x_n. The x_n was fixed at 2549, 2572, and 2586 cm^{-1} for the interacting peak with the donor (hexamethylbenzene) via S–H/π interaction, self-association of *p*-thiocresol, and for the non-interacting thiol peak, respectively.
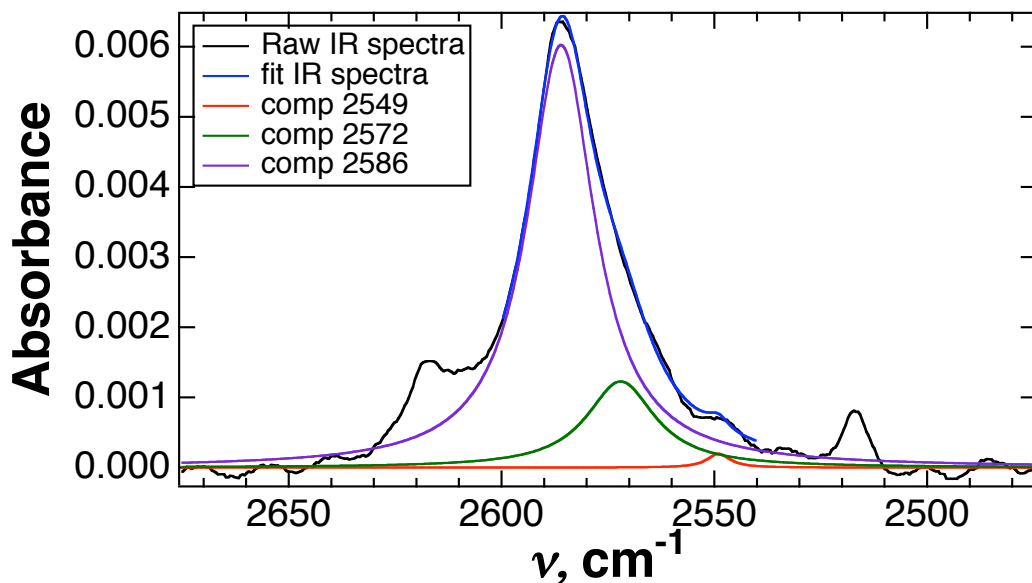
Figure S37. Fit and deconvolution of the infrared spectrum for the S–H stretching frequency of *p*-thiocresol in 12.5 mM hexamethylbenzene in CCl_4 (black). The S–H/π interactions are indicated: thiol association with hexamethylbenzene (2549 cm^{-1}, red), *p*-thiocresol self-association (2572 cm^{-1}, green), and the non-interacting *p*-thiocresol thiol (2586 cm^{-1}, purple).
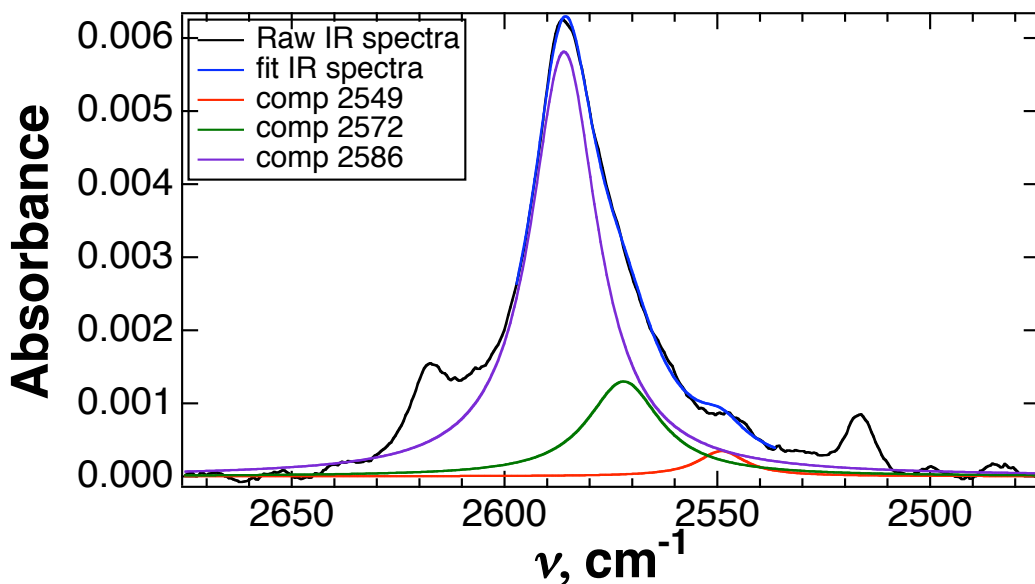
Figure S38. Fit and deconvolution of the infrared spectrum for the S–H stretching frequency of *p*-thiocresol in 25 mM hexamethylbenzene in CCl_4 (black). The S–H/π interactions are indicated: thiol association with hexamethylbenzene (2549 cm^{-1}, red), *p*-thiocresol self-association (2572 cm^{-1}, green), and the non-interacting *p*-thiocresol thiol (2586 cm^{-1}, purple).
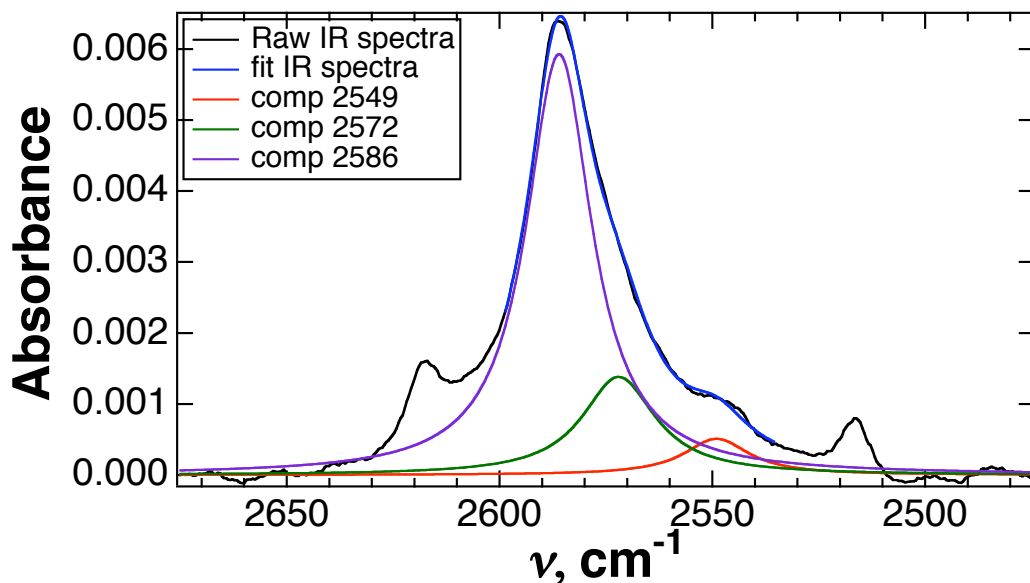
Figure S39. Fit and deconvolution of the infrared spectrum for the S–H stretching frequency of *p*-thiocresol in 50 mM hexamethylbenzene in CCl$_4$ (black). The S–H/π interactions are indicated: thiol association with hexamethylbenzene (2549 cm^{-1}, red), *p*-thiocresol self-association (2572 cm^{-1}, green), and the non-interacting *p*-thiocresol thiol (2586 cm^{-1}, purple).
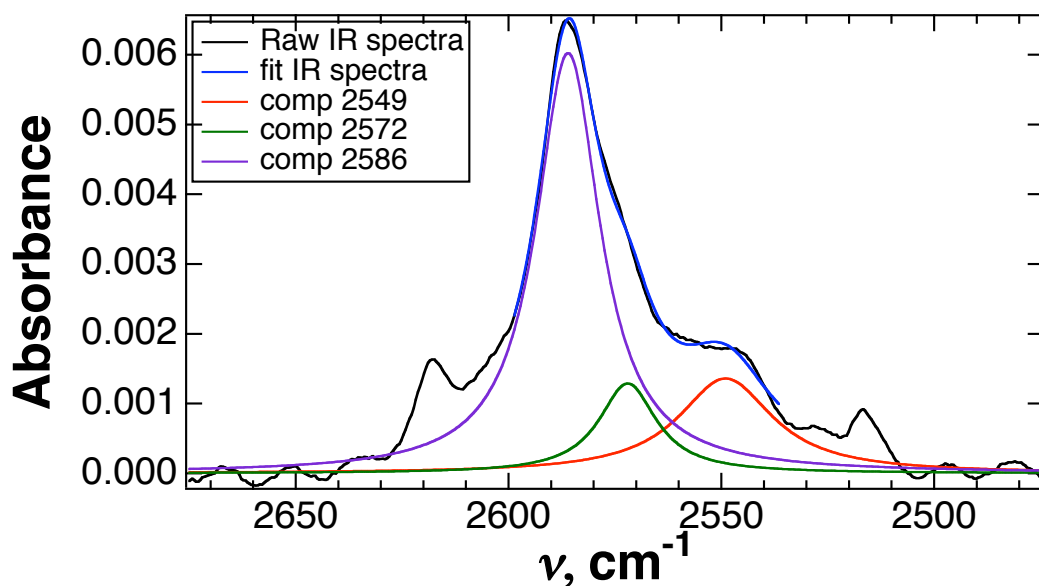
Figure S40. Fit and deconvolution of the infrared spectrum for the S–H stretching frequency of *p*-thiocresol in 100 mM hexamethylbenzene in CCl$_4$ (black). The S–H/π interactions are indicated: thiol association with hexamethylbenzene (2549 cm^{-1}, red), *p*-thiocresol self-association (2572 cm^{-1}, green), and the non-interacting *p*-thiocresol thiol (2586 cm^{-1}, purple).

Figure S41. Fit and deconvolution of the infrared spectrum for the S–H stretching frequency of *p*-thiocresol in 200 mM hexamethylbenzene in CCl$_4$ (black). The S–H/π interactions are indicated: thiol association with hexamethylbenzene (2549 cm^{-1}, red), *p*-thiocresol self-association (2572 cm^{-1}, green), and the non-interacting *p*-thiocresol thiol (2586 cm^{-1}, purple).

Figure S42. Fit and deconvolution of the infrared spectrum for the S–H stretching frequency of *p*-thiocresol in 400 mM hexamethylbenzene in CCl$_4$ (black). The S–H/π interactions are indicated: thiol association with hexamethylbenzene (2549 cm^{-1}, red), *p*-thiocresol self-association (2572 cm^{-1}, green), and the non-interacting *p*-thiocresol thiol (2586 cm^{-1}, purple).

Figure S43. Fit and deconvolution of the infrared spectrum for the S–H stretching frequency of *p*-thiocresol in 800 mM hexamethylbenzene in CCl_4 (black). The S–H/π interactions are indicated: thiol association with hexamethylbenzene (2549 cm^{-1}, red), *p*-thiocresol self-association (2572 cm^{-1}, green), and the non-interacting *p*-thiocresol thiol (2586 cm^{-1}, purple).

Titration of *p*-thiocresol with mesitylene
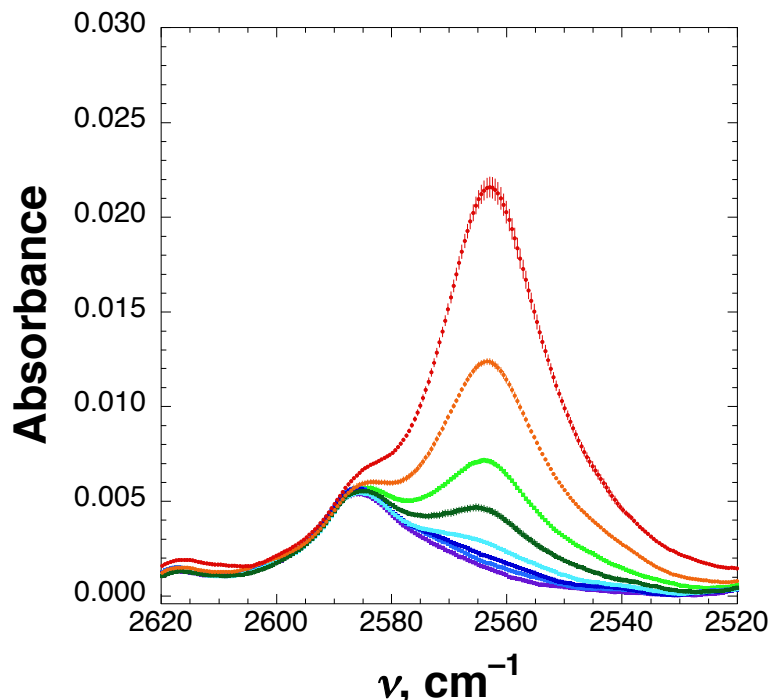
Figure S44. Infrared spectroscopy of the S–H stretching frequency of *p*-thiocresol (55 mM) in the presence of different concentrations of mesitylene in CCl_4 (25 mM (purple), 50 mM (light blue), 100 mM (blue), 200 mM (cyan), 400 mM (dark green), 800 mM (green), 1600 mM (orange), and 3200 mM (red)). The peak at 2586 cm^{-1} corresponds to the non-interacting S–H stretching frequency of *p*-thiocresol. The peak at 2563 cm^{-1} corresponds to the S–H stretching frequency for the thiol hydrogen interacting with mesitylene via an S–H/π interaction. The peak at 2563 cm^{-1} increases in intensity with increasing mesitylene concentration, consistent with increased binding of the aromatic donor to the thiol hydrogen of *p*-thiocresol via an S–H/π interaction. The shoulder at 2572 cm^{-1} is due to the S–H stretching of *p*-thiocresol self-association. Error bars indicate standard error.

Each of the IR spectra was fit with a three-component Lorentzian distribution function with the general formula

$$Y = Y_0 + \sum_{n=1}^{3} \frac{A_n}{(x - x_n)^2 + B_n}$$

where Y_0 is the offset in y-axis and A_n and B_n are maximum intensity and width of the distribution around the peak position at x_n. The x_n was fixed at 2563, 2572, and 2586 cm^{-1} for the interacting peak with the donor (mesitylene), self-association of *p*-thiocresol, and for the non-interacting thiol peak, respectively.
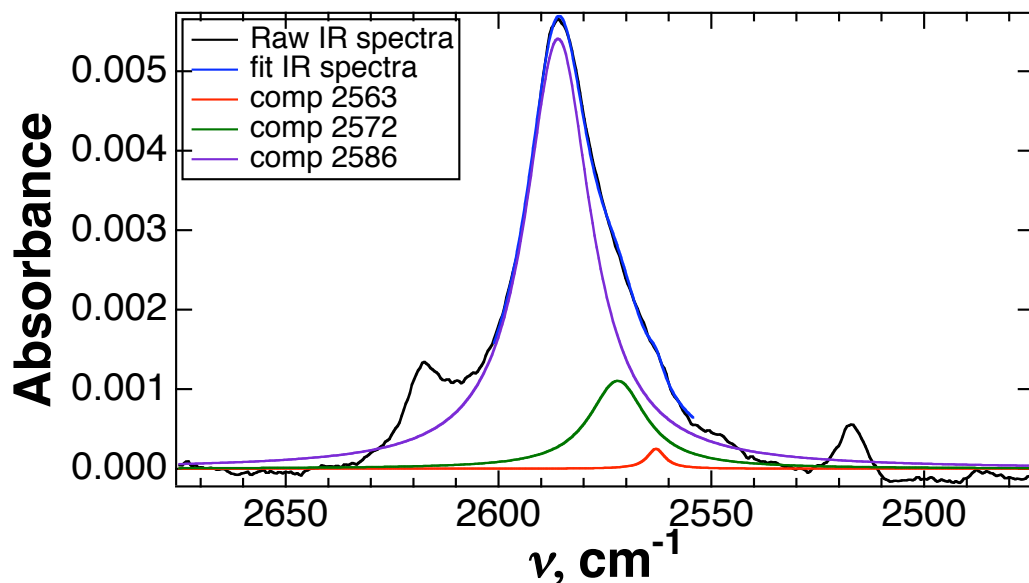
Figure S45. Fit and deconvolution of the infrared spectrum for the S–H stretching frequency of *p*-thiocresol in 25 mM mesitylene in CCl$_4$ (black). The S–H/π interactions are indicated: thiol association with mesitylene (2563 cm^{-1}, red), *p*-thiocresol self-association (2572 cm^{-1}, green), and the non-interacting *p*-thiocresol thiol (2586 cm^{-1}, purple).
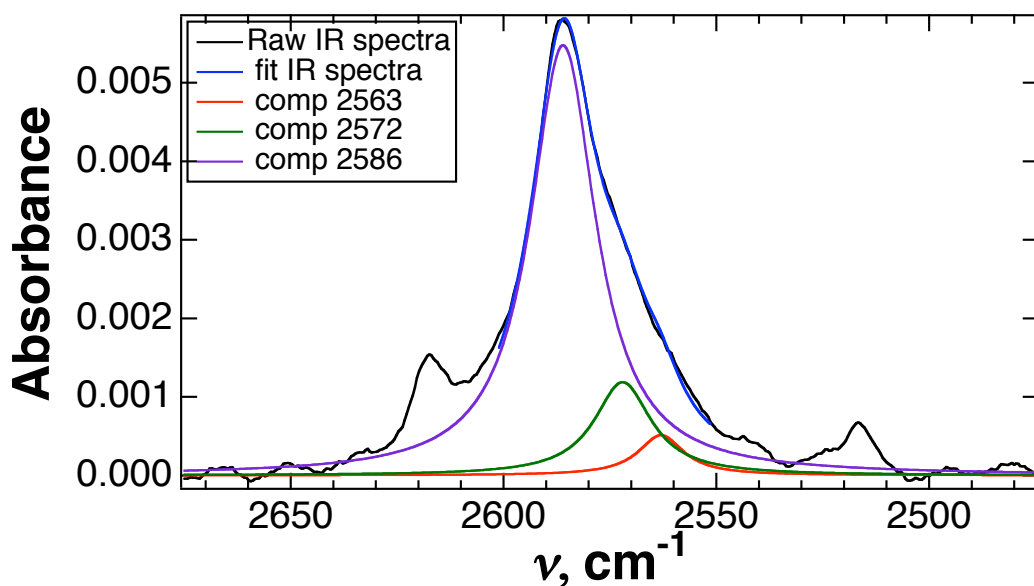
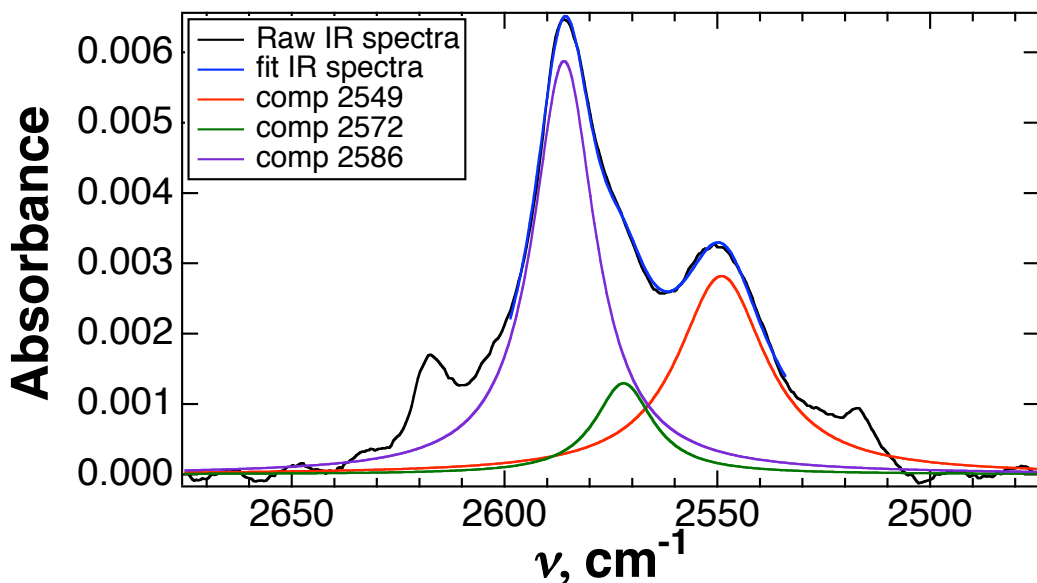**Figure S46**. Fit and deconvolution of the infrared spectrum for the S–H stretching frequency of *p*-thiocresol in 50 mM mesitylene in CCl$_4$ (black). The S–H/π interactions are indicated: thiol association with mesitylene (2563 cm^{-1}, red), *p*-thiocresol self-association (2572 cm^{-1}, green), and the non-interacting *p*-thiocresol thiol (2586 cm^{-1}, purple).
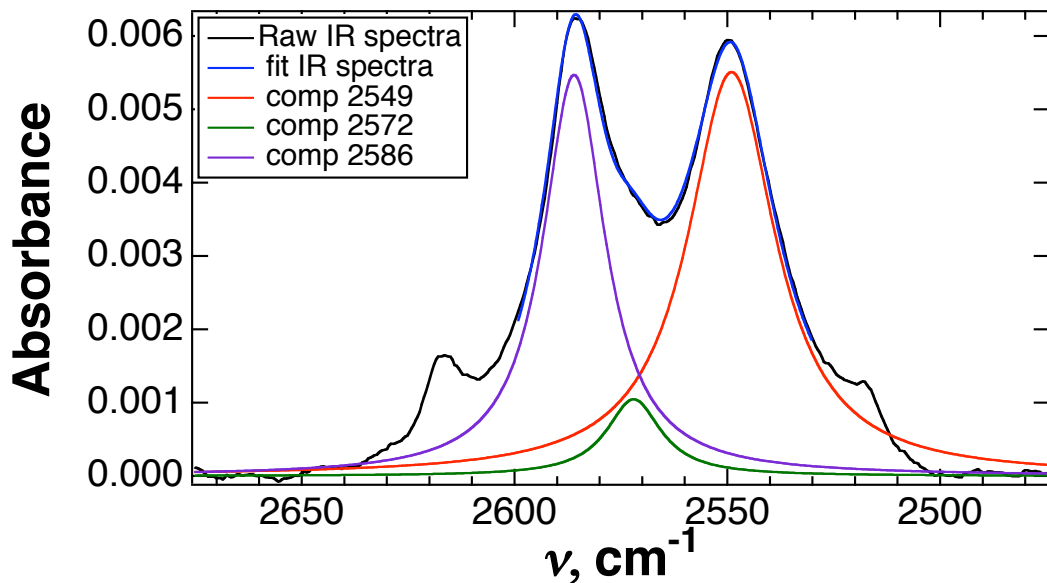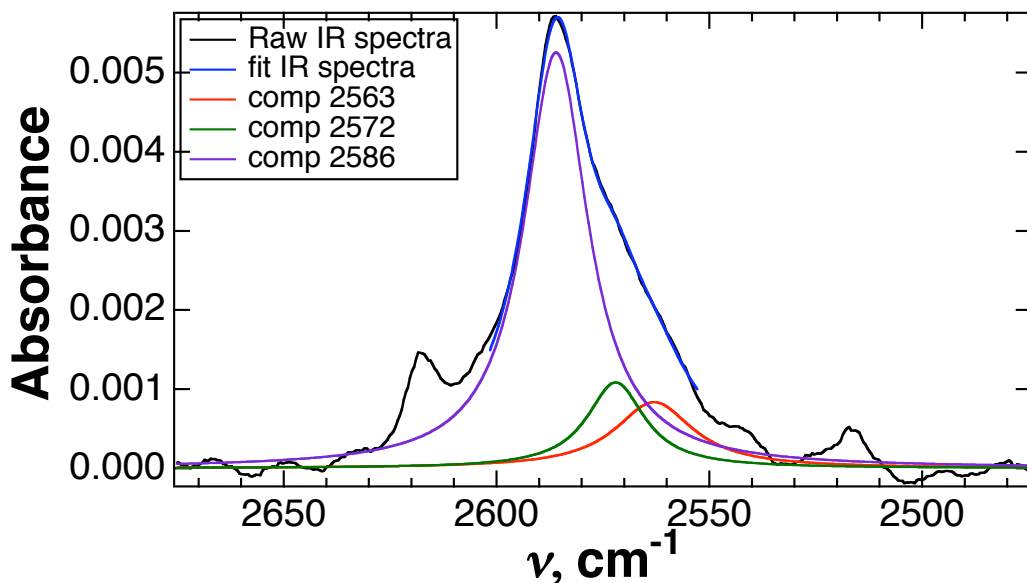
Figure S47. Fit and deconvolution of the infrared spectrum for the S–H stretching frequency of *p*-thiocresol in 100 mM mesitylene in CCl$_4$ (black). The S–H/π interactions are indicated: thiol association with mesitylene (2563 cm^{-1}, red), *p*-thiocresol self-association (2572 cm^{-1}, green), and the non-interacting *p*-thiocresol thiol (2586 cm^{-1}, purple).

Figure S48. Fit and deconvolution of the infrared spectrum for the S–H stretching frequency of *p*-thiocresol in 200 mM mesitylene in CCl$_4$ (black). The S–H/π interactions are indicated: thiol association with mesitylene (2563 cm^{-1}, red), *p*-thiocresol self-association (2572 cm^{-1}, green), and the non-interacting *p*-thiocresol thiol (2586 cm^{-1}, purple).

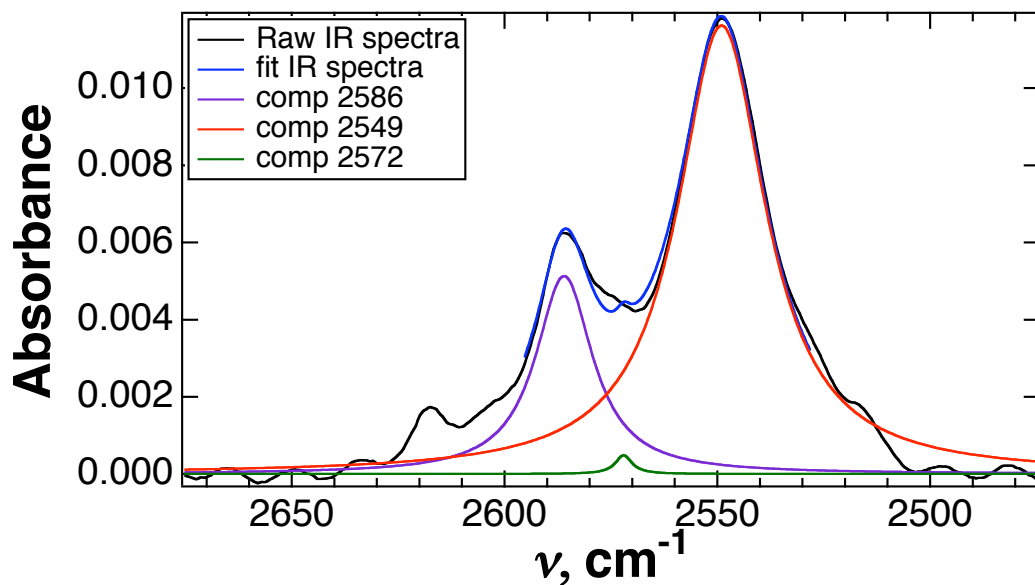**Figure S49**. Fit and deconvolution of the infrared spectrum for the S–H stretching frequency of *p*-thiocresol in 400 mM mesitylene in CCl$_4$ (black). The S–H/π interactions are indicated: thiol association with mesitylene (2563 cm^{-1}, red), *p*-thiocresol self-association (2572 cm^{-1}, green), and the non-interacting *p*-thiocresol thiol (2586 cm^{-1}, purple).

Figure S50. Fit and deconvolution of the infrared spectrum for the S–H stretching frequency of *p*-thiocresol in 800 mM mesitylene in CCl$_4$ (black). The S–H/π interactions are indicated: thiol association with mesitylene (2563 cm^{-1}, red), *p*-thiocresol self-association (2572 cm^{-1}, green), and the non-interacting *p*-thiocresol thiol (2586 cm^{-1}, purple).

Figure S51. Fit and deconvolution of the infrared spectrum for the S–H stretching frequency of *p*-thiocresol in 1600 mM mesitylene in CCl$_4$ (black). The S–H/π interactions are indicated: thiol association with mesitylene (2563 cm^{-1}, red), *p*-thiocresol self-association (2572 cm^{-1}, green), and the non-interacting *p*-thiocresol thiol (2586 cm^{-1}, purple).

Figure S52. Fit and deconvolution of the infrared spectrum for the S–H stretching frequency of *p*-thiocresol in 3200 mM mesitylene in CCl$_4$ (black). The S–H/π interactions are indicated: thiol association with mesitylene (2563 cm^{-1}, red), *p*-thiocresol self-association (2572 cm^{-1}, green), and the non-interacting *p*-thiocresol thiol (2586 cm^{-1}, purple).

**Titration of *p*-thiocresol with 1-methylindole**
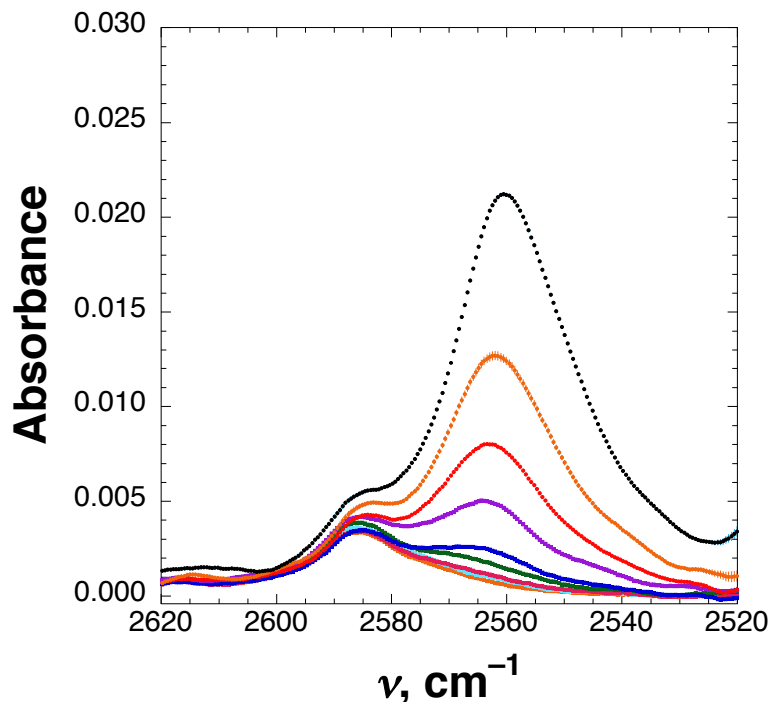
Figure S53. Infrared spectroscopy of the S–H stretching frequency of *p*-thiocresol (55 mM) in the presence of different concentrations of 1-methylindole in CCl$_4$ (12.5 mM (magenta), 25 mM (cyan), 50 mM (red), 100 mM (dark green), 200 mM (blue), 400 mM (purple), 800 mM (green), 1600 mM (orange), and 3200 mM (black)). The peak at 2586 cm^{-1} corresponds to the non-interacting S–H stretching frequency of *p*-thiocresol. The peak at 2561 cm^{-1} corresponds to the S–H stretching frequency for the thiol hydrogen interacting with 1-methylindole via an S–H/π interaction. The peak at 2561 cm^{-1} increases in intensity with increasing 1-methylindole concentration, consistent with increased binding of the aromatic donor to the thiol hydrogen of *p*-thiocresol via an S–H/π interaction. The shoulder at 2572 cm^{-1} is due to the S–H stretching of *p*-thiocresol self-association. Error bars indicate standard error.

Each of the IR spectra was fit with a three-component Lorentzian distribution function with the general formula

$$Y = Y_0 + \sum_{n=1}^{3} \frac{A_n}{(x - x_n)^2 + B_n}$$

where Y_0 is the offset in y-axis, A_n and B_n are maximum intensity and width of the distribution around the peak position at x_n. The x_n was fixed at 2561, 2572, and 2586 cm^{-1} for the interacting peak with the donor (1-methylindole), for the self-association of *p*-thiocresol, and for the non-interacting thiol peak, respectively.

Figure S54. Fit and deconvolution of the infrared spectrum for the S–H stretching frequency of *p*-thiocresol in 12.5 mM 1-methylindole in CCl_4 (black). The S–H/π interactions are indicated: thiol association with 1-methylindole (2561 cm^{-1}, red), *p*-thiocresol self-association (2572 cm^{-1}, green), and the non-interacting *p*-thiocresol thiol (2586 cm^{-1}, purple).
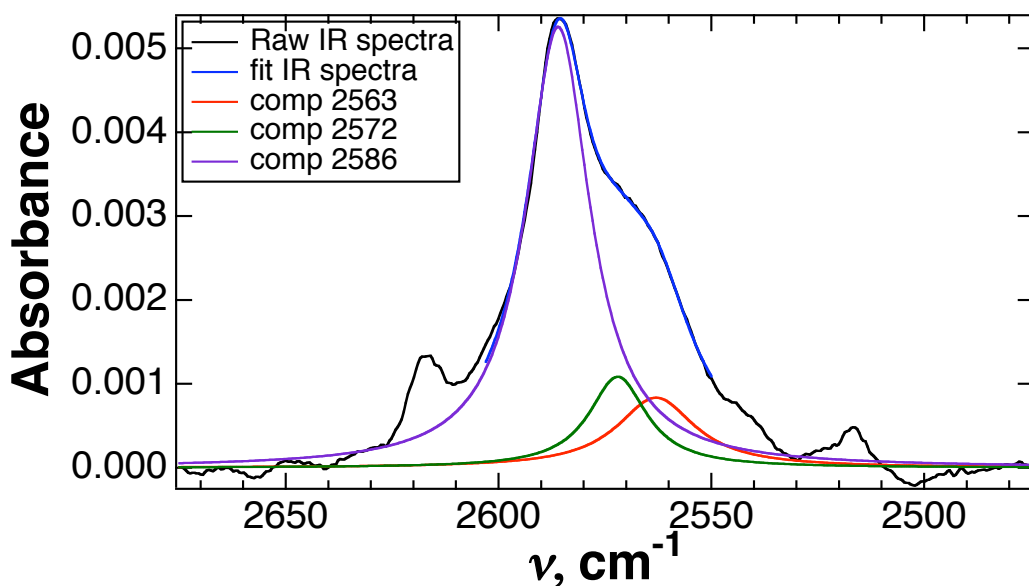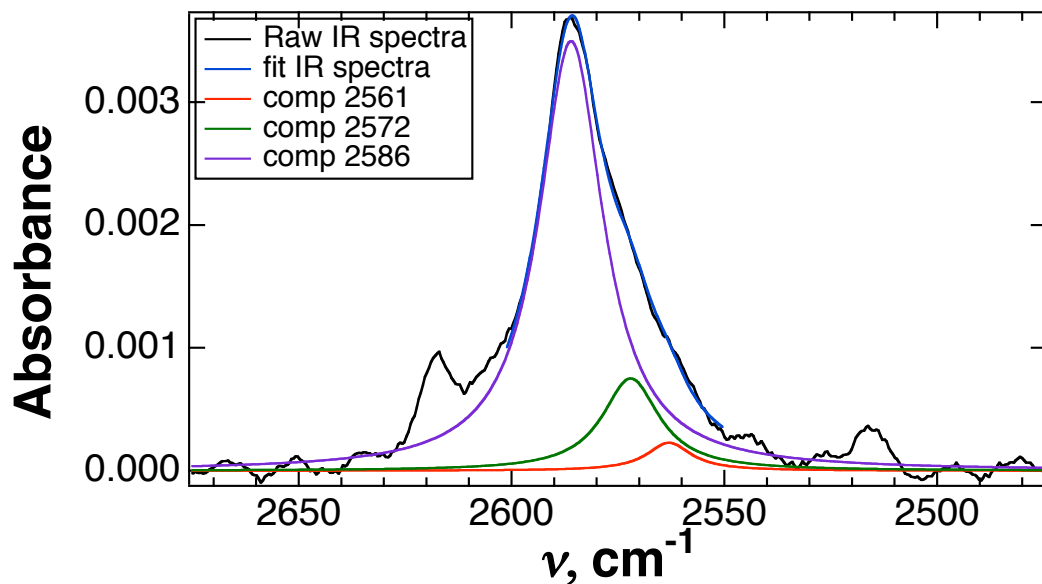

Figure S55. Fit and deconvolution of the infrared spectrum for the S–H stretching frequency of *p*-thiocresol in 25 mM 1-methylindole in CCl_4 (black). The S–H/π interactions are indicated: thiol association with 1-methylindole (2561 cm^{-1}, red), *p*-thiocresol self-association (2572 cm^{-1}, green), and the non-interacting *p*-thiocresol thiol (2586 cm^{-1}, purple).
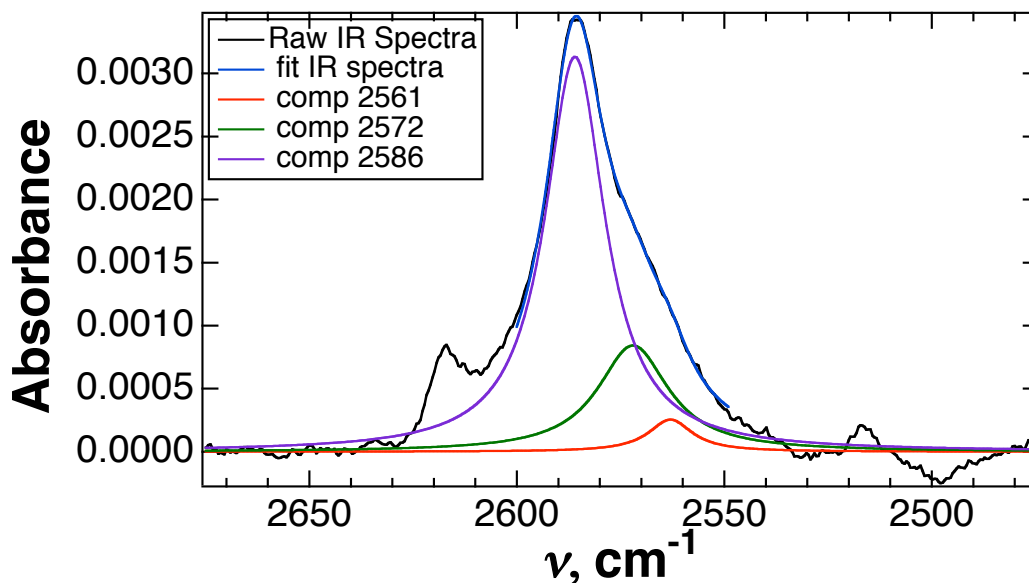
Figure S56. Fit and deconvolution of the infrared spectrum for the S–H stretching frequency of *p*-thiocresol in 50 mM 1-methylindole in CCl_4 (black). The S–H/π interactions are indicated: thiol association with 1-methylindole (2561 cm^{-1}, red), *p*-thiocresol self-association (2572 cm^{-1}, green), and the non-interacting *p*-thiocresol thiol (2586 cm^{-1}, purple).
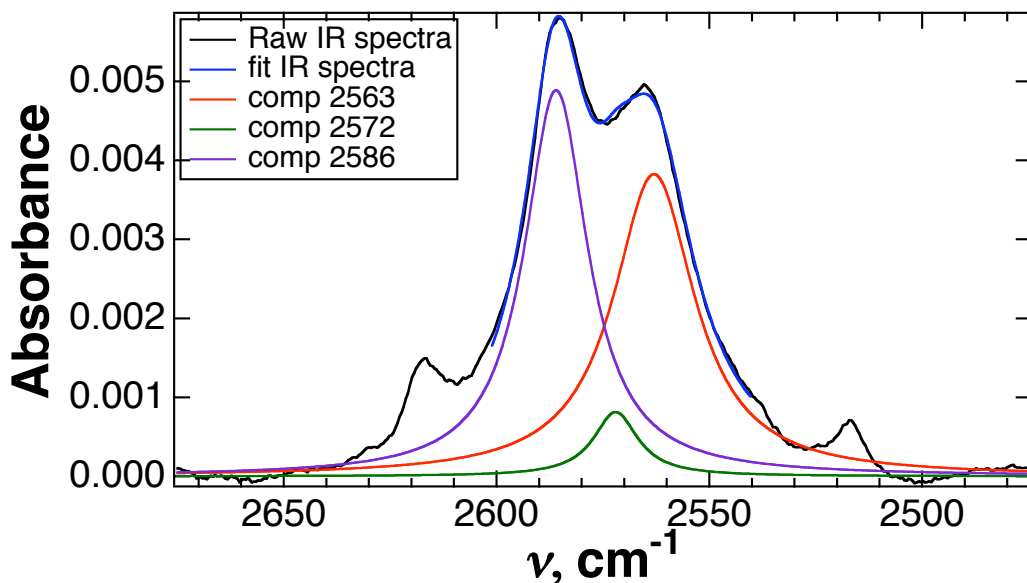

Figure S57. Fit and deconvolution of the infrared spectrum for the S–H stretching frequency of *p*-thiocresol in 100 mM 1-methylindole in CCl_4 (black). The S–H/π interactions are indicated: thiol association with 1-methylindole (2561 cm^{-1}, red), *p*-thiocresol self-association (2572 cm^{-1}, green), and the non-interacting *p*-thiocresol thiol (2586 cm^{-1}, purple).
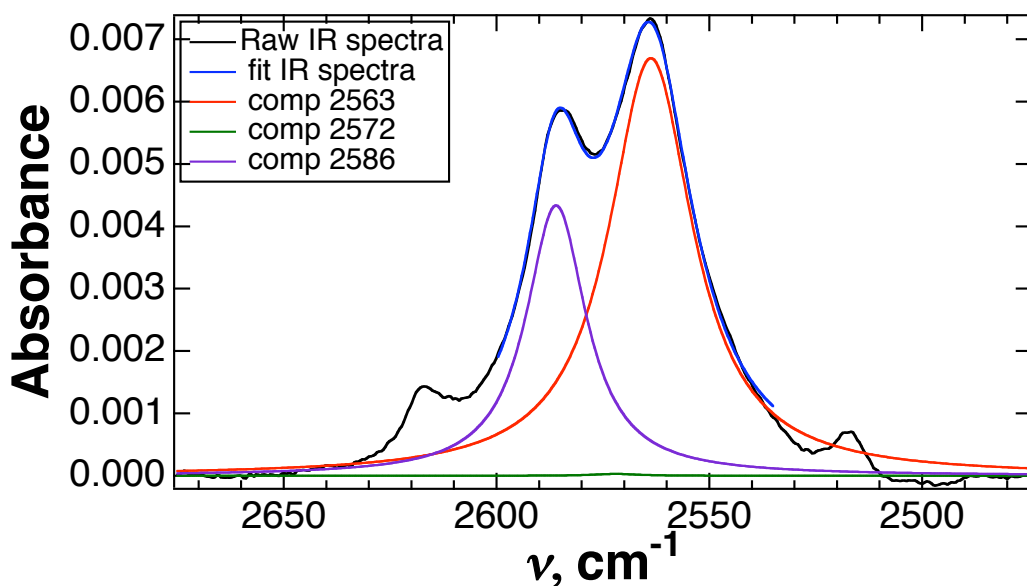
Figure S58. Fit and deconvolution of the infrared spectrum for the S–H stretching frequency of *p*-thiocresol in 200 mM 1-methylindole in CCl$_4$ (black). The S–H/π interactions are indicated: thiol association with 1-methylindole (2561 cm^{-1}, red), *p*-thiocresol self-association (2572 cm^{-1}, green), and the non-interacting *p*-thiocresol thiol (2586 cm^{-1}, purple).
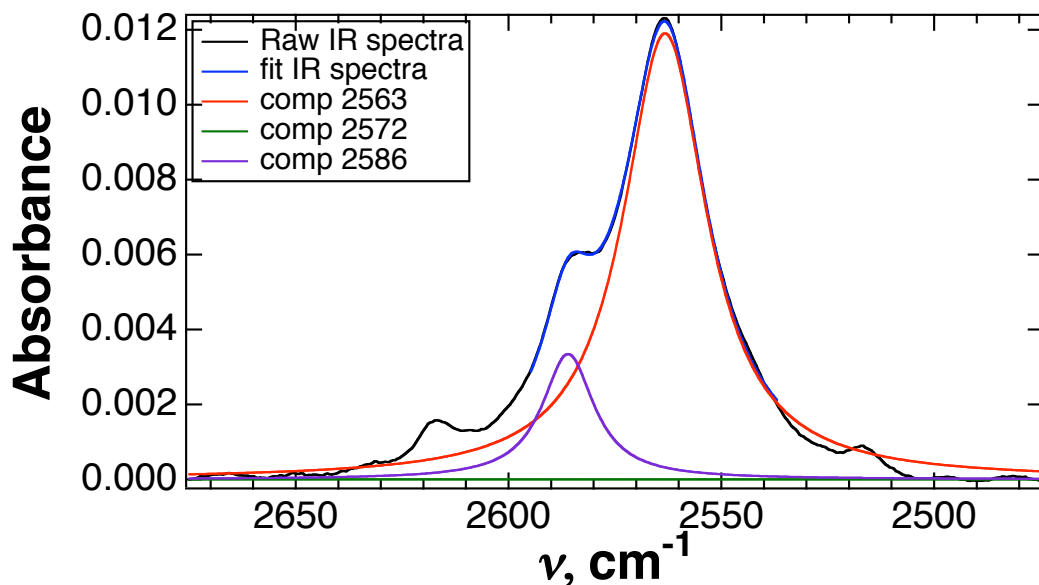

Figure S59. Fit and deconvolution of the infrared spectrum for the S–H stretching frequency of *p*-thiocresol in 400 mM 1-methylindole in CCl$_4$ (black). The S–H/π interactions are indicated: thiol association with 1-methylindole (2561 cm^{-1}, red), *p*-thiocresol self-association (2572 cm^{-1}, green), and the non-interacting *p*-thiocresol thiol (2586 cm^{-1}, purple).
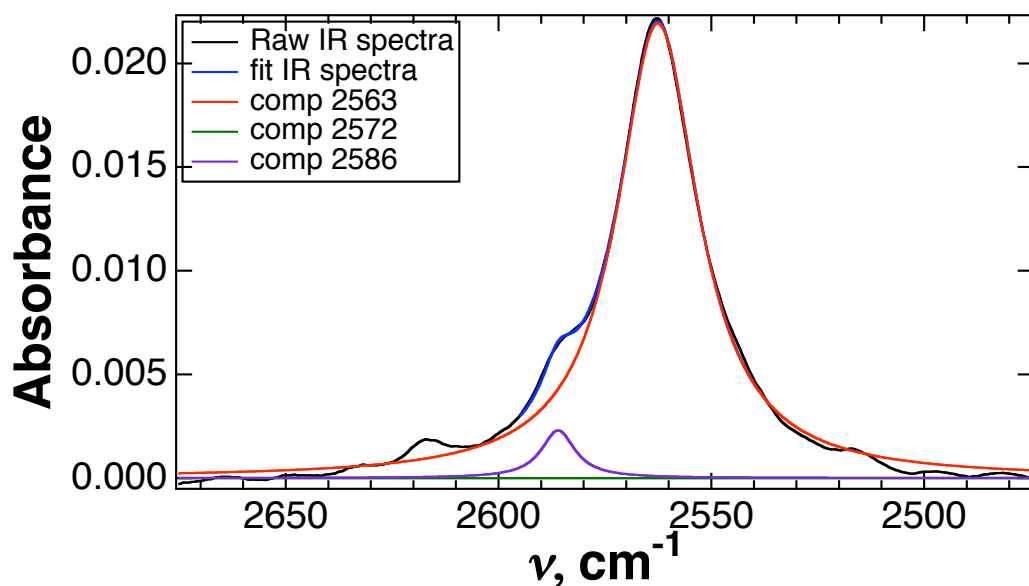
Figure S60. Fit and deconvolution of the infrared spectrum for the S–H stretching frequency of *p*-thiocresol in 800 mM 1-methylindole in CCl_4 (black). The S–H/π interactions are indicated: thiol association with 1-methylindole (2561 cm^{-1}, red), *p*-thiocresol self-association (2572 cm^{-1}, green), and the non-interacting *p*-thiocresol thiol (2586 cm^{-1}, purple).

Figure S61. Fit and deconvolution of the infrared spectrum for the S–H stretching frequency of *p*-thiocresol in 1600 mM 1-methylindole in CCl_4 (black). The S–H/π interactions are indicated: thiol association with 1-methylindole (2561 cm^{-1}, red), *p*-thiocresol self-association (2572 cm^{-1}, green), and the non-interacting *p*-thiocresol thiol (2586 cm^{-1}, purple).

Figure S62. Fit and deconvolution of the infrared spectrum for the S–H stretching frequency of *p*-thiocresol in 3200 mM 1-methylindole in CCl$_4$ (black). The S–H/π interactions are indicated: thiol association with 1-methylindole (2561 cm^{-1}, red), *p*-thiocresol self-association (2572 cm^{-1}, green), and the non-interacting *p*-thiocresol thiol (2586 cm^{-1}, purple).

Titration of *p*-thiocresol with toluene
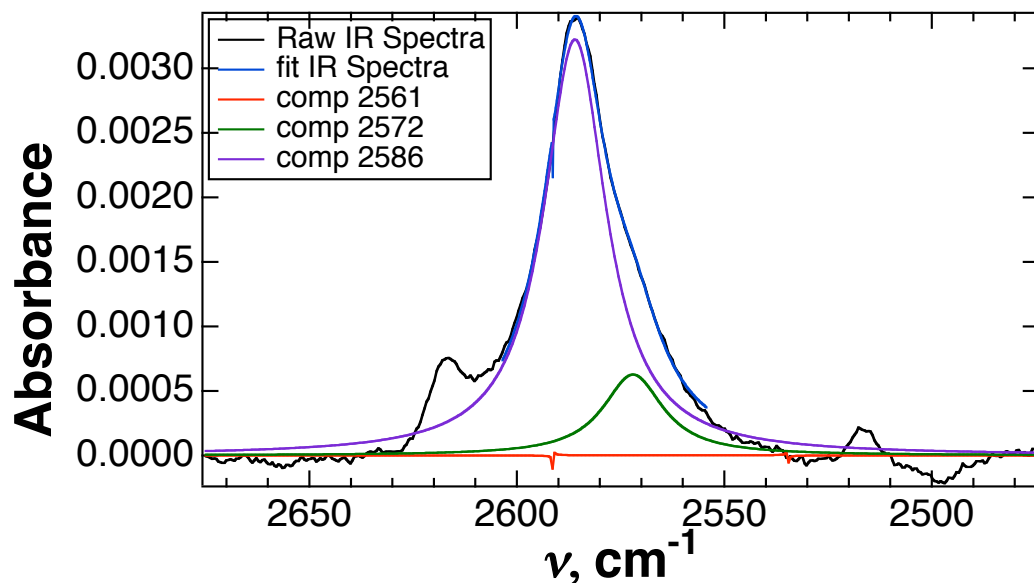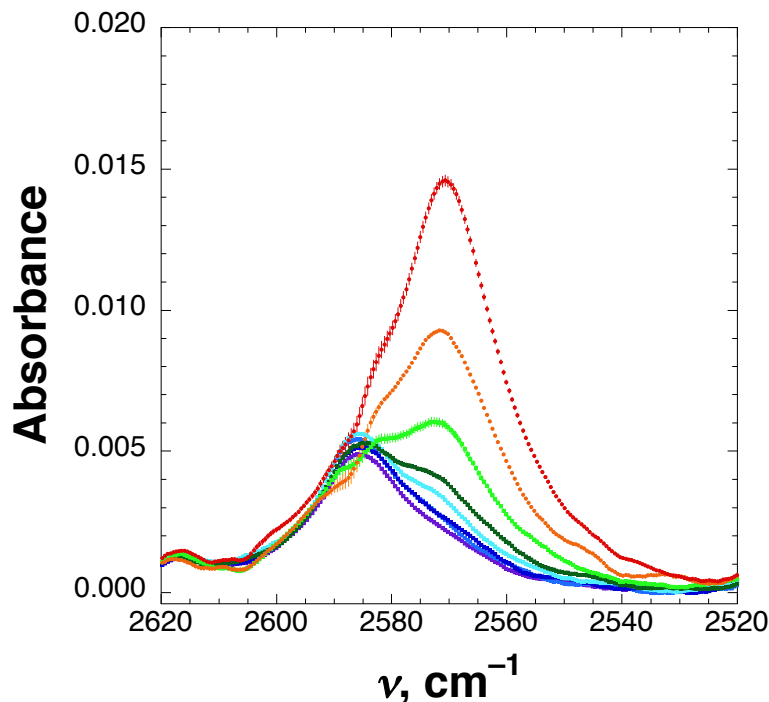

Figure S63. Infrared spectroscopy of the S–H stretching frequency of *p*-thiocresol (55 mM) in the presence of different concentrations of toluene in CCl_4 (25 mM (purple), 50 mM (light blue), 100 mM (blue), 200 mM (cyan), 400 mM (dark green), 800 mM (green), 1600 mM (orange), and 3200 mM (red)). The peak at 2586 cm^{-1} corresponds to the non-interacting S–H stretching frequency of *p*-thiocresol. The peak at 2571 cm^{-1} corresponds to the S–H stretching frequency for the thiol hydrogen interacting with toluene via an S–H/π interaction. The peak at 2571 cm^{-1} increases in intensity with increasing toluene concentration, consistent with increased binding of the aromatic donor to the thiol hydrogen of *p*-thiocresol via an S–H/π interaction. Due to overlap of the S–H stretching frequency of *p*-thiocresol interacting with toluene (2571 cm^{-1}) S–H stretching of *p*-thiocresol due to self-association (2572 cm^{-1}) is not resolved separately. Error bars indicate standard error.

Each of the IR spectra was fit with a two-component Lorentzian distribution function with the general formula

$$Y = Y_0 + \sum_{n=1}^{2} \frac{A_n}{(x - x_n)^2 + B_n}$$

where Y_0 is the offset in y-axis and A_n and B_n are maximum intensity and width of the distribution around the peak position at x_n. x_n was fixed at 2571 and 2586 cm^{-1} for the interacting peak with the donor (toluene), and for the non-interacting thiol peak, respectively.
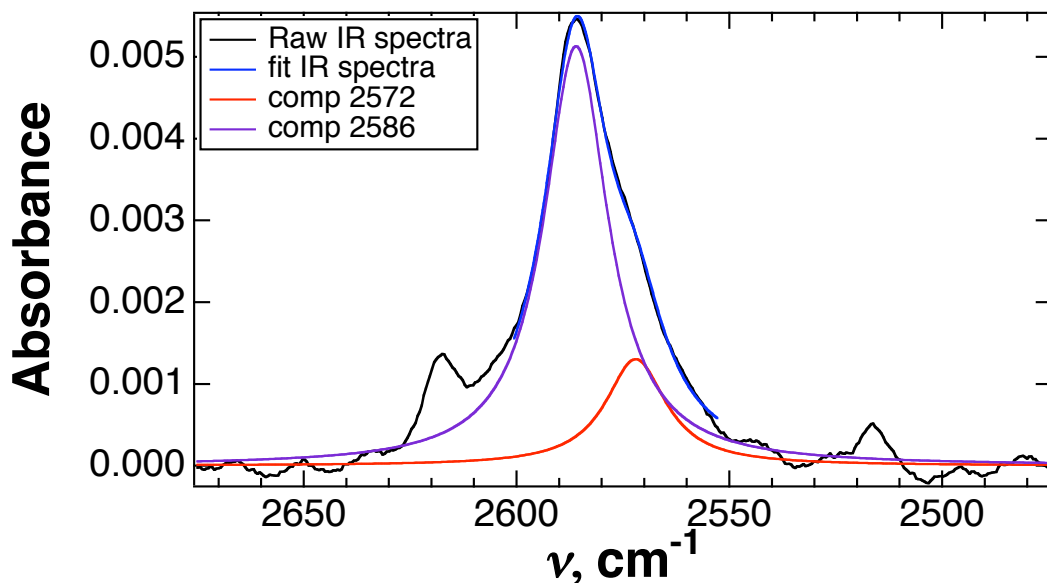
Figure S64. Fit and deconvolution of the infrared spectrum for the S–H stretching frequency of *p*-thiocresol in 50 mM toluene in CCl$_4$ (black). The S–H/π interactions are indicated: thiol association with toluene (2571 cm^{-1}, red) and the non-interacting *p*-thiocresol thiol (2586 cm^{-1}, purple).
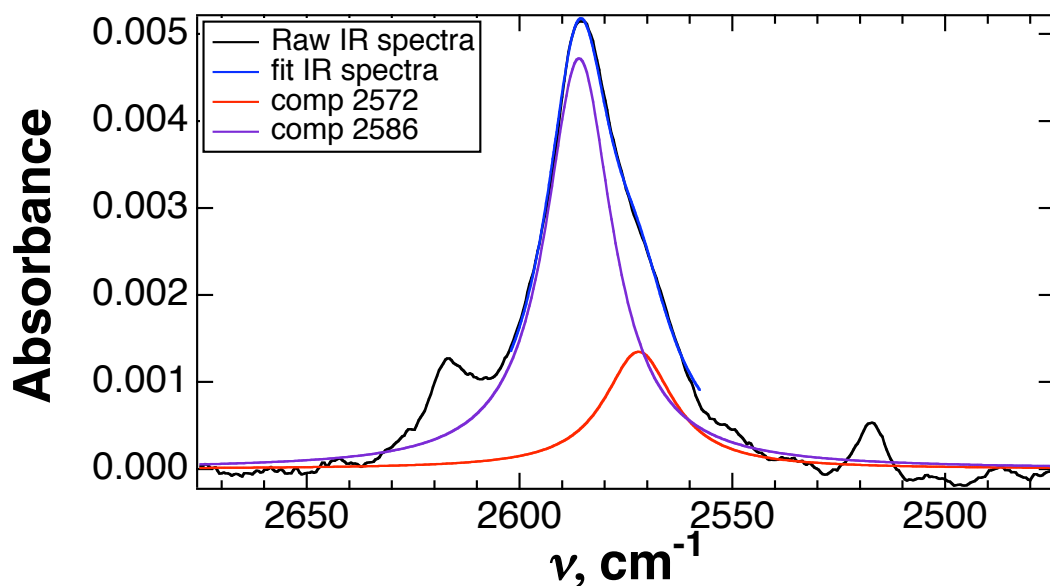
Figure S65. Fit and deconvolution of the infrared spectrum for the S–H stretching frequency of *p*-thiocresol in 100 mM toluene in CCl$_4$ (black). The S–H/π interactions are indicated: thiol association with toluene (2571 cm^{-1}, red) and the non-interacting *p*-thiocresol thiol (2586 cm^{-1}, purple).
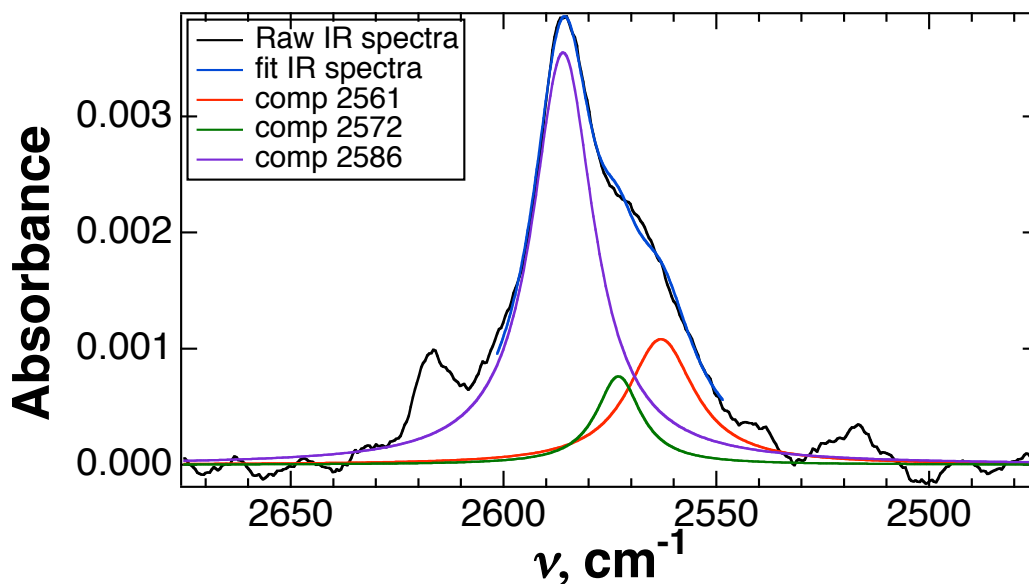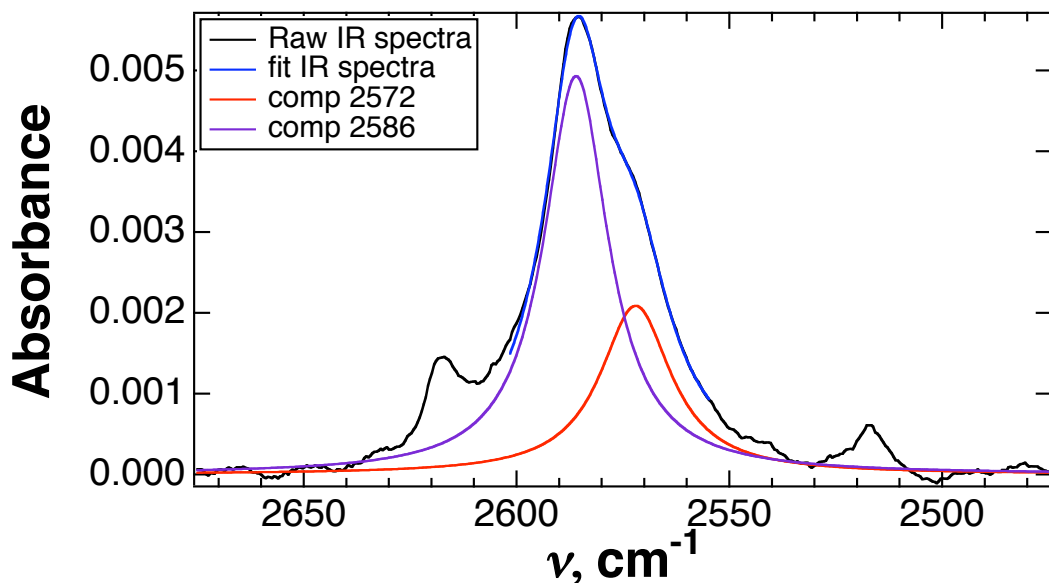
Figure S66. Fit and deconvolution of the infrared spectrum for the S–H stretching frequency of *p*-thiocresol in 200 mM toluene in CCl_4 (black). The S–H/π interactions are indicated: thiol association with toluene (2571 cm^{-1}, red) and the non-interacting *p*-thiocresol thiol (2586 cm^{-1}, purple).
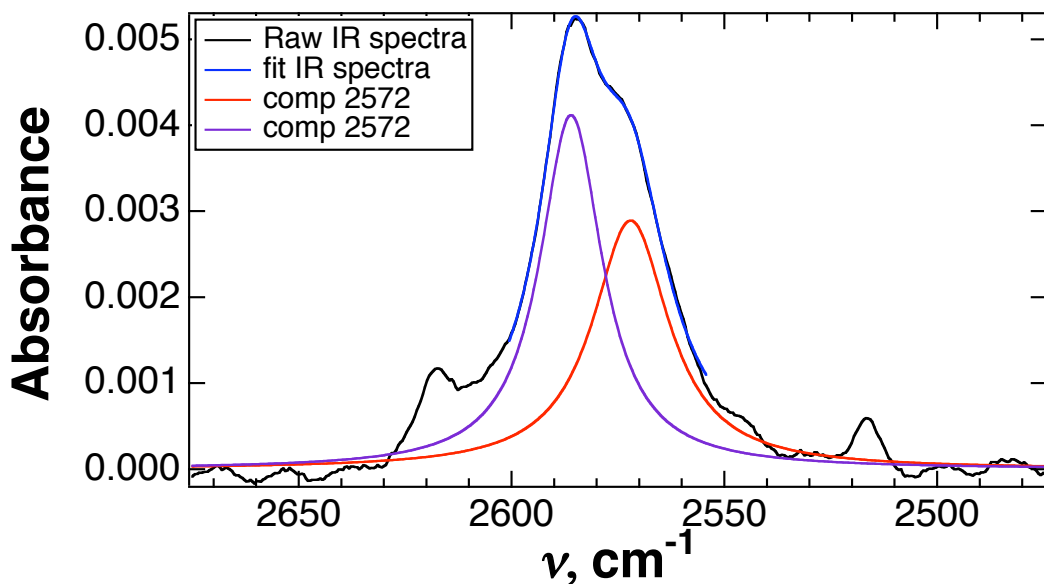
Figure S67. Fit and deconvolution of the infrared spectrum for the S–H stretching frequency of *p*-thiocresol in 400 mM toluene in CCl_4 (black). The S–H/π interactions are indicated: thiol association with toluene (2571 cm^{-1}, red) and the non-interacting *p*-thiocresol thiol (2586 cm^{-1}, purple).
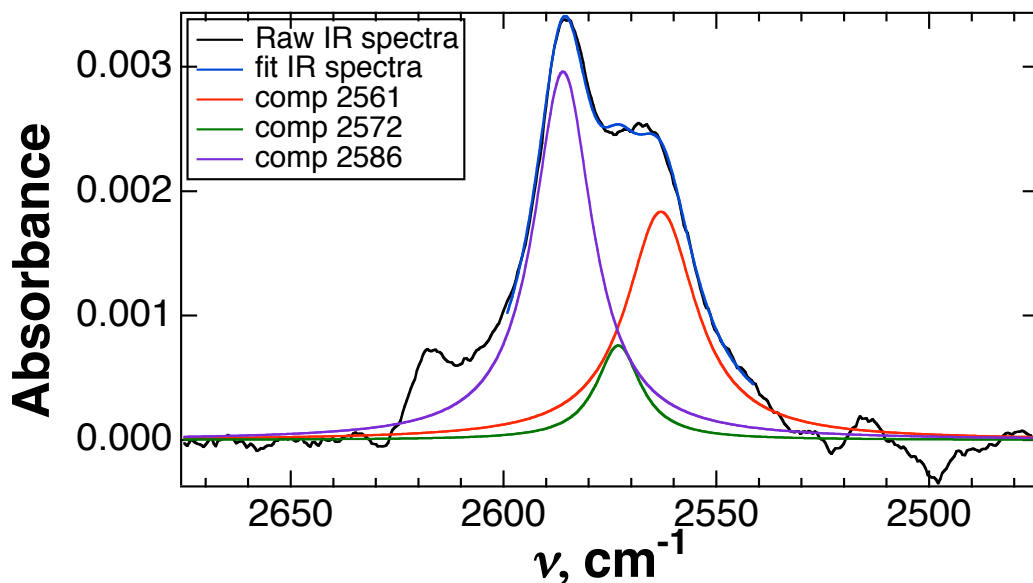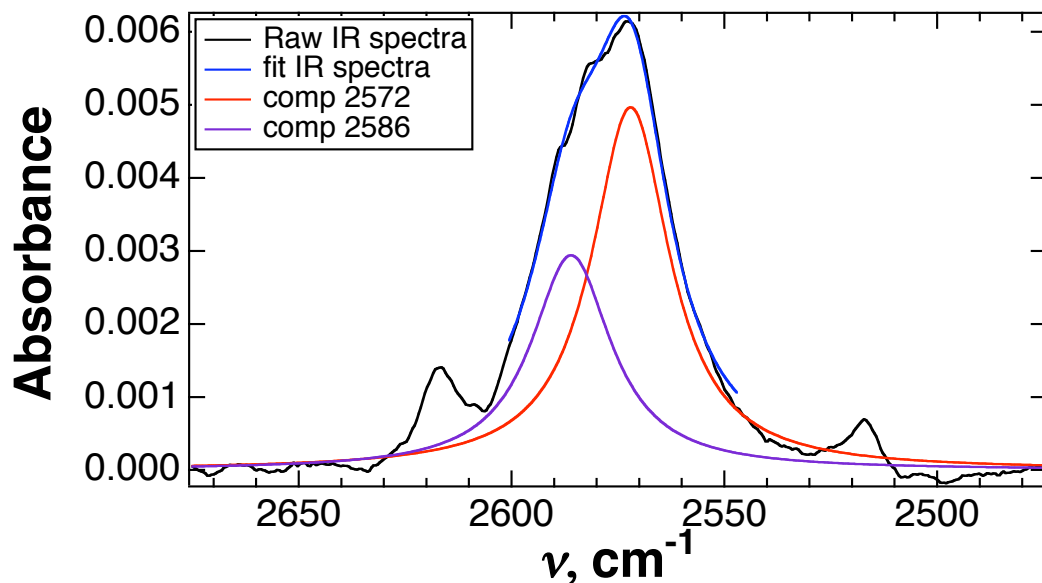
Figure S68. Fit and deconvolution of the infrared spectrum for the S–H stretching frequency of *p*-thiocresol in 800 mM toluene in CCl_4 (black). The S–H/π interactions are indicated: thiol association with toluene (2571 cm^{-1}, red) and the non-interacting *p*-thiocresol thiol (2586 cm^{-1}, purple).
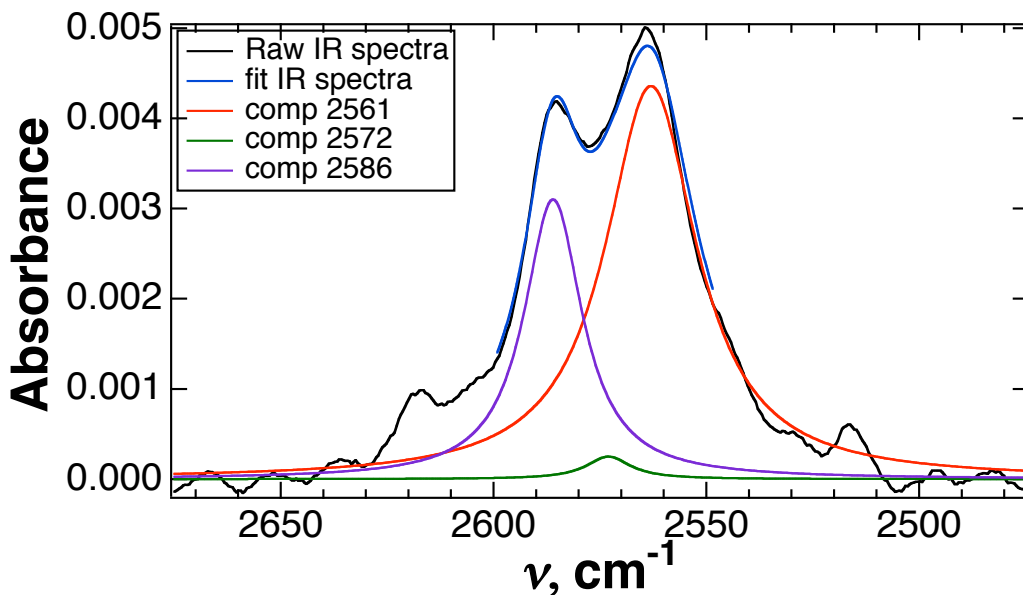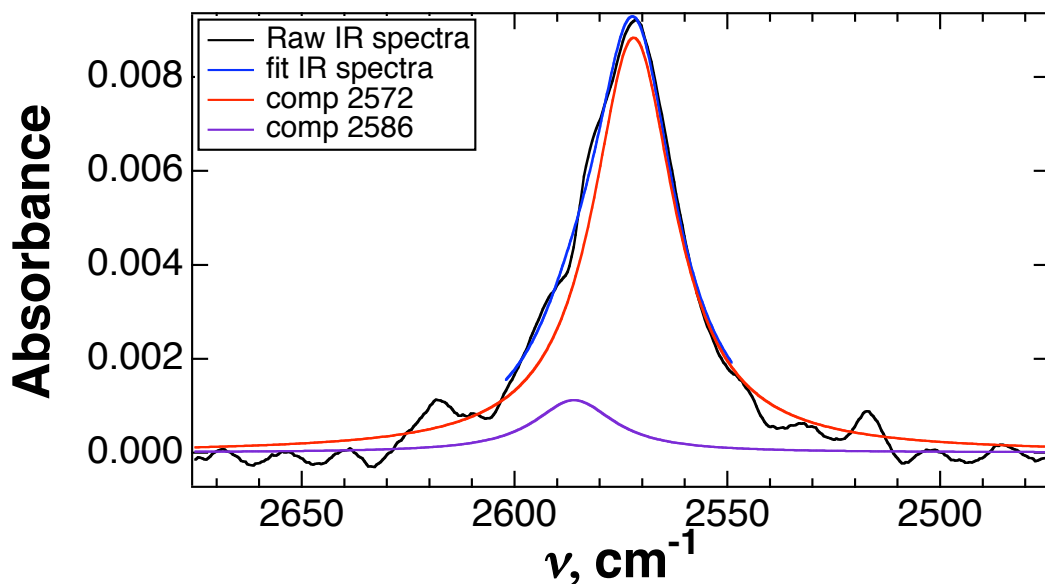

Figure S69. Fit and deconvolution of the infrared spectrum for the S–H stretching frequency of *p*-thiocresol in 1600 mM toluene in CCl_4 (black). The S–H/π interactions are indicated: thiol association with toluene (2571 cm^{-1}, red) and the non-interacting *p*-thiocresol thiol (2586 cm^{-1}, purple).
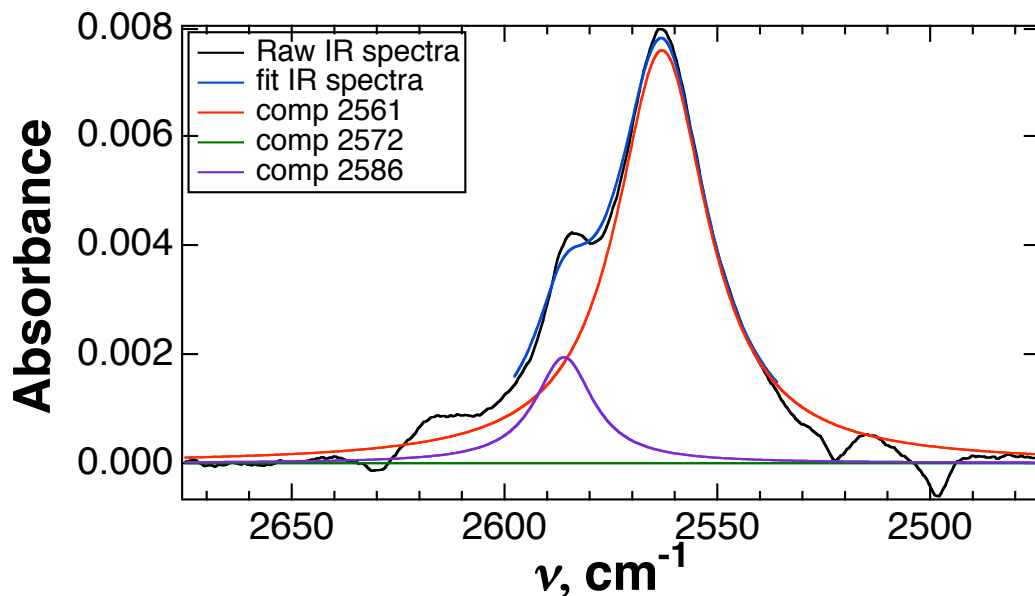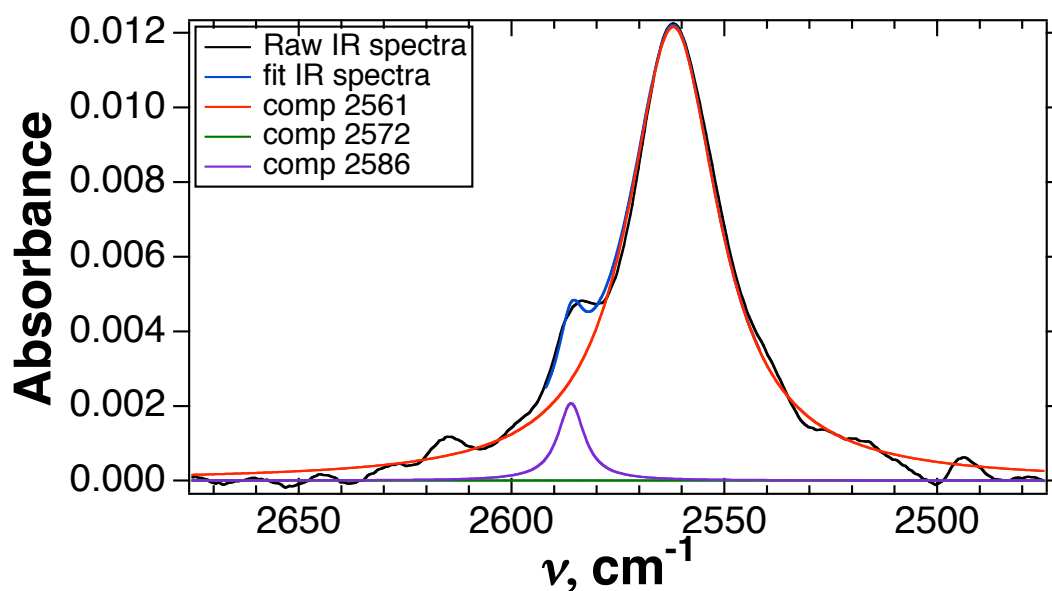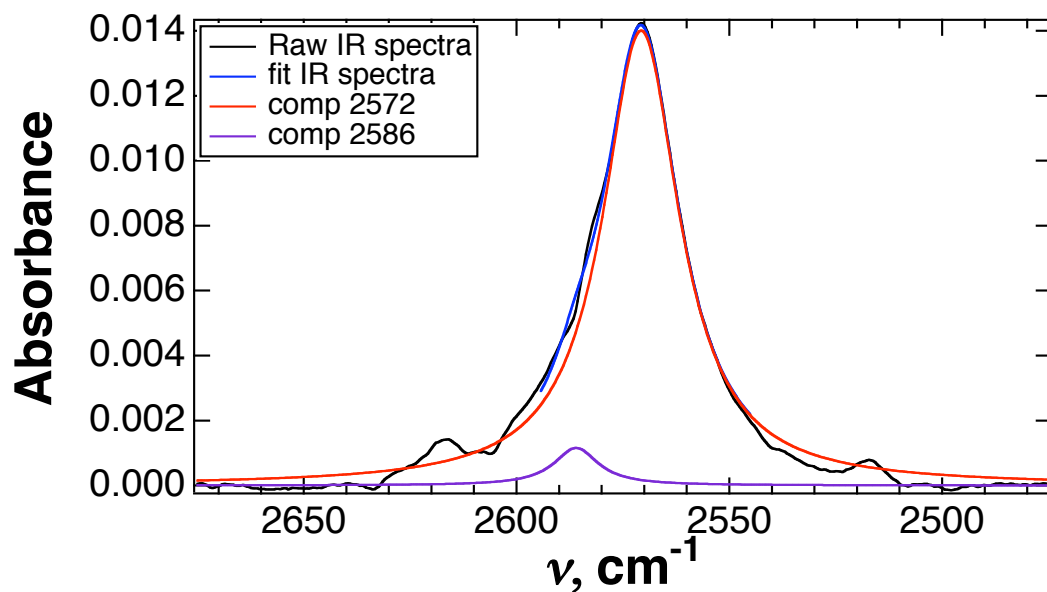
Figure S70. Fit and deconvolution of the infrared spectrum for the S–H stretching frequency of *p*-thiocresol in 3200 mM toluene in CCl$_4$ (black). The S–H/π interactions are indicated: thiol association with toluene (2571 cm^{-1}, red) and the non-interacting *p*-thiocresol thiol (2586 cm^{-1}, purple).

Titration of *p*-thiocresol with *m*-dichlorobenzene
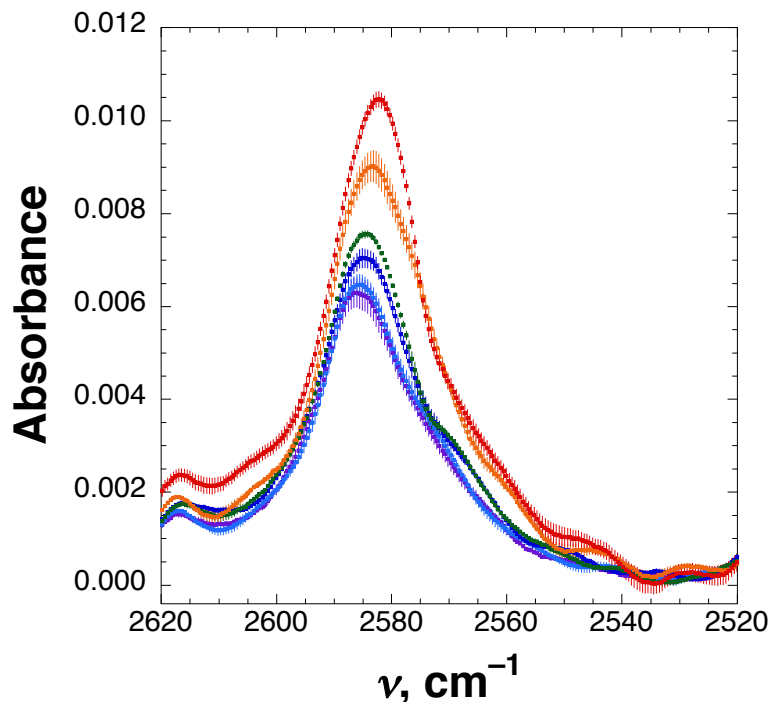
Figure S71. Infrared spectroscopy of the S–H stretching frequency of *p*-thiocresol (55 mM) in the presence of different concentrations of *m*-dichlorobenzene in CCl_4 (50 mM (magenta), 400 mM (light blue), 800 mM (blue), 1600 mM (dark green), 3200 mM (orange), and 4800 mM (red). The peak at 2586 cm^{-1} corresponds to the non-interacting S–H stretching frequency of *p*-thiocresol. The peak at 2581 cm^{-1} corresponds to the S–H stretching frequency for the thiol hydrogen interacting with *m*-dichlorobenzene via an S–H/π interaction. The peak at 2581 cm^{-1} increases in intensity with increasing 1-methylindole concentration, consistent with increased binding of the aromatic donor to the thiol hydrogen of *p*-thiocresol via an S–H/π interaction. The shoulder at 2572 cm^{-1} is due to the S–H stretching of *p*-thiocresol self-association. Error bars indicate standard error.

Each of the IR spectra was fit with a three-component Lorentzian distribution function with the general formula

$$Y = Y_0 + \sum_{n=1}^{3} \frac{A_n}{(x - x_n)^2 + B_n}$$

where Y_0 is the offset in y-axis and A_n and B_n are maximum intensity and width of the distribution around the peak position at x_n. x_n was fixed at 2581, 2572, and 2586 cm^{-1} for the interacting peak with the donor (*m*-dichlorobenzene), for the self-association of *p*-thiocresol, and for the non-interacting thiol peak, respectively.
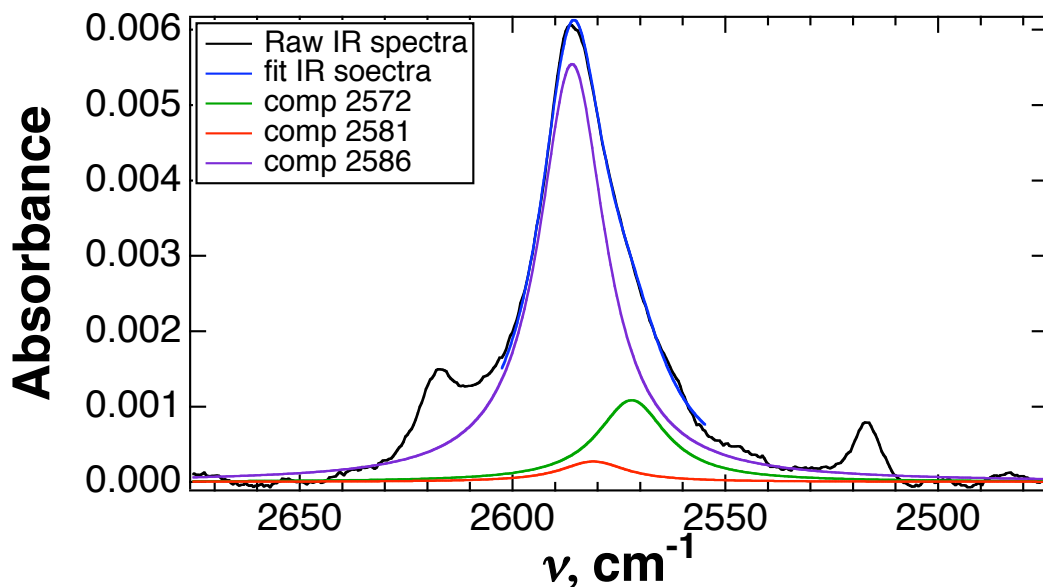
Figure S72. Fit and deconvolution of the infrared spectrum for the S–H stretching frequency of *p*-thiocresol in 50 mM *m*-dichlorobenzene in CCl$_4$ (black). The S–H/π interactions are indicated: thiol association with *m*-dichlorobenzene (2581 cm^{-1}, red), *p*-thiocresol self-association (2572 cm^{-1}, green), and the non-interacting *p*-thiocresol thiol (2586 cm^{-1}, purple).
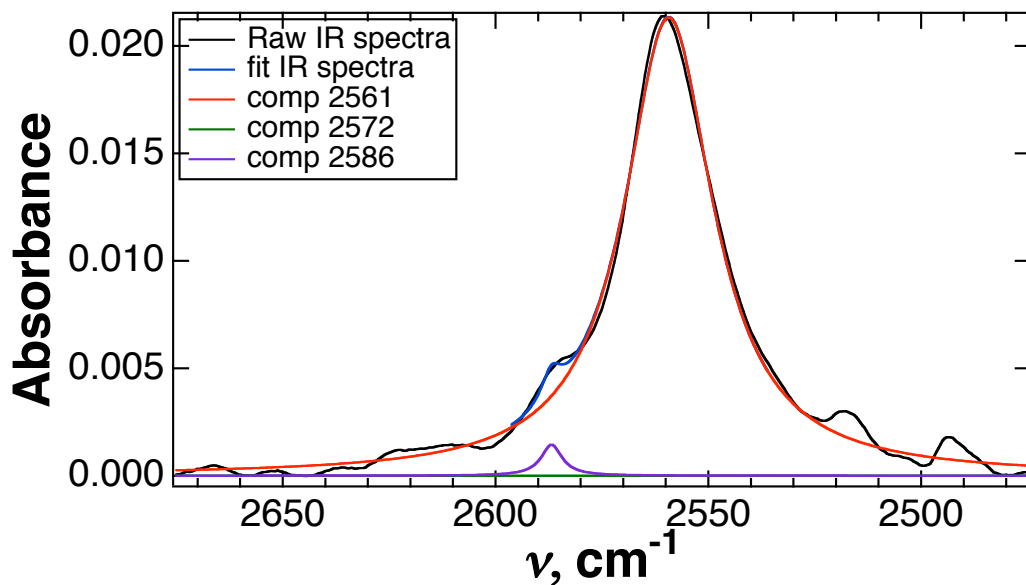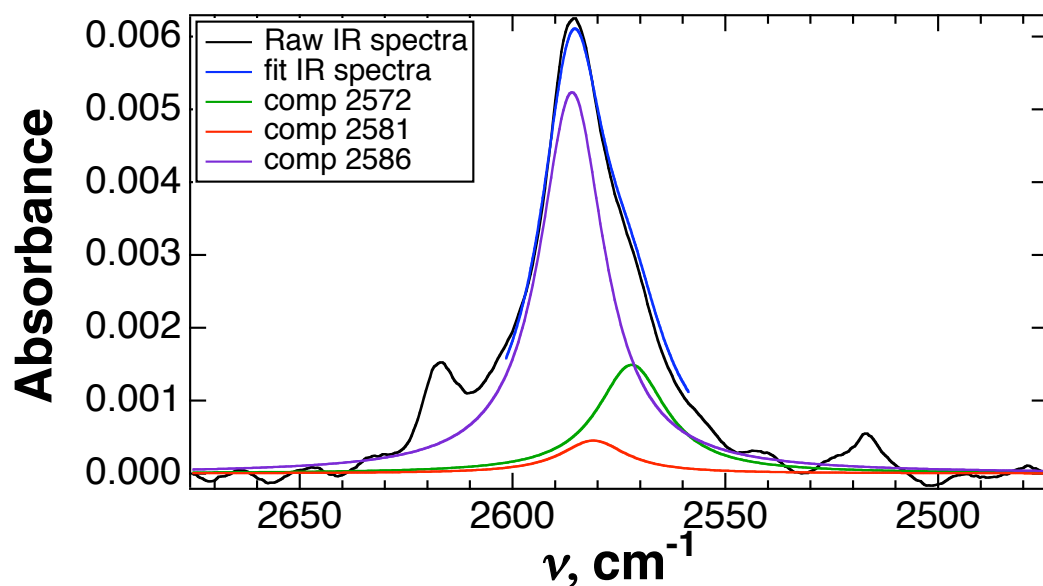

Figure S73. Fit and deconvolution of the infrared spectrum for the S–H stretching frequency of *p*-thiocresol in 400 mM *m*-dichlorobenzene in CCl$_4$ (black). The S–H/π interactions are indicated: thiol association with *m*-dichlorobenzene (2581 cm^{-1}, red), *p*-thiocresol self-association (2572 cm^{-1}, green), and the non-interacting *p*-thiocresol thiol (2586 cm^{-1}, purple).
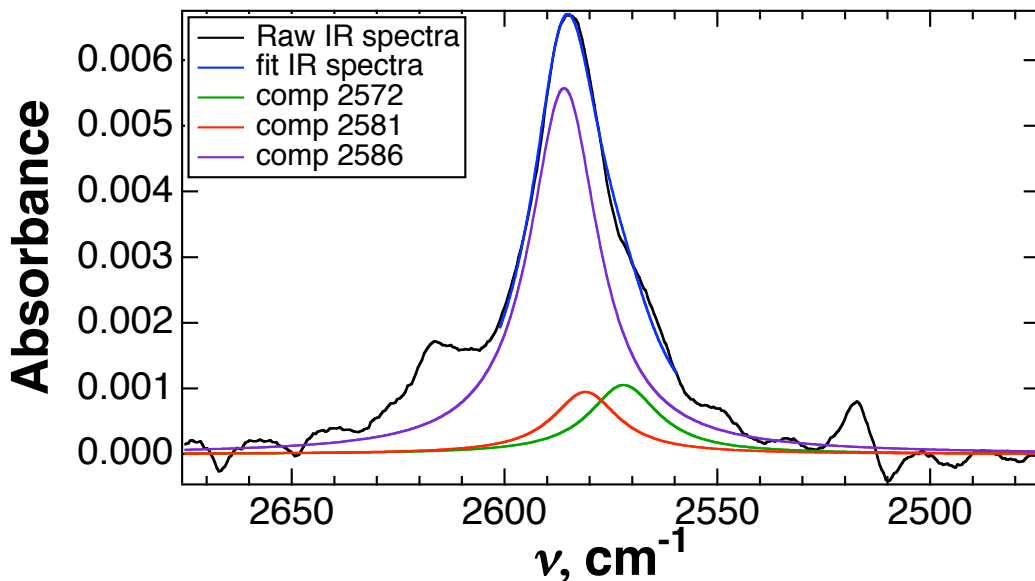
Figure S74. Fit and deconvolution of the infrared spectrum for the S–H stretching frequency of *p*-thiocresol in 800 mM *m*-dichlorobenzene in CCl_4 (black). The S–H/π interactions are indicated: thiol association with *m*-dichlorobenzene (2581 cm^{-1}, red), *p*-thiocresol self-association (2572 cm^{-1}, green), and the non-interacting *p*-thiocresol thiol (2586 cm^{-1}, purple).
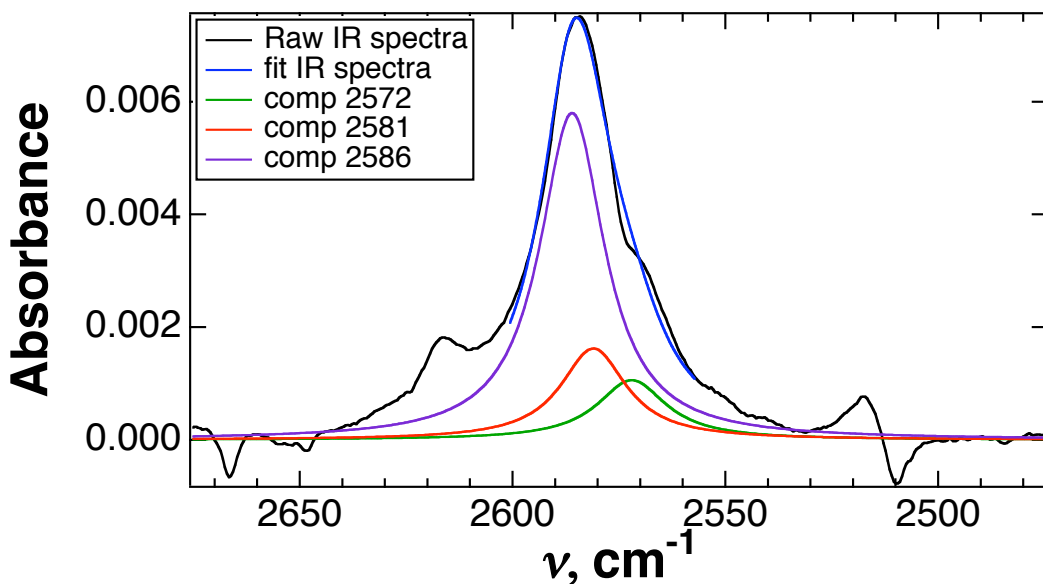
Figure S75. Fit and deconvolution of the infrared spectrum for the S–H stretching frequency of *p*-thiocresol in 1600 mM *m*-dichlorobenzene in CCl_4 (black). The S–H/π interactions are indicated: thiol association with *m*-dichlorobenzene (2581 cm^{-1}, red), *p*-thiocresol self-association (2572 cm^{-1}, green), and the non-interacting *p*-thiocresol thiol (2586 cm^{-1}, purple).
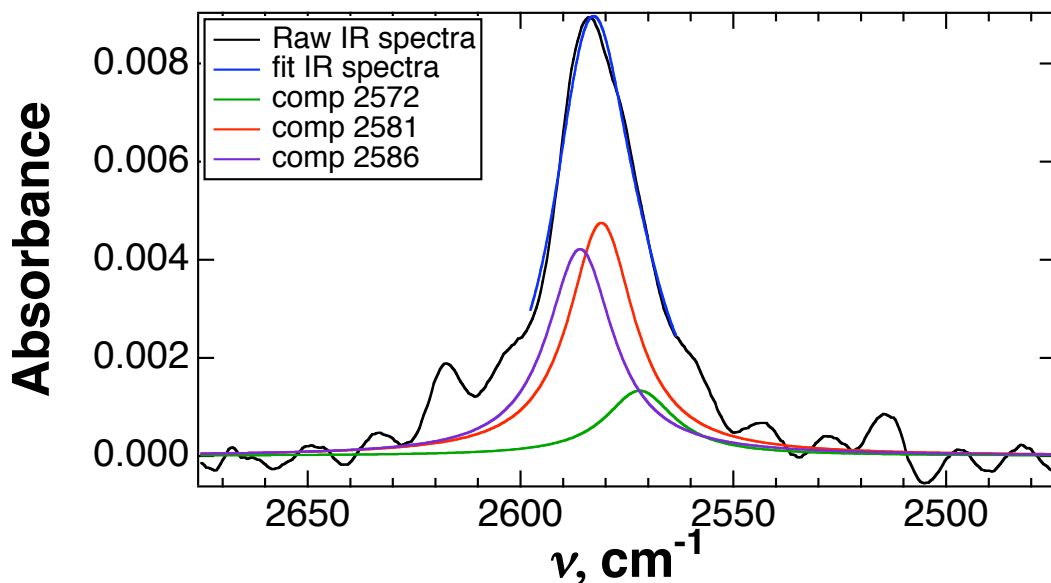
Figure S76. Fit and deconvolution of the infrared spectrum for the S–H stretching frequency of *p*-thiocresol in 3200 mM *m*-dichlorobenzene in CCl_4 (black). The S–H/π interactions are indicated: thiol association with *m*-dichlorobenzene (2581 cm^{-1}, red), *p*-thiocresol self-association (2572 cm^{-1}, green), and the non-interacting *p*-thiocresol thiol (2586 cm^{-1}, purple).
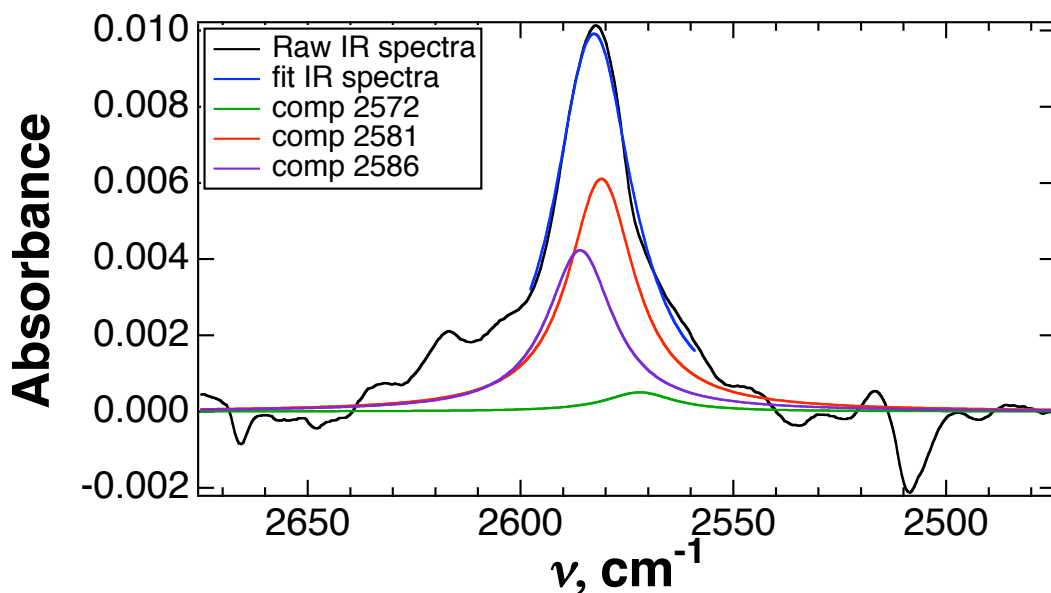
Figure S77. Fit and deconvolution of the infrared spectrum for the S–H stretching frequency of *p*-thiocresol in 4800 mM *m*-dichlorobenzene in CCl_4 (black). The S–H/π interactions are indicated: thiol association with *m*-dichlorobenzene (2581 cm^{-1}, red), *p*-thiocresol self-association (2572 cm^{-1}, green), and the non-interacting *p*-thiocresol thiol (2586 cm^{-1}, purple).

Table S12. Fitting parameters for Lorentzian deconvolution of the observed IR spectra (S–H stretching region) for *p*-thiocresol in the presence of different concentrations of aromatic donors. "Interacting" thiol component refers to the component of the IR spectrum that is due to association of the thiol with the aromatic donor, the "self-association" thiol component refers the component that is due to *p*-thiocresol dimerization, and the "non-interacting" thiol component refers to the component due to free thiol.

	Concentration (mM)	"Interacting" thiol component			"Self-association" thiol component			"Non-interacting" thiol component		
		Intensity (A1)	Peak (x1)	width (B1)	Intensity (A2)	Peak (x2)	width (B2)	Intensity (A3)	peak (x3)	width (B3)
hexamethylbenzene	12.5	0.0021	2549	10.6	0.11823	2572	96.25	0.55481	2586	92.057
	25	0.016186	2549	46.737	0.25841	2572	151.93	0.59644	2586	89.907
	50	0.04442	2549	87.06	0.15144	2572	109.57	0.51967	2586	87.626
	100	0.24852	2549	182.96	0.086763	2572	67.376	0.49961	2586	82.916
	200	0.44963	2549	159.52	0.088938	2572	68.649	0.45995	2586	78.276
	400	0.8612	2549	156.34	0.063471	2572	60.642	0.43246	2586	79.033
	800	1.8355	2549	157.89	0.0027185	2572	5.5905	0.34161	2586	66.562
1-methylindole	12.5	-0.000458	2561	-802.66	0.048668	2572	77.673	0.26903	2586	83.474
	25	0.0090527	2561	39.708	0.0495	2572	65.908	0.2931	2586	83.803
	50	0.010554	2561	41.4	0.090871	2572	107.78	0.24273	2586	77.48
	100	0.087586	2561	99.035	0.065904	2572	78.672	0.26447	2586	76.162
	200	0.14129	2561	96.893	0.14096	2572	142.95	0.18154	2586	66.107
	400	0.57802	2561	132.4	0.019338	2573	40	0.25036	2586	77.989
	800	1.1971	2561	155.91	0	2572	n.a.	0.14562	2586	70
	1600	1.8293	2561	151.25	0	2572	n.a.	0.13504	2586	70
	3200	3.3919	2561	160.96	0	2572	n.a.	0.01939	2586	10.51
mesitylene	25	-0.00010336	2563	6.28	0.18758	2572	148.93	0.40852	2586	85.372
	50	0.020376	2563	41.4	0.079376	2572	65.9	0.44195	2586	87.602
	100	0.11178	2563	128.84	0.075624	2572	68.16	0.44133	2586	86.489
	200	0.23415	2563	147.3	0.066159	2572	68.16	0.38905	2586	82.708
	400	0.51657	2563	135.06	0.032541	2572	40	0.39745	2586	81.274
	800	0.96582	2563	144.24	0.0011836	2572	40	0.31901	2586	73.577
	1600	1.6987	2563	142.71	0	2572	n.a.	0.18227	2586	54.455
	3200	2.7458	2563	135.54	0	2572	n.a.	0.06639	2586	28.776

Table S12 cont.

	Concentration (mM)	"Interacting" thiol component Intensity (A1)	Peak (x1)	width (B1)	"Self-association" thiol component Intensity (A2)	Peak (x2)	width (B2)	"Non-interacting" thiol component Intensity (A3)	peak (x3)	width (B3)
toluene	25	0.084829	2571	88.95	n.a.	n.a.	n.a.	0.41018	2586	89.181
	50	0.098218	2571	79.545	n.a.	n.a.	n.a.	0.42377	2586	85.446
	100	0.14115	2571	102.17	n.a.	n.a.	n.a.	0.42656	2586	91.388
	200	0.19954	2571	96.791	n.a.	n.a.	n.a.	0.39699	2586	79.945
	400	0.35317	2571	119.53	n.a.	n.a.	n.a.	0.35963	2586	83.414
	800	0.63168	2571	124.24	n.a.	n.a.	n.a.	0.34296	2586	106.63
	1600	1.257	2571	142.85	n.a.	n.a.	n.a.	0.13271	2586	77.86
	3200	1.6874	2570.6	117.82	n.a.	n.a.	n.a.	0.067063	2586	40
m-dichlorobenzene	50	0.024254	2581	88.39	0.12686	2572	97	0.56101	2586	88.521
	400	0.043575	2581	88.39	0.1447	2572	97	0.51153	2586	84.052
	800	0.12037	2581	88.39	0.13904	2572	97	0.47225	2586	81.547
	1600	0.19255	2581	88.39	0.10948	2572	97	0.4068	2586	73.315
	3200	0.42045	2581	88.39	0.1579	2572	97	0.37081	2586	75.543
	4800	0.54123	2581	88.39	0.099708	2572	97	0.41319	2586	90

Determination of the dissociation constants for *p*-thiocresol•aromatic donor complexes

The combined total area under the curve for the self-associated and non-associated *p*-thiocresol signals is expected to approach zero at limiting high concentration of the aromatic donor, following a 1:1 binding with the dissociation constant (K_d) according to the scheme shown below:

SH   **D$_L$**

p*-thiocresol**   **aromatic donor**   ***complex formation
                                              via S–H/π interaction
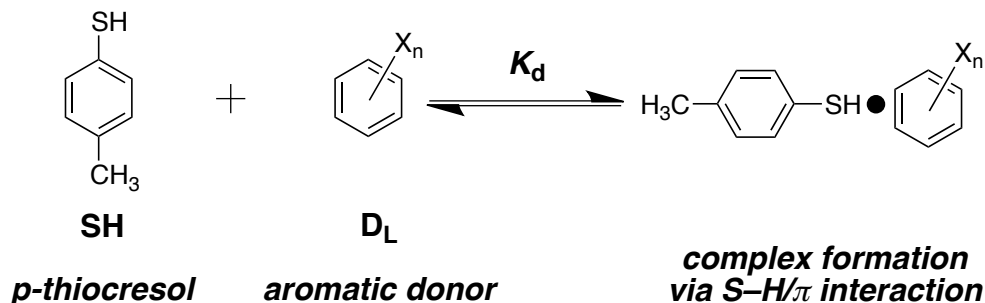
The total area of the observed components then varies according to the 1:1 binding equation as

$$Y = \frac{Y_0}{SH_t} \times \frac{\left[-(D_L + K_d - SH_t) + \sqrt{(D_L + K_d - SH_t)^2 + 4(SH_t)(K_d)}\right]}{2}$$

[Equation S2]

where D_L = concentration of the aromatic donor
       SH_t = total concentration of *p*-thiocresol
       K_d = dissociation constant
       Y_0 = signal in absence of donor.
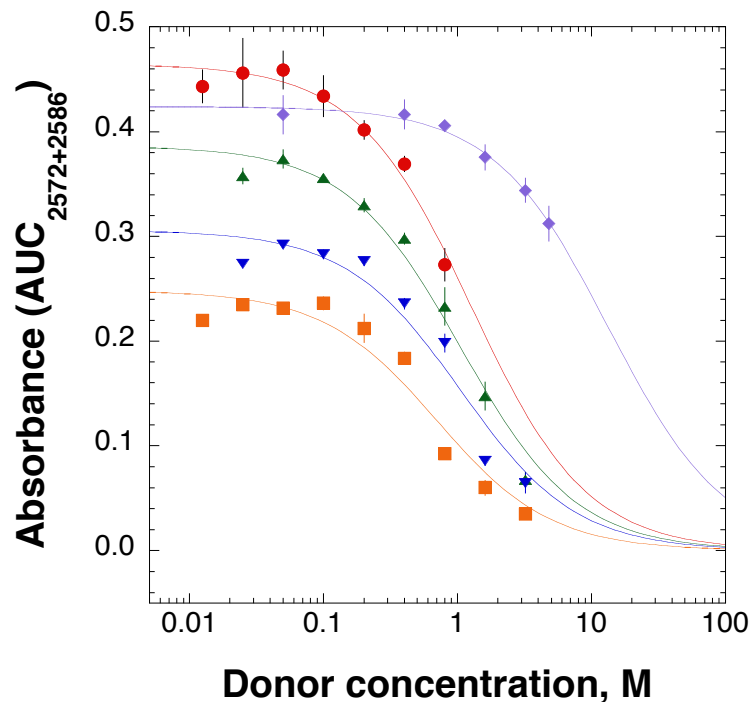
Figure S78. Determination of the dissociation constant for the complex of each interacting aromatic compound with *p*-thiocresol, measured as a function of the observed disappearance of the "non-interacting" thiol signal and the dimerized *p*-thiocresol species. The y-axis represents the total area under the curve (AUC) in the observed IR spectrum for the "non-interacting" and "self-associating" signals for *p*-thiocresol when titrated with aromatic donors: hexamethylbenzene (red, circles), 1-methylindole (orange, squares) mesitylene (green, triangles), toluene (blue, inverted triangles), and *m*-dichlorobenzene (violet, diamonds). The solid lines represent the best fit to the experimental data according to equation S2. Dissociation constants estimated from the disappearance of "non-interacting" and "self-interacting" species have the inherent limit of zero signal at complete saturation. Estimated dissociation constants are reported in Table S13. Error bars indicate standard error.

The dissociation constant can also be determined via the analysis of the area of the "interacting" thiol species by plotting its total area under the curve (AUC) as a function of the concentration of the aromatic donor. The total area for the interacting species follows the following equation:

$$Y = \frac{Y_0}{SH_t} \times \frac{\left[(D_L + K_d + SH_t) - \sqrt{(D_L + K_d + SH_t)^2 - 4(SH_t)(D_L)} \right]}{2}$$

[Equation S3]

where D_L = concentration of the aromatic donor
SH_t = total concentration of p-thiocresol
K_d = dissociation constant
Y_0 = signal in absence of donor.
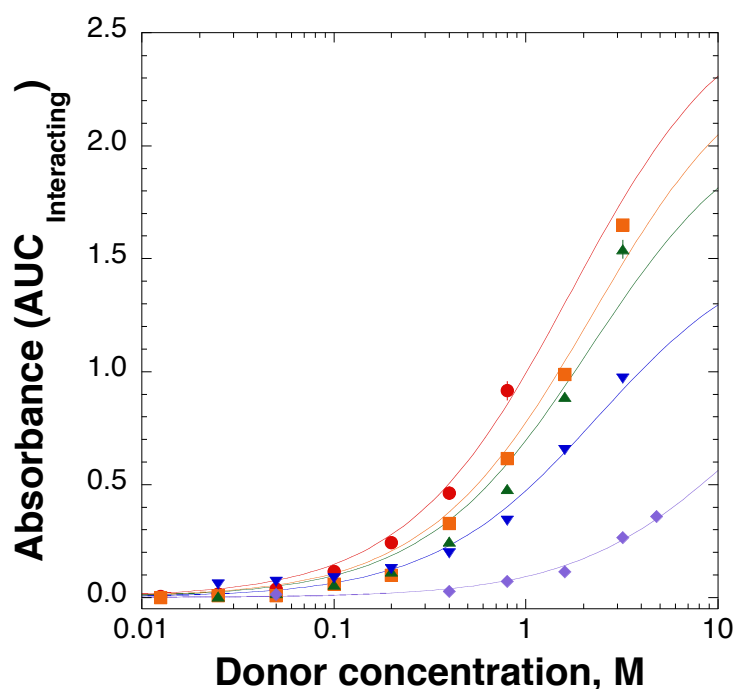
Figure S79. Determination of the dissociation constant for the complex of each interacting aromatic compound with p-thiocresol, measured as a function of the increasing "interacting" species. The y-axis represents the combined area under the curve (AUC) for the IR signal associated with the interaction of p-thiocresol when titrated with aromatic donors: hexamethylbenzene (red, circles), 1-methylindole (orange, squares) mesitylene (green, triangles), toluene (blue, inverted triangles), and m-dichlorobenzene (violet, diamonds). The solid lines represent the best fit for the experimental data according to equation S3. Dissociation constants estimated from the S–H stretching frequency due to interaction with aromatic compounds also have the additional error associated with the absence of saturation in the binding isotherms, and thus include the error in the extinction coefficient of the interacting form and in the maximum signal at saturation. Estimated dissociation constants are reported in Table S13. Error bars indicate standard error.

Table S13. Dissociation constants for S–H/π interactions. K_d values determined from the disappearance of the IR signal associated with the "non-interacting" thiol and the "self-interacting" thiol signal of *p*-thiocresol are listed as K_d non-interacting. Values based on the appearance of the interacting peak are indicated as K_d interacting. Dissociation constants estimated from the S–H stretching frequency due to interaction with aromatic compounds also have the additional error associated with the absence of saturation in binding isotherms, and thus include the additional errors, in the extinction coefficient of the interacting form and in the maximum signal at saturation. Dissociation constants estimated from the disappearance of "non-interacting" and "self-interacting" species have the inherent limit of zero signal at complete saturation.

donor	K_d, kcal mol^{-1}	
	Determined via non-interacting peak	**Determined via interacting peak**
m–dichlorobenzene	13.5 ± 0.9	13.1 ± 0.6
toluene	1.03 ± 0.13	2.34 ± 0.14
mesitylene	1.03 ± 0.13	2.12 ± 0.25
1-methylindole	0.69 ± 0.11	2.18 ± 0.17
hexamethylbenzene	1.25 ± 0.14	1.68 ± 0.09

Estimation of ΔH and ΔS for the S–H/π interaction: Temperature-dependent IR spectroscopy of *p*-thiocresol in the presence of aromatic donors

An in-house temperature-controlled cell holder was built by wrapping copper tubing around the standard IR cell and connecting the tubing to a chiller with temperature control. Temperatures were read directly from the cell holder using a thermocouple. The temperature readings from the chiller and the thermocouple were within ± 0.5 ˚C. Samples were allowed to equilibrate for at least 30 minutes prior to acquisition of each IR spectrum. Data were fit to a two-component Lorentzian function. The area under the curve for the non-interacting thiol species at 2586 cm^{-1} was used to determine the fraction bound and unbound.
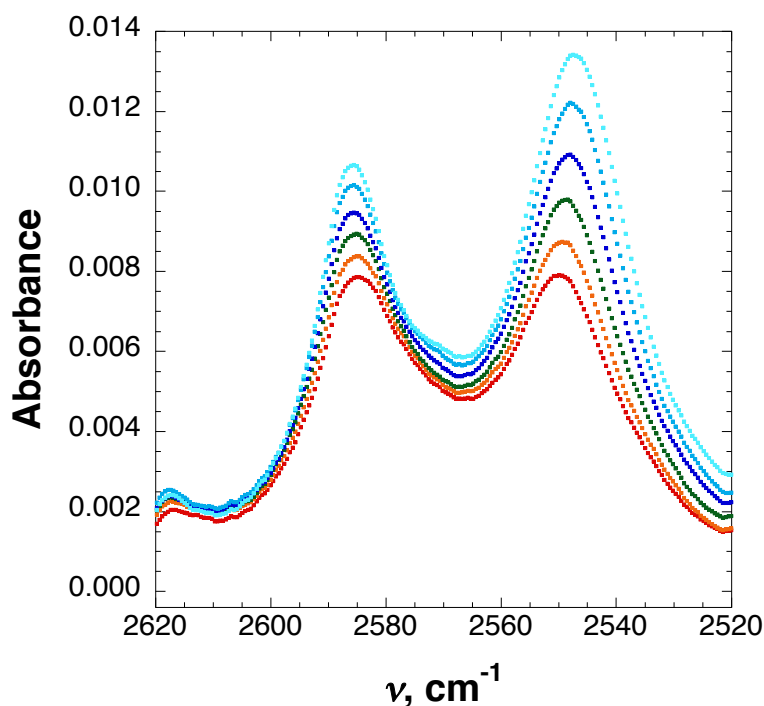
Figure S80. Temperature-dependent infrared spectroscopy of the S–H stretching frequency of *p*-thiocresol (55 mM) in presence of 400 mM hexamethylbenzene at –8 ˚C (cyan), 0 ˚C (indigo), 10 ˚C (blue), 20 ˚C (green), 30 ˚C (orange), and 40 ˚C (red).
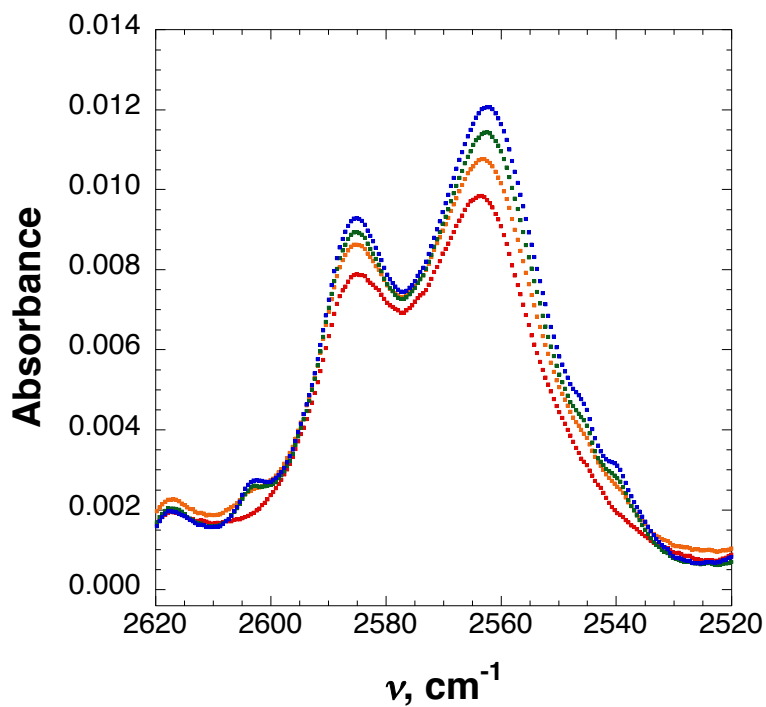
Figure S81. Temperature-dependent infrared spectroscopy of the S–H stretching frequency of *p*-thiocresol (55 mM) in presence of 400 mM mesitylene at –4.8 ˚C (blue), 0 ˚C (green), 10 ˚C (orange), and 20 ˚C (red).
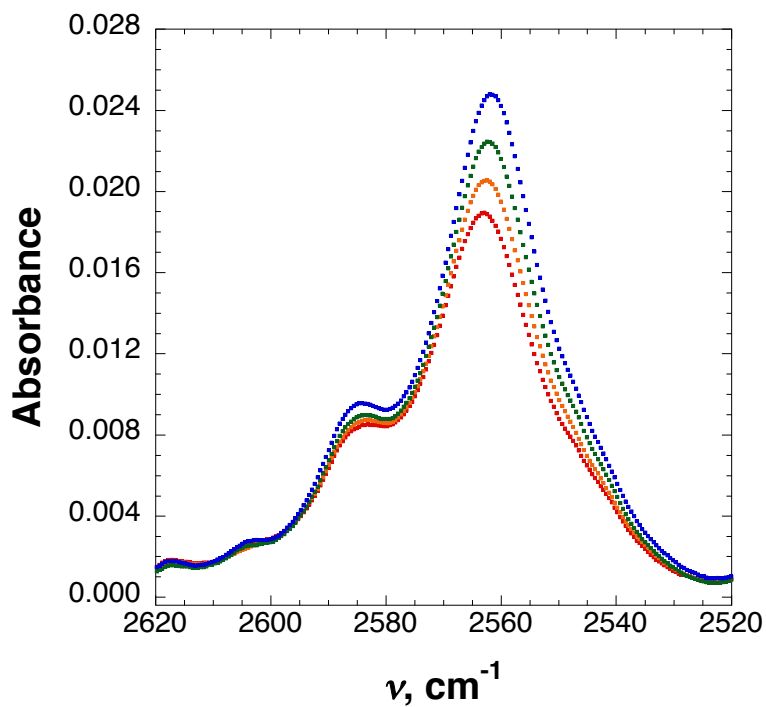
Figure S82. Temperature-dependent infrared spectroscopy of the S–H stretching frequency of *p*-thiocresol (55 mM) in presence of 1600 mM mesitylene at –9 ˚C (blue), 0 ˚C (green), 10 ˚C (orange), and 20 ˚C (red).
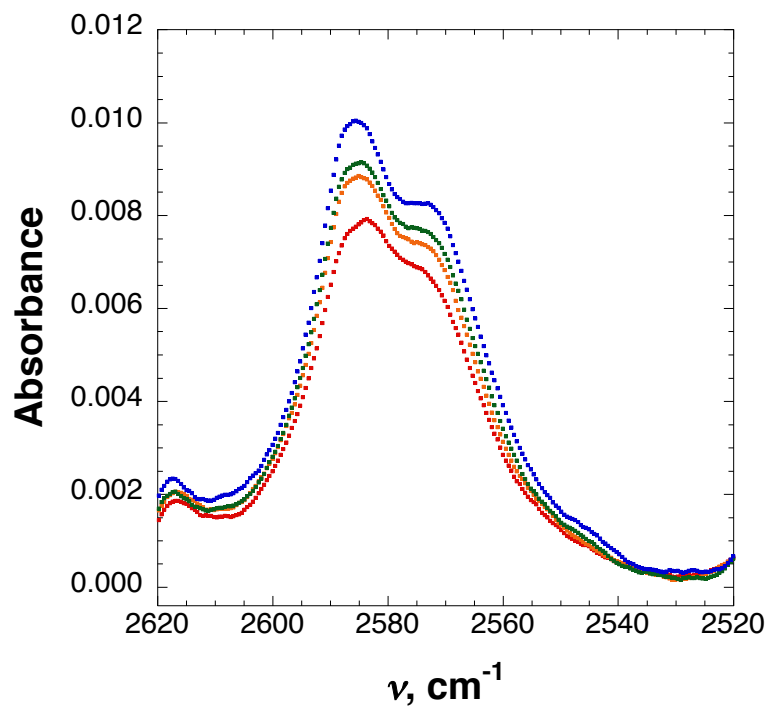
Figure S83. Temperature-dependent infrared spectroscopy for the S–H stretching frequency of *p*-thiocresol (55 mM) in presence of 400 mM toluene at 0 ˚C (blue), 10 ˚C (green), 20 ˚C (orange), and 30 ˚C (red).
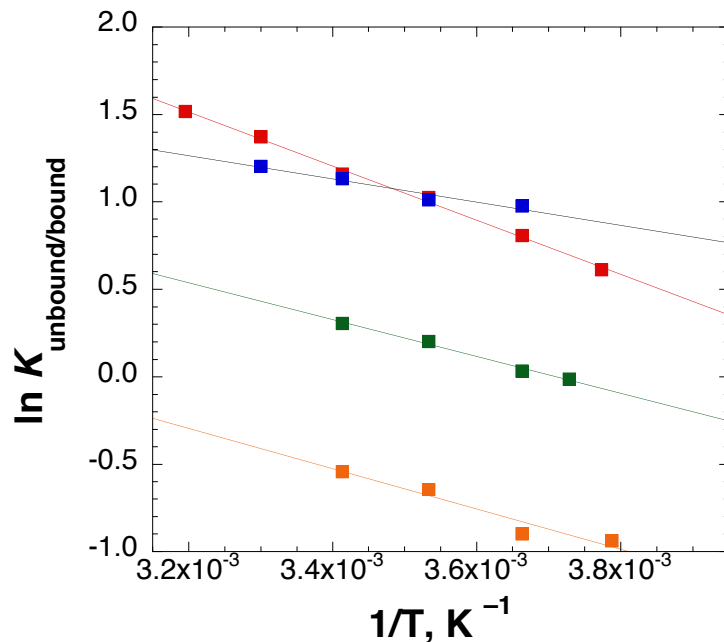
Figure S84. van't Hoff plots for the interactions of *p*-thiocresol with 400 mM hexamethylbenzene (red), 400 mM mesitylene (green), 1600 mM mesitylene (orange), and 400 mM toluene (blue). All experiments were conducted on a single sample with 55 mM *p*-thiocresol.

Table S14. Calculated enthalpy (ΔH) and entropy (ΔS) for the dissociation of the thiol-aromatic complex to the free, non-interacting thiol.

Aromatic Donor	ΔH, kcal mol^{-1}	ΔS, cal mol^{-1} K^{-1}
400 mM hexamethylbenzene	2.9 ± 0.3	12.6 ± 1.3
450 mM hexamethylbenzene	3.1 ± 0.1	12.9 ± 0.8
400 mM mesitylene	2.1 ± 0.1	7.8 ± 0.4
1600 mM mesitylene	2.3 ± 0.4	6.8 ± 1.2
400 mM toluene	1.3 ± 0.2	6.7 ± 1.0

Solid-State Magic-Angle-Spinning (MAS) ^{13}C NMR of Boc-L-4-thiolphenylalanine *tert*-butyl ester (1) and *p*-thiocresol

^{13}C CP/MAS experiments were conducted using a 4.0 mm HX or a 3.2 mm HCN solid-state magic-angle-spinning (MAS) probe on a Bruker Avance III spectrometer operating at a proton Larmor frequency of 500.13 MHz. All spectra were obtained at 298 ± 2 K and CP/MAS experiments were carried out with a sample spinning rate of 10,000 ± 2 Hz with a 4 mm rotor or 14,000 ± 2 Hz with a 3.2 mm rotor. TPPM decoupling during CP/MAS data acquisition was provided by a 104.2-kHz proton decoupling field. For CP/MAS spectra, the contact time was 3 ms. Solid-state ^{13}C-^{1}H HETCOR spectra were acquired with a 3.2 mm HCN MAS probe at a spinning rate of 14,000 Hz. The mixing time was set to either 300 or 1000 µsec. During the t_1 evolution period, proton homonuclear decoupling with the FSLG scheme was applied to enhance proton resolution.[2]

All ^{13}C chemical shifts were referenced externally via the resonance of adamantane at an isotropic chemical shift relative to tetramethylsilane (TMS) of 38.55 ppm.

Solid samples of *p*-thiocresol were used as purchased, consistent with the crystals used in X-ray diffraction and in obtaining the crystalline FT-IR spectrum. Solid samples of **1** were obtained by precipitation from hexanes, and the solids were filtered and dried. The solids were redissolved in 20% ethyl acetate in hexanes and the solution was warmed until all of the material had dissolved, and the sample was allowed to recrystallize. The sample appeared to contain a mixture of solids and crystals. FT-IR spectroscopy conducted after CP/MAS NMR indicated an identical IR spectrum to that obtained on crystalline material. ^{13}C chemical shift assignments for *p*-thiocresol were obtained from HSQC and HMBC experiments in CDCl$_3$, and were compared by analogy to the chemical shifts observed in the solid-state NMR spectra. ^{13}C chemical shift assignments for **1** were obtained directly from solid-state ^{13}C-^{1}H HETCOR spectra.

Table S15. ^{13}C and ^{1}H chemical shift assignments for **1** in solution (CDCl$_3$) and in the solid state. Carbon chemical shifts were assigned using the ^{1}H-^{13}C HMBC NMR spectrum in solution and the solid-state ^{13}C-^{1}H HETCOR NMR spectrum (Figure S85, S87).

Carbon #

Proton #
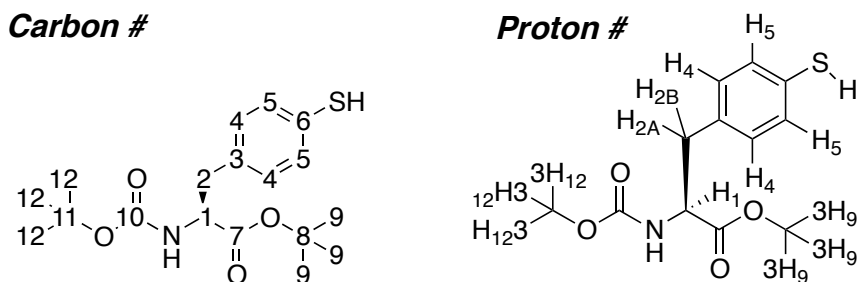
Atom #	Assignment	CDCl$_3$ δ, ppm	Solid State δ, ppm	Δδ, ppm
C7	Carbonyl, *tert*-butyl ester	170.8	175.4	4.7
C10	Carbonyl, Boc	155.0	156.3	1.3
C3	C$_{Aro}$, ipso	134.0	135.1	1.1
C5	C$_{Aro}$, meta	130.3	131.4[a]	1.2
C4	C$_{Aro}$, ortho	129.5	131.4[a]	1.9
C6	C$_{Aro}$, para	128.9	129.6	0.8
C8	C, *tert*-butyl ester	82.2	82.2	0.0
C11	C, Boc	79.7	80.4	0.7
C1	Cα	54.7	58.9	4.3
C2	Cβ	37.9	36.0	–1.9
C12	CH$_3$, Boc	28.3	28.6[a]	0.3
C9	CH$_3$, *tert*-butyl ester	28.0	28.6[a]	0.6
SH	Thiol	3.4	6.2	2.8
NH	Carbamate	5.0	7.4	2.4
H5	H$_{Aro}$, meta	7.2	7.6[a]	0.4
H4	H$_{Aro}$, ortho	7.0	7.6[a]	0.6
H1	Hα	4.4	4.6	0.2
H2A, H2B	Hβ	3.0	3.3	0.3
H12	Methyl, Boc	1.4	1.7[a]	0.3
H9	Methyl, *tert*-butyl ester	1.4	1.7[a]	0.3

[a] Peaks were not resolved in solid-state NMR spectra.
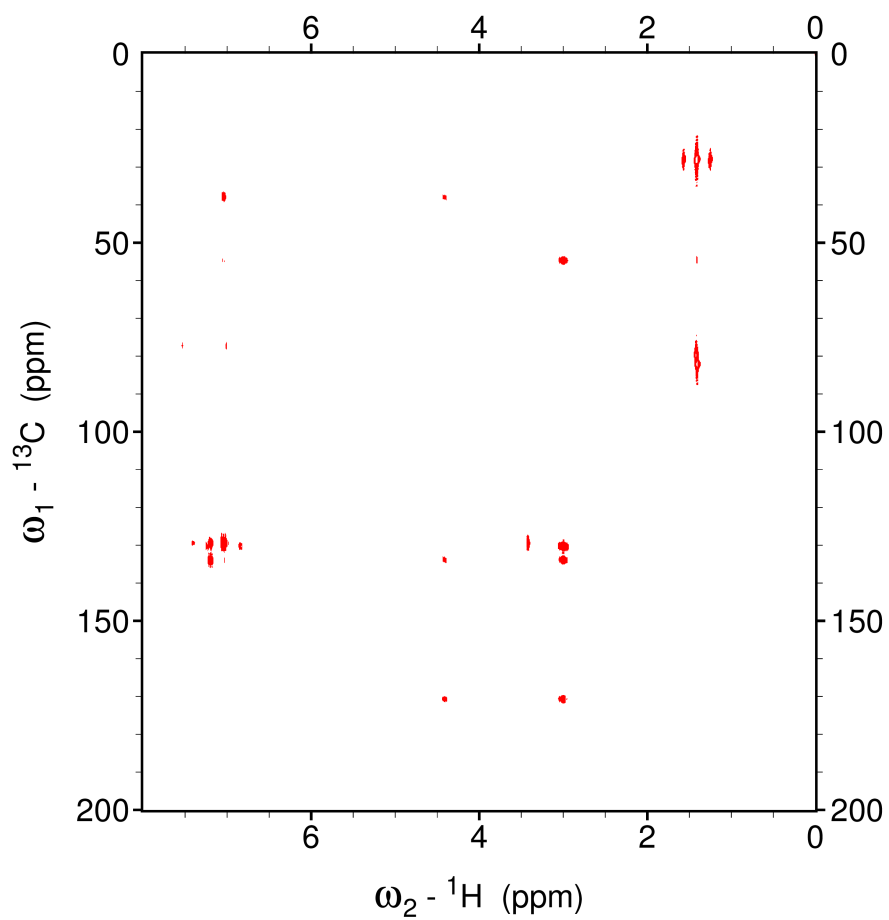
Figure S85. Solution ^1H-^{13}C HMBC spectrum of **1** in $CDCl_3$.
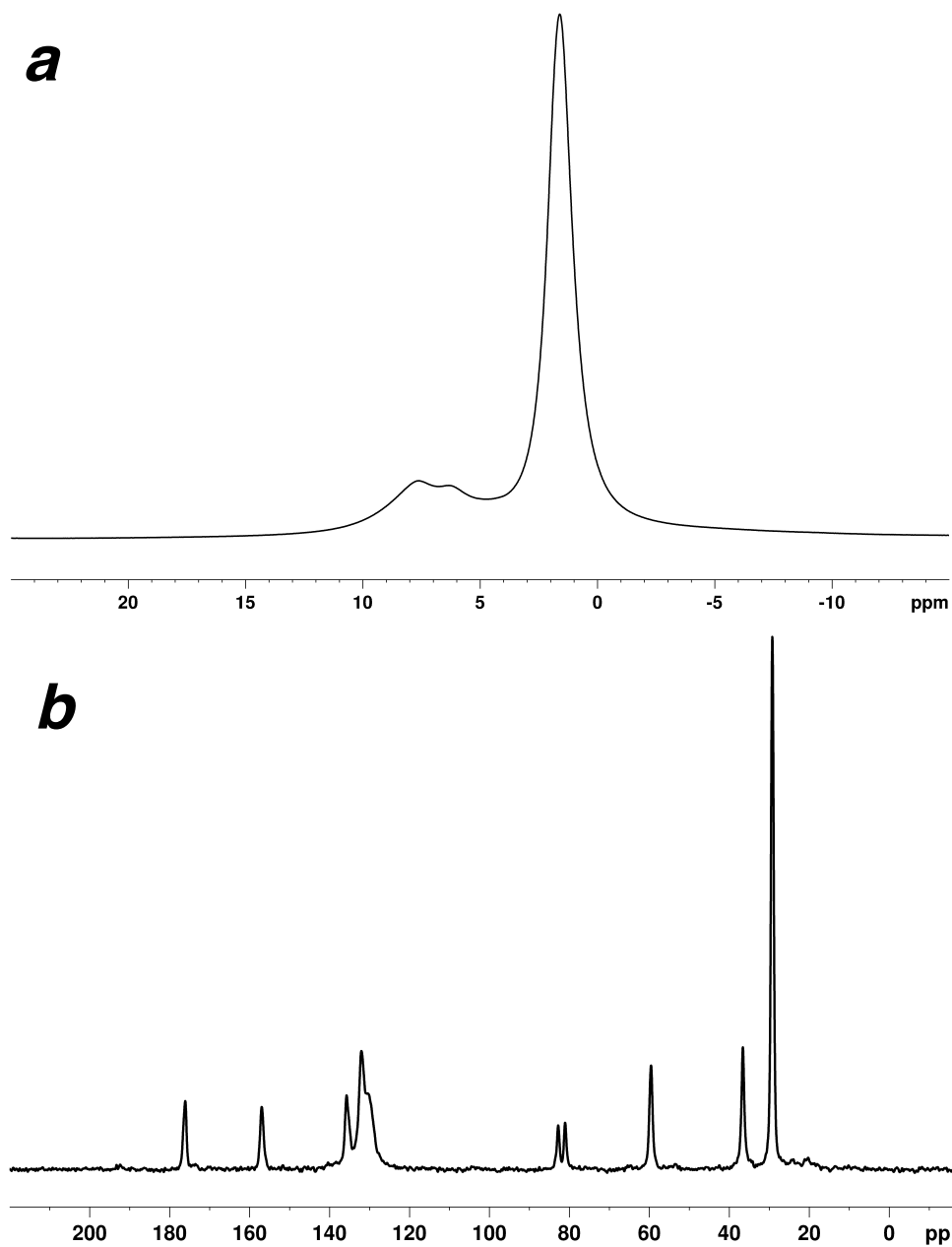
Figure S86. Solid-state NMR spectra of **1**. (a) ¹H MAS NMR spectrum and (b) ¹³C CP/MAS NMR spectrum.
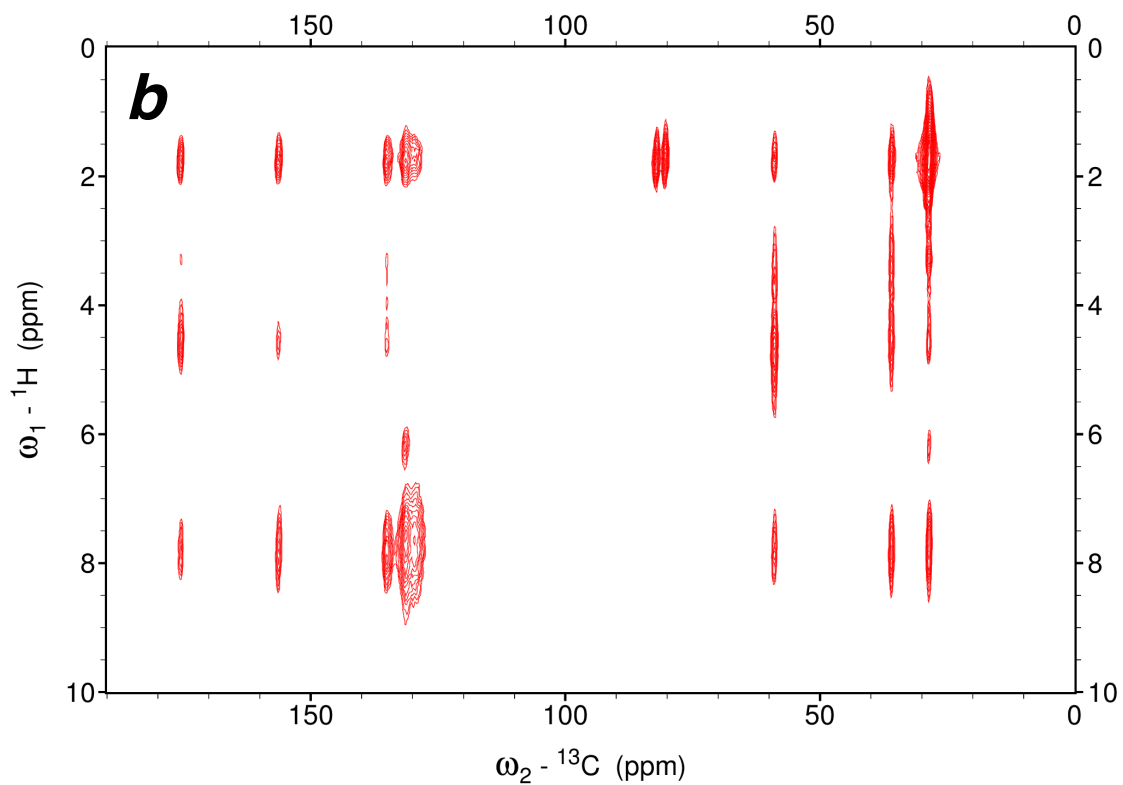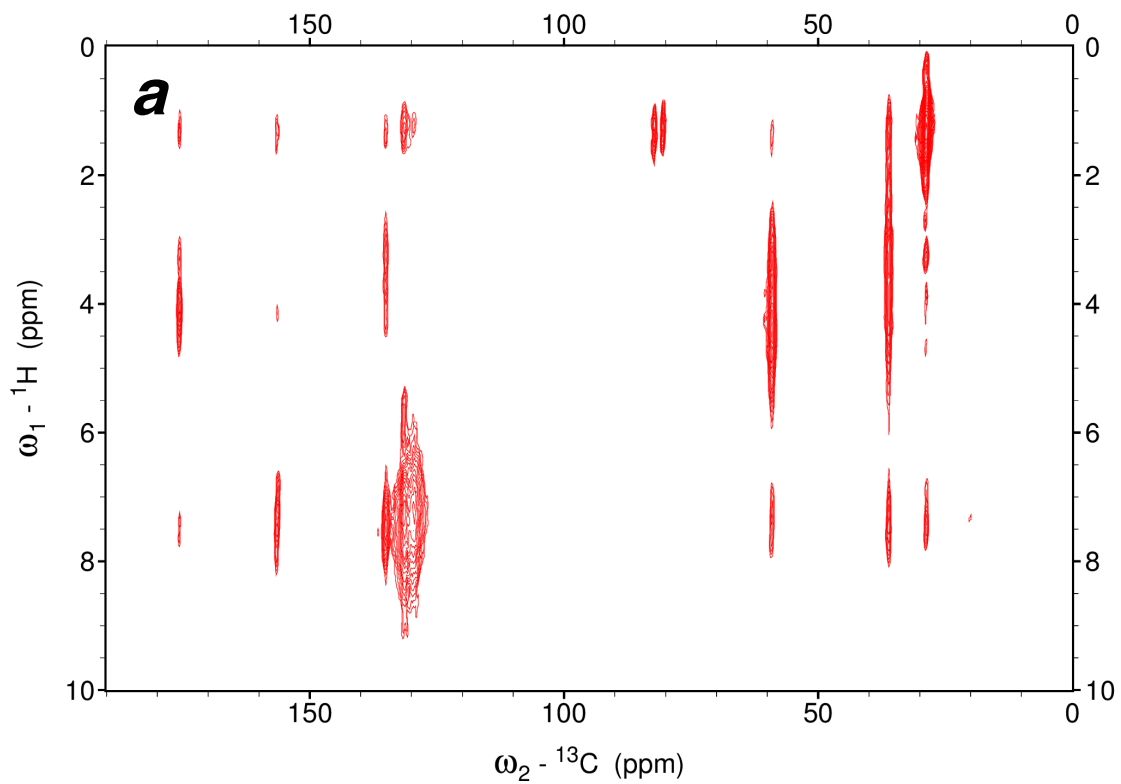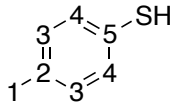
Figure S87. Solid-state ^{13}C-^{1}H HETCOR spectrum of **1** using a mixing time of (a) 300 μsec or (b) 1000 μsec.
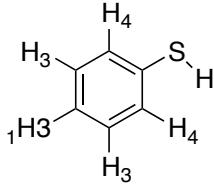
Table S16. ^{13}C and ^{1}H chemical shift assignments for *p*-thiocresol in solution (CDCl$_3$) and in the solid state. Carbon chemical shifts in CDCl$_3$ were assigned using ^{1}H-^{13}C HMBC, ^{1}H-^{13}C HSQC, NMR spectra in solution and the solid-state ^{13}C-^{1}H HETCOR NMR spectrum (Figure S88-89, S93).

Carbon #   *Proton #*

atom#	Assignment	CDCl$_3$ δ, ppm	Solid State δ, ppm	Δδ, ppm
C2	C$_{Aro}$, ipso	135.6	133.0	2.6
C4	C$_{Aro}$, meta	129.9	129.5	0.4
C3	C$_{Aro}$, ortho	129.8	128.3	1.5
C5	C$_{Aro}$, para	126.6	126.8	–0.2
C1	CH$_3$	20.9	20.2	0.7
SH	Thiol	3.4	5.0, 3.2	1.6,–0.2
H4	H$_{Aro}$, meta	7.0	7.1^a	0.1
H3	H$_{Aro}$, ortho	7.2	7.1^a	–0.1
H1	Methyl	2.3	2.4	0.1

^{a} Peaks were not resolved in solid-state NMR spectra.
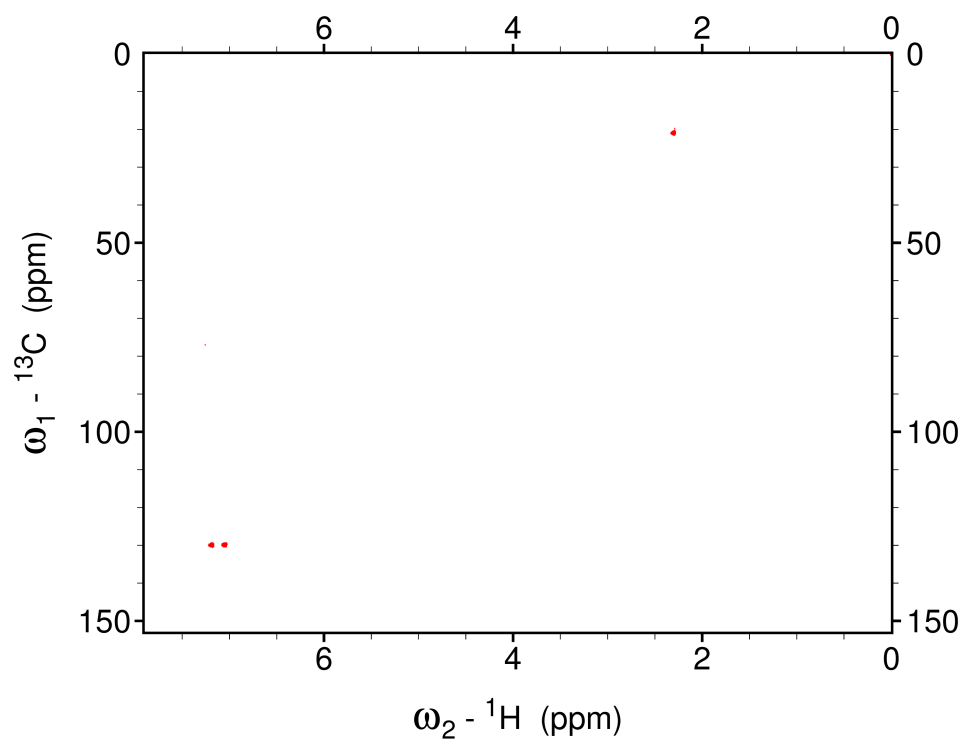
Figure S88. Solution ^{1}H-^{13}C HSQC spectrum of *p*-thiocresol in CDCl$_3$.
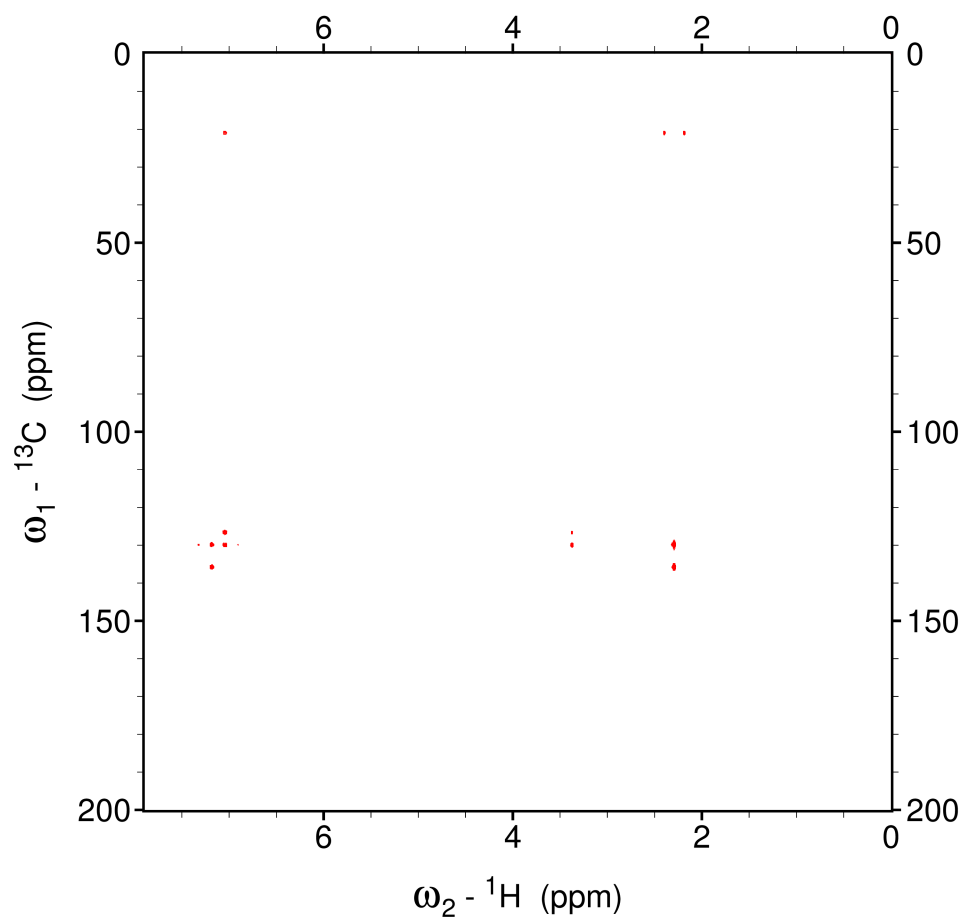
Figure S89. Solution ^{1}H-^{13}C HMBC spectrum of *p*-thiocresol in CDCl$_3$.
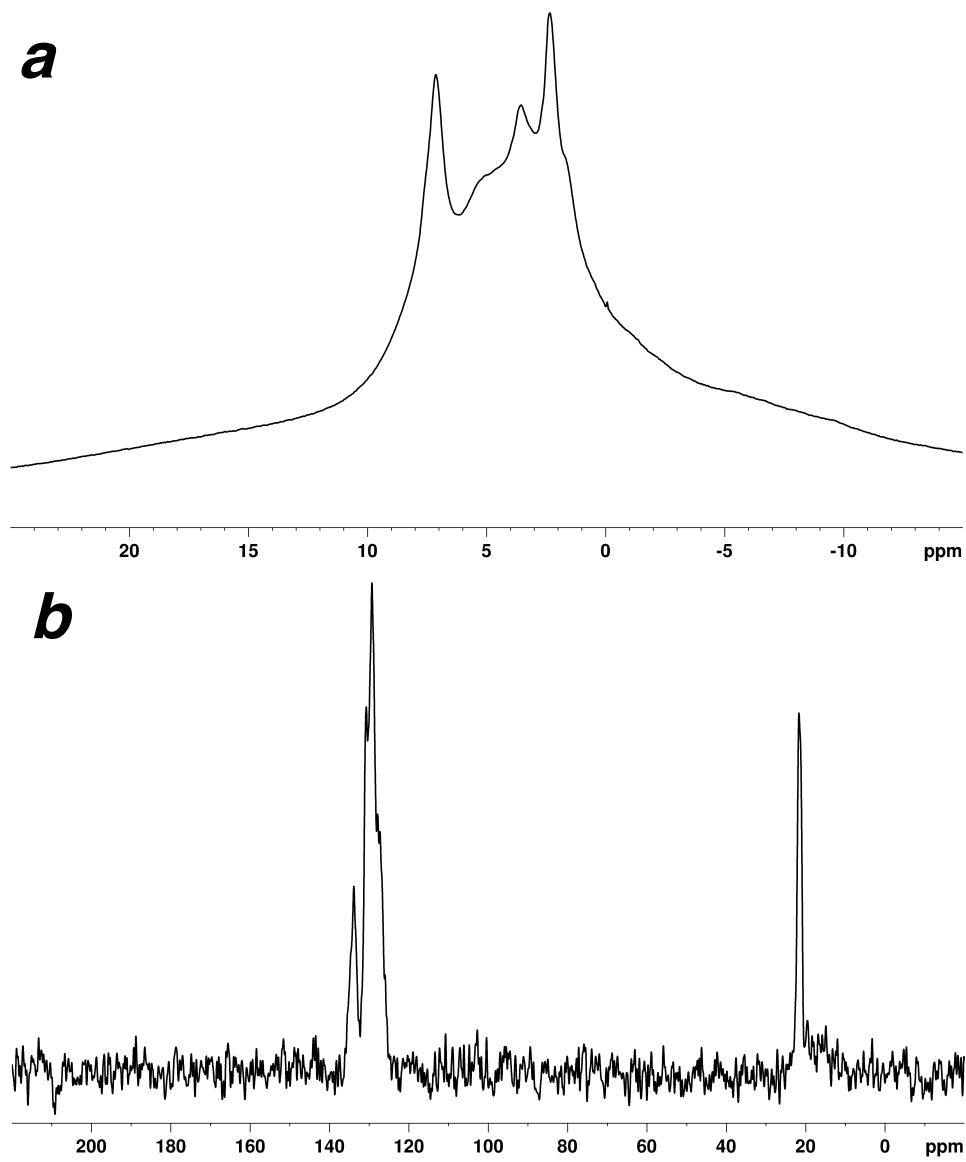
Figure S90. Solid-state NMR spectra of *p*-thiocresol. (a) ^{1}H MAS NMR spectrum and (b) ^{13}C CP/MAS NMR spectrum.
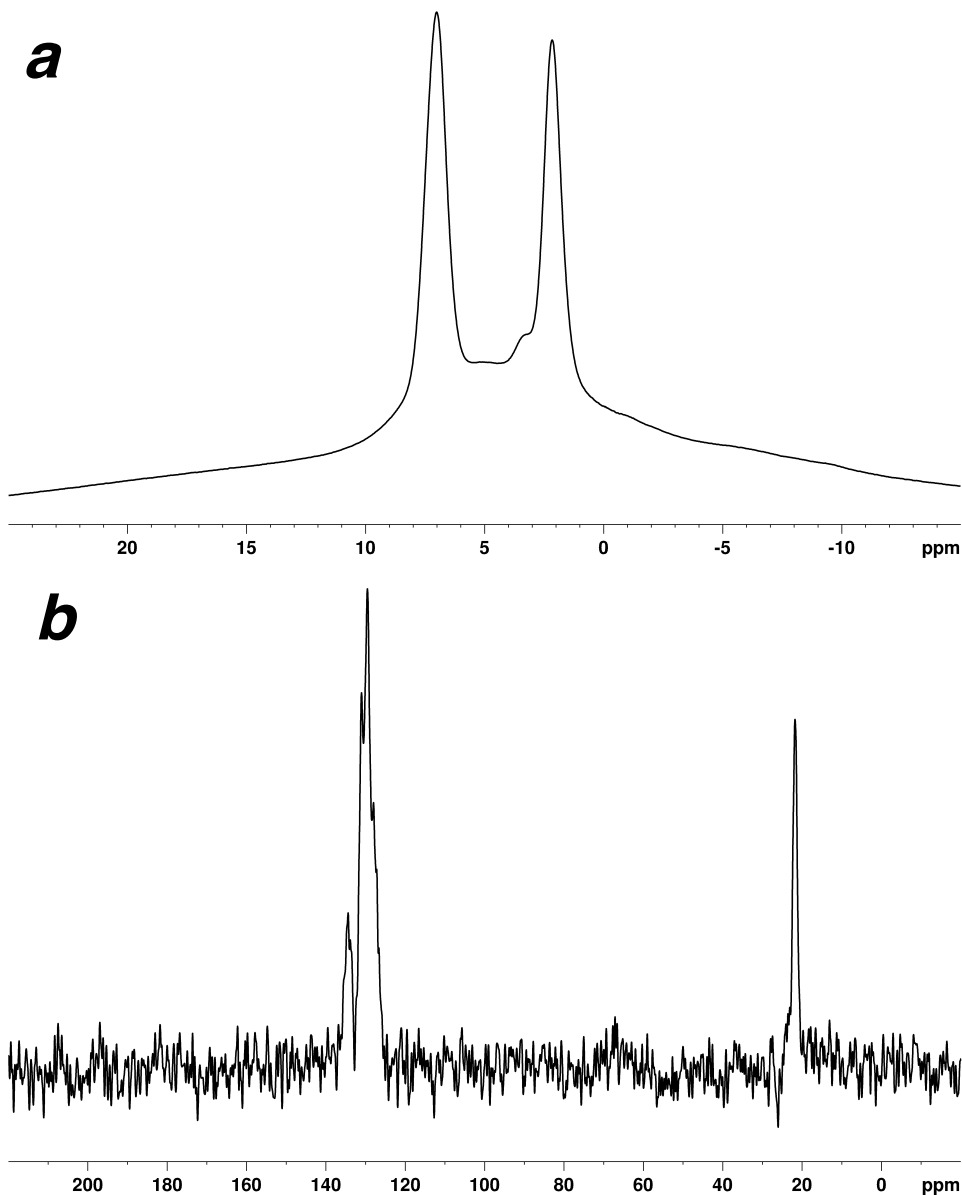
Figure S91. Solid-state NMR spectra of deuterated *p*-thiocresol. (a) ^{1}H MAS NMR spectrum and (b) ^{13}C CP/MAS NMR spectrum. Deuteration of *p*-thiocresol was completed by dissolving the sample in methanol-d$_4$ (50 mg/mL) and then warming to 90 °C for 5 minutes or until the sample had completely dissolved. The sample was cooled to 50 °C and incubated for 12 hours. The sample was cooled to room temperature, where crystals readily formed. The crystals were filtered and dried, and then redissolved in methanol-d$_4$ (50 mg/mL). The process was repeated three times.
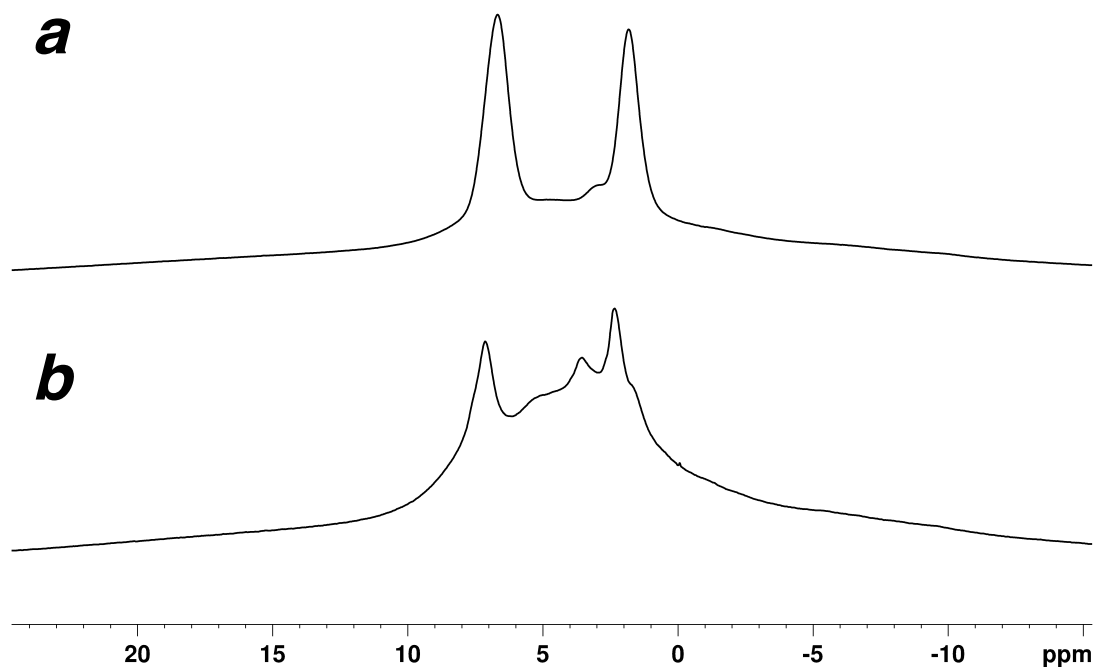
Figure S92. Comparison of solid-state MAS ^{1}H NMR spectra of *p*-thiocresol as (a) deuterated *p*-thiocresol and (b) protonated *p*-thiocresol. Deuteration of *p*-thiocresol was completed by dissolving the sample in methanol-d$_4$ (50 mg/mL) and then warming to 90 °C for 5 minutes or until the sample had completely dissolved. The sample was cooled to 50 °C and incubated for 12 hours. The sample was cooled to room temperature, where crystals readily formed. The crystals were filtered and dried, and then redissolved in methanol-d$_4$ (50 mg/mL). The process was repeated three times. The peaks at 5.0 ppm and 3.2 ppm are present in the protonated sample but absent in the deuterated sample, indicating that both resonances are due to thiol protons, which are in different environments in the crystalline form.
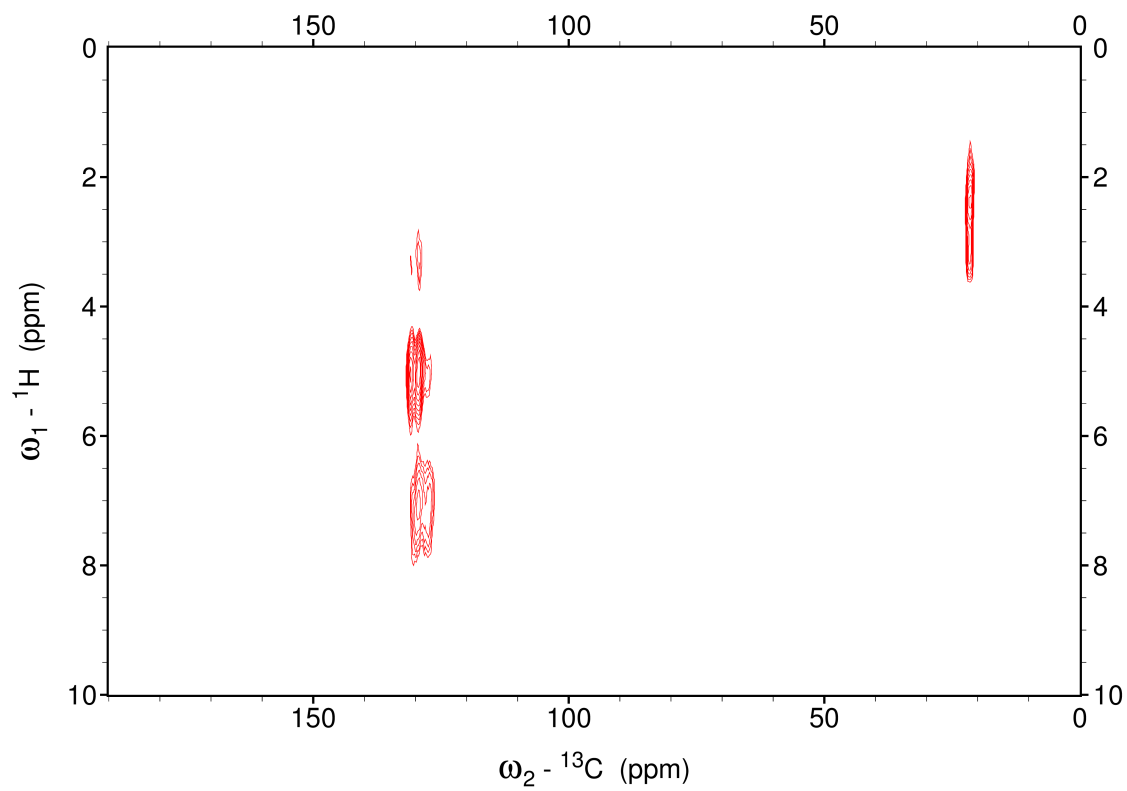
Figure S93. Solid-state ^{13}C-^{1}H HETCOR spectrum of *p*-thiocresol using a mixing time of 300 μsec.

ab initio **calculations on the crystal structure of Boc-L-4-thiolphenylalanine *tert*-butyl ester (1) as a truncated dimer**

All calculations were performed using the Gaussian 09 program package.[3] To reduce calculation time, the crystal structure of **1** was truncated to remove atoms so that only the dimeric and monomeric *p*-thiocresol molecules remained (Figure S94). The structure was optimized at B3LYP level of theory with the 6-311+G(2d,p) basis set followed by frequency calculations to ensure that all structures were true minima. The natural bond orbital (NBO) analysis was performed using the NBO program available in the Gaussian 09 software at B3LYP and MP2 levels of theory using various basis sets for the experimental crystal structure of the molecule.[4] The atomic charges were computed using CHELPG (CHarges from Electrostatic Potentials using a Grid-based method) at both B3LYP and MP2 level of theories for both crystal structure and optimized structures.[5] GAUSSVIEW was utilized for graphics preparation for this study.[3]
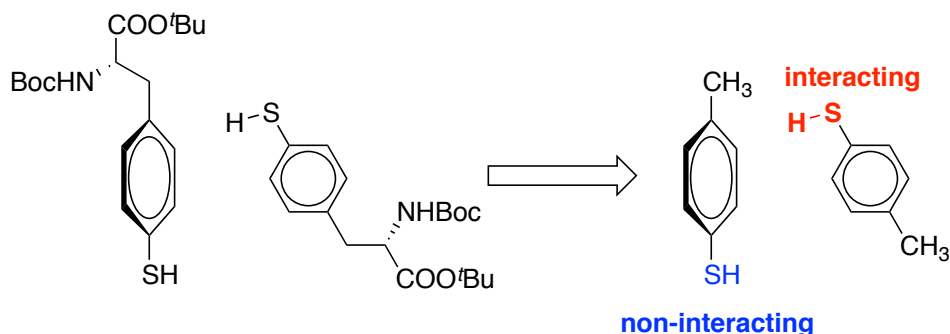
Figure S94. Based on the atomic coordinates from the orthorhombic crystals of **1** (left), a *p*-thiocresol dimer was generated for calculations (right). The two thiol groups are either "interacting" or "non-interacting" with respect to the aromatic ring, as indicated. Calculations were completed on the crystallographically observed S–H bond length of 1.26 Å and on the standardized S–H bond distance of 1.338 Å.[7]

$d_{H-centroid} = 2.9$ Å
$d_{S-centroid} = 4.0$ Å
Angle $\theta = 9.6°$
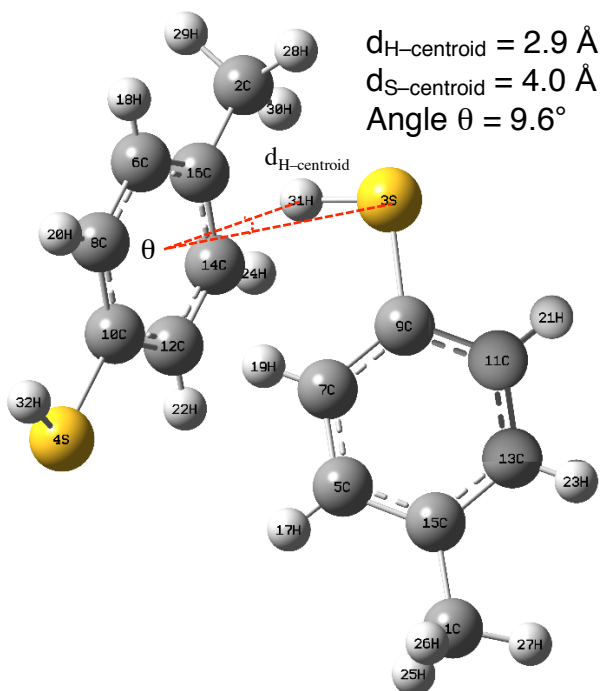
Figure S95. Structure of the *p*-thiocresol dimer, based on the atomic coordinates from the atomic orthorhombic crystals of **1**. Atom numbers are indicated.

The energy and atomic charges for the *p*-thiocresol dimer were examined based on atomic coordinates obtained from the crystal structure of **1** (Figure S95). The geometrical parameters $d_{S-centroid}$, $d_{H-centroid}$ (the distances between the thiol sulfur or hydrogen atom and the aromatic centroid of phenyl ring of the interacting subunit, respectively), and the angle θ (defined as the angle S–centroid–H) are shown in Figure S95. The analyses of atomic charges at both B3LYP and MP2 levels of theories using 6-311+G(2d,p) and aug-cc-pvdz basis sets are shown in Table S17. To assess the electrostatic component of the S–H/π interaction, the atomic charges of the *p*-thiocresol monomer were computed using these same basis sets, and the deviation of atomic charges (Δq) from the monomeric structure of *p*-thiocresol for sulfur and hydrogen atoms of two σ_{S-H} bonds are tabulated in the Table S18. These data indicate that the σ_{S-H} bond is polarized through intermolecular interaction with the aromatic ring. Polarization of the thiol bond is also expected to influence the Columbic electrostatic interaction energy between σ_{S-H} bond and aromatic ring, and these data are included in Table S18. The electrostatic energy between the σ_{S-H} bond and aromatic ring provides an important insight for the interaction between them.

Table S17. Calculated atomic charges of the *p*-thiocresol dimer based on crystallographic coordinates of **1** at B3LYP and MP2 levels of theories using 6-311+G(2d,p) and aug-cc-pvdz basis sets, obtained from the CHELPG method. Atoms are numbered according to the legend below: (a) carbon and (b) hydrogen. The thiol groups are highlighted in yellow, where atoms ^{a}31 (H) and ^{a}3 (S) represent the thiol interacting with the aromatic ring, and atoms 32 (H) and 4 (S) represent the thiol that is not interacting with the aromatic ring.
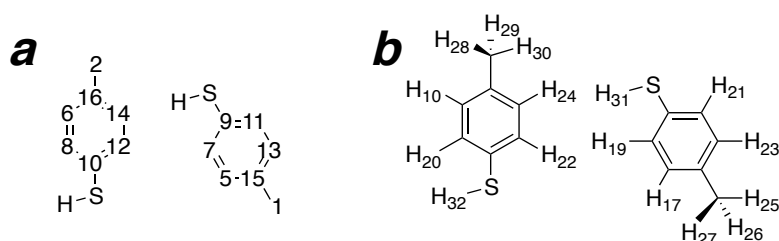
S.NO	Atom #	B3LYP		MP2	
		6-311+G (2d,p)	aug-cc-vdz	6-311+G (2d,p)	aug-cc-pvdz
1	C	-0.213	-0.191	-0.204	-0.228
2	C	-0.339	-0.310	-0.323	-0.356
^{a}**3**	**S**	**-0.344**	**-0.348**	**-0.345**	**-0.345**
4	S	-0.287	-0.289	-0.291	-0.290
5	C	-0.218	-0.207	-0.215	-0.222
6	C	-0.226	-0.218	-0.217	-0.228
7	C	-0.119	-0.106	-0.105	-0.120
8	C	-0.108	-0.098	-0.099	-0.110
9	C	0.094	0.093	0.079	0.087
10	C	0.072	0.076	0.065	0.068
11	C	-0.077	-0.065	-0.063	-0.075
12	C	-0.011	-0.004	-0.002	-0.010
13	C	-0.303	-0.286	-0.298	-0.309
14	C	-0.359	-0.341	-0.356	-0.367
15	C	0.254	0.242	0.246	0.257
16	C	0.327	0.315	0.315	0.329
17	H	0.121	0.115	0.121	0.126
18	H	0.139	0.133	0.138	0.143
19	H	0.095	0.087	0.087	0.095
20	H	0.083	0.077	0.080	0.084
21	H	0.151	0.141	0.147	0.153
22	H	0.131	0.122	0.126	0.132
23	H	0.141	0.129	0.138	0.145
24	H	0.154	0.143	0.153	0.160
25	H	0.051	0.044	0.048	0.055
26	H	0.054	0.048	0.053	0.059
27	H	0.059	0.054	0.058	0.064
28	H	0.106	0.098	0.102	0.111
29	H	0.071	0.062	0.066	0.076
30	H	0.090	0.083	0.088	0.096
^{a}**31**	**H**	**0.209**	**0.206**	**0.206**	**0.213**
32	H	0.202	0.196	0.203	0.209

^{a}indicates the thiol group which is interacting with the aromatic ring.

Table S18. Summary of the electronic polarization, associated electrostatic interaction, and NBO analyses for the S–H/π interaction of the *p*-thiocresol dimer based on the atomic coordinates from the crystal structure of **1** at B3LYP and MP2 levels of theories using 6-311+G(2d,p) and aug-cc-pvdz basis sets.

			B3LYP		MP2	
	S.NO		6-311+G (2d,p)	aug-cc-pvdz	6-311+G (2d,p)	aug-cc-pvdz
Δq (e)		^{a}S	0.0656	0.0715	0.0598	0.0640
		^{a}H	-0.0211	-0.0263	-0.0094	-0.0254
		S	0.0083	0.0127	0.0053	0.0095
		H	-0.0140	-0.0165	0.0061	-0.0215
$\Delta\Delta q$ S (e)			-0.057	-0.059	-0.054	-0.055
$\Delta\Delta q$ H (e)			0.007	0.010	0.003	0.004
ΔE_{el}(kcal/mol)			-0.866	-0.745	-1.07	-0.72
$E^{(2)}_{i\rightarrow j^*}$ (kcal/mol)			0.70(0.75)	1.19 (1.26)	0.76 (0.80)	1.45 (1.52)
	$\langle\pi_{Aro}|\sigma^*_{S-H}\rangle$		0.1048	0.1261	0.1070	0.1064
α	σ^*_{S-H}		0.0075	0.0079	0.00524	0.0056
	π_{Aro}		1.690	1.691	1.685	1.685

^{a}indicates the thiol group which is interacting with the aromatic ring.

Δq	is the deviation of atomic charges from the *p*-thiocresol monomer and the calculated atomic charges from the crystal structure of **1**.
$\Delta\Delta q$	is the difference of atomic charges between the "interacting" and "non-interacting" thiol groups
E_{el}	is the energy due to the electrostatic interaction
$E^{(2)}_{i\rightarrow j^*}$	is the interaction energy between donor NBO (σ^*_j) and acceptor NBO (σ_i).
$\langle\pi_{Aro}|\sigma^*_{S-H}\rangle$	is the energy between the orbitals π_{Aro} and σ^*_{S-H}
α	is electron occupancy for the indicated orbitals
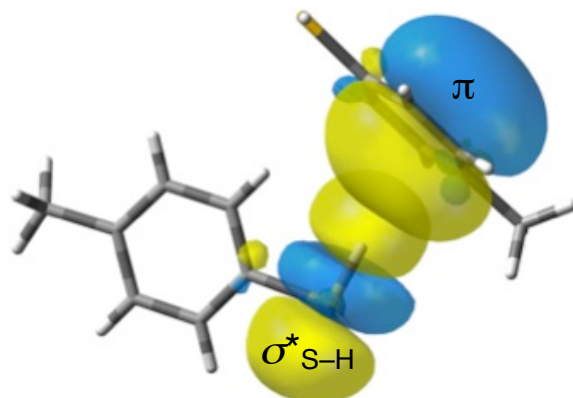
Figure S96. Orbital overlap between the π orbital of the aromatic ring and the antibonding σ^*_{S-H} orbital of the S–H bond. NBO analysis indicates favorable overlap between these orbitals.

To examine the $\sigma*_{S-H}$/aromatic interaction in greater detail, we performed NBO analysis for the two structures at B3LYP and MP2 levels of theory using 6-311+G(2d,p) and aug-cc-pvdz basis sets. NBO analysis can be applied to quantitatively determine the strength of the $\sigma*_{S-H}$/aromatic interaction present in this S–H/π interaction. This interaction might be viewed as a Lewis interaction, where the occupied π orbital of aromatic ring behaves as a Lewis acid-Lewis base, transferring electron density to the empty σ^*_{S-H}, which acts as a Lewis acid. The magnitude of the interaction energy, $E^{(2)}_{i \to j^*}$, between a donor NBO, σ_j^*, and an acceptor NBO, σ_i, can be estimated using the second order perturbation theory:

$$E^{(2)}_{i \to j^*} = q_i \frac{|\langle \sigma_j^* | \hat{F} | \sigma_i \rangle|^2}{\varepsilon_j^* - \varepsilon_i},$$

where i and j denote the donor and acceptor orbitals, q_i is the occupancy of bonding orbital, ε_i and ε_j^* correspond to their respective orbital energies, and $\hat{F}$ is the Fock operator respectively. The data indicate that the primary interaction is between the unoccupied σ^*_{S-H} and one of the occupied π orbitals of the aromatic ring. The values of occupancy, α, of these respective orbitals are included Table S18. The extent of overlap between these respective orbitals is shown in Figure S96, as obtained from NBO calculation on the experimental structure **1** at MP2 level of theory using the aug-cc-pvdz basis set. The overlap between the π_{Aro} and σ^*_{S-H} NBOs was quantified by calculating the overlap integral between them, $\langle \pi_{Aro} | \sigma^*_{S-H} \rangle$, at B3LYP and MP2 levels of theories using 6-311+G (2d,p) and aug-cc-pvdz basis sets; these data are included in Table S18. The overlap integral and the figure indicate that there is significant in-phase overlap between the π_{Aro} and σ^*_{S-H} NBOs. The possible pair of $E^{(2)}_{i \to j^*}$ interaction energies for the σ^*_{S-H} orbital and all other orbitals as obtained from NBO calculation at B3LYP and MP2 levels of theory using 6-311+G (2d,p) and aug-cc-pvdz basis sets are presented in Table S18.

The data indicate that there is a significant σ^*_{S-H}–π_{Aro} interaction present in the crystal structure of **1**. Furthermore, to examine the interaction between σ^*_{S-H} and all other possible orbitals, we deleted all orbitals except for the σ^*_{S-H} and the π_{Aro} under interrogation and measured the energy of stabilization. The calculation was performed for both structures at B3LYP and MP2 levels of theory using 6-311+G (2d,p) and aug-cc-pvdz basis sets, and the associated stabilization energies are also included in Table S18. The data indicate that the interaction between the σ^*_{S-H} and the π orbitals stabilizes the overall system in a significant

manner. It is noteworthy that these calculations were conducted on the *p*-thiocresol dimer with an S–H bond length of 1.26 Å, as determined by X-ray crystallography. At the more likely S–H bond length of 1.34 Å, the extent of orbital overlap and energetic stabilization between the σ^*_{S-H} and the π orbitals would potentially be even greater.

Based on the described computational analysis, the S–H bond becomes more polarized on interaction with an aromatic ring, and there is a significant electrostatic interaction present between the σ^*_{S-H} bond and aromatic ring. The calculations at higher levels on both the experimental structures do not alter these findings. Through NBO analysis, it was revealed that there is significant in-phase overlap between the antibonding σ^*_{S-H} orbital and the π orbital of the aromatic ring. Therefore, we can conclude that the σ^*_{S-H}–π_{Aro} interaction is important for stability of this intermolecular, non-covalent interaction.

Analysis of ν_{S-H} as a function of S–H bond length and interaction with the aromatic ring

The *p*-thiocresol dimer model was further examined by DFT calculations as a function of the length of the S–H bond, with all other atoms held at fixed positions. The S–H bond length was varied systematically within a dimer (interacting S–H) and monomer (non-interacting S–H) context to identify the effects of bond length and interaction with the aromatic ring on S–H stretching frequency. The initial experiments were conducted using the computationally inexpensive B3LYP method with the cc-pvtz basis set. After identification of the 1.360 Å bond length as generating frequencies most similar to the IR data, these structures were re-examined using the TPSSh method. These data, while not expected to quantitatively identify the bond length in solution, indicate that longer bond lengths are associated with lower S–H frequencies, and that interaction with the aromatic ring both decreases the frequency and increases the intensity of the absorbance at the S–H stretching frequency. These calculations also indicated a downfield change in the thiol H chemical shift with increasing S–H bond length.

Table S19. DFT calculations on the effect of S–H bond length and interaction with the aromatic ring on IR properties of the S–H bond.

Thiol structure	S–H bond length, Å	S–H frequency, cm^{-1}	Intensity	method	basis set
monomer (non-interacting)	1.261	3319	0.95	B3LYP	cc-pvtz
	1.338	2722	0.21	B3LYP	cc-pvtz
	1.350	2641		B3LYP	cc-pvtz
	1.360	2575	1.5	B3LYP	cc-pvtz
	1.360	**2584**	**2.1**	**TPSSh**	**cc-pvtz**
	1.375	2477	2.1	B3LYP	cc-pvtz
	1.400	2311	2.7	B3LYP	cc-pvtz
dimer (interacting)	1.261	3320	19.1	B3LYP	cc-pvtz
	1.338	2714	29.5	B3LYP	cc-pvtz
	1.350	2634	31.8	B3LYP	cc-pvtz
	1.360	2568	33.8	B3LYP	cc-pvtz
	1.360	**2568**	**37.2**	**TPSSh**	**cc-pvtz**
	1.375	2470	37.2	B3LYP	cc-pvtz
	1.400	2305	43.6	B3LYP	cc-pvtz

Cambridge Structural Database Search Parameters and Results

A search was conducted on the Cambridge Structural Database (version 5.36, released in November, 2014) for entries containing non-bonded contacts between thiols (motif Z–S–H, Z = any non-hydrogen atom) or cations (Li$^+$, Na$^+$, K$^+$, Rb$^+$, Cs$^+$, or Ag$^+$) and a 6-membered phenyl ring containing only carbon. The release of the database used in the current study contained over 710,000 molecules. Searches were conducted using ConQuest (version 1.17 Cambridge Crystallographic Data Centre, 2014).

The initial search parameters placed restrictions on the distance between the aromatic-centroid and the interacting atom, either the thiol sulfur atom for thiol-aromatic interactions or Li$^+$, Na$^+$, K$^+$, Rb$^+$, Cs$^+$, or Ag$^+$ (generalized as M$^+$) for cation-aromatic interactions (Figure S97). Intermolecular and intramolecular contacts (2 bonds or more) were included within the search parameters. For the transition metal Ag$^+$, only intermolecular interactions were considered. Only error-free, non-disordered structures where R < 0.10 were included in the search, and powder pattern structures were excluded. For cation-aromatic interactions, the range was defined as $d_{M^+-centroid} \leq 4.2$ Å (for cations Li$^+$, Na$^+$, and K$^+$) or $d_{M^+-centroid} \leq 4.8$ Å (for cations Rb$^+$, Cs$^+$, and Ag$^+$). For thiol-aromatic interactions, the range was defined as $d_{S-centroid} \leq 4.8$ Å. The interacting 6-membered aromatic ring contained only carbon atoms, and heteroaromatic rings were excluded from this study. For thiol-aromatic interactions, two lists were generated with different coordinates for hydrogen atom location: one with the coordinates as reported in the CSD, and one where the S–H bond length was normalized to 1.338 Å.[6] For bond length normalization, the coordinates of the hydrogen atom were adjusted along the vector of the S–H bond directly using ConQuest 1.17, Cambridge Crystallographic Data Centre, 2014. Data and statistics obtained from the thiol structures with fixed S–H bond lengths are indicated as "normalized" entries.

$d_{M-centroid} \leq 4.2$ Å
for M$^+$ = Li$^+$, Na$^+$, K$^+$
$d_{M-centroid} \leq 4.8$ Å
for M$^+$ = Rb$^+$, Cs$^+$, Ag$^+$

$d_{S-centroid} \leq 4.8$ Å
Z = any non-hydrogen atom
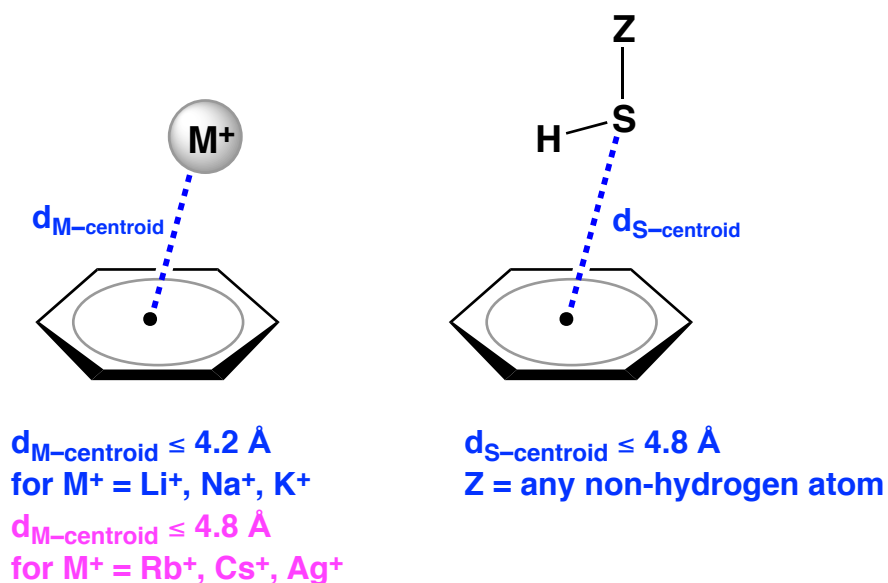
Figure S97. Initial search parameters for cation/π and S–H/π interactions in the Cambridge Structural Database. The interacting 6-membered aromatic ring only contained carbon atoms; heteroaromatic rings were excluded from this study. Cation/π aromatic interactions (left) and S–H/π aromatic interactions (right) were examined and compared in this study.

For all entries obtained from the initial search parameters, distances and bond angles were calculated. The measurements on the crystal structures included distances from the interacting atom (M^+, thiol S, or thiol H, generalized as "X") to the aromatic ring. The measurements included: $d_{X-centroid}$, distance to the calculated centroid of the aromatic ring; d_{X-Cmin}, the shortest distance from X to any aromatic carbon atom; and d_{plane}, the normal distance from X to the plane of the aromatic ring (Figure S98). The radius (r) was defined as the distance from the aromatic centroid to the projection of X in the plane of the aromatic ring, and was calculated from measured distances as $\sqrt{d_{X-centroid}^2 - d_{plane}^2}$. For the thiol entries, measurements were also obtained for the bond length S–H (range 0.86 Å-1.42 Å), for the Z–S–H bond angle (range 80°-120°), and for the angle S–H–centroid. Thiol structures that had S–H bond lengths or Z–S–H bond angles outside of these criteria were excluded.
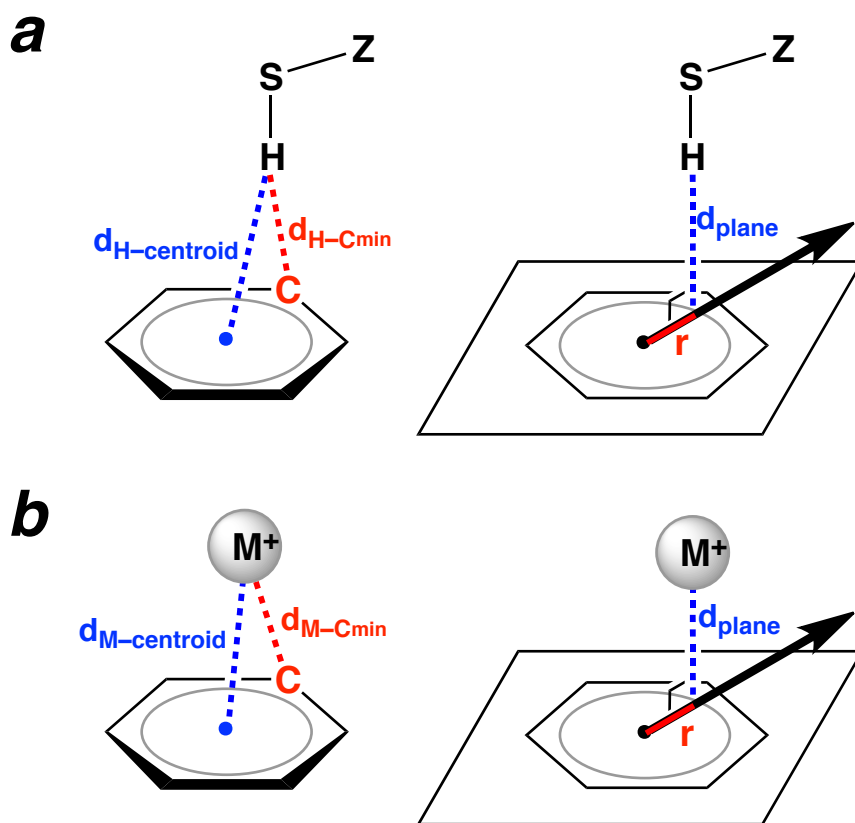
Figure S98. Defined distances accumulated from crystal structures within defined parameters for (a) S–H/π interactions and (b) cation-π interactions. and $d_{X-centroid}$ refers to the distance between the atom X (where X = M^+, S or H) and the centroid of the aromatic ring; d_{X-Cmin} refers to the distance between the atom X (where X = M^+, S or H) and the nearest carbon atom of the aromatic ring; d_{plane} refers to the distance between the atom X (where X = M^+, S or H) and the plane of the aromatic ring; *r* refers to the projected distance from atom M^+, S, or H within the plane of the aromatic ring to the centroid, which was calculated from measured distances as $\sqrt{d_{X-centroid}^2 - d_{plane}^2}$.

In order to identify and study entries with close cation- or thiol-aromatic interactions, the accumulated entries from the CSD were constrained by a geometric "cylinder" based on the plane of the aromatic ring (Figure S99). Only entries with interacting atom coordinates within the defined cylinder were examined further. The base of the cylinder was defined by r ≤ 3.00 Å for M^+ and thiol hydrogens. The size of the base was designed to be slightly larger than twice the radius of benzene. For thiol sulfur atoms, the base of the cylinder was defined as r ≤ 4.20 Å, which was twice the radius of benzene (3.00 Å) and an additional 1.20 Å to account for the S–H bond. The height of the cylinder was defined for each X as d_{plane} ≤ (1.25 × ΣvdWr for carbon and X, where ΣvdWr refers to the sum of van der Waals radii). The ionic radii for Li^+, Na^+, K^+, Rb^+, Cs^+, and Ag^+ were defined as 0.60 Å, 0.95 Å, 1.33 Å, 1.48 Å, 1.69 Å, and 1.26 Å respectively;[6] the van der Waals radii for C, H, and S were defined as 1.70 Å, 1.20 Å, and 1.80 Å respectively.[6, 7] Using these definitions, the ΣvdWr for $C{\cdot\cdot}Li^+$, $C{\cdot\cdot}Na^+$, $C{\cdot\cdot}K^+$, $C{\cdot\cdot}Rb^+$, $C{\cdot\cdot}Cs^+$, $C{\cdot\cdot}Ag^+$, C··H, and C··S were defined as 2.30 Å, 2.65 Å, 3.03 Å, 3.18 Å, 3.39 Å, 2.96 Å, 2.90 Å, and 3.50 Å respectively.[6, 7] The cylinder restrictions and defined distances used for this study are shown in Figure S99.

After applying the cylinder restraints on the atomic coordinates of each cation, hydrogen, or sulfur atom, the individual structures were manually examined and annotated for features that could potentially affect the geometry of the cation- or thiol-aromatic interaction. The entries were manually annotated with the following criteria: (A) polycyclic rings; (A1) complex macrocylic rings; (B) carbanions within or adjacent to the interacting aromatic rings; (C) in thiol structures, where thiol groups were "pointed away" from the plane of the aromatic ring (as defined by $(d_{S–plane} − d_{H–plane)}$ ≥ –0.10 Å); (D) in thiol structures, where the sulfur atom is apparently tri-coordinate; (E) redundant structures or entries; (F) unusual structures; or (G) in cation structures, where the cation was interacting with a crown ether. The resultant number of structures after each level of parsing are shown in Table S20. The Ag^+ database was not manually parsed.

The geometries of S–H/π interactions were further compared to O–H/π interactions, which were expected to have a greater electrostatic component, and potentially different geometries of interaction. A search of the CSD was conducted for entries containing intermolecular non-bonded contacts between alcohols (motif C–O–H) and a 6-membered phenyl ring containing only carbon atoms. Non-bonded contacts were initially identified as $d_{O–centroid}$ ≤ 4.8 Å (similar to the right panel, Figure S97). Only intermolecular contacts were included within the search parameters. Only error-free, non-disordered structures where R < 0.05 were included in the search, and powder pattern structures were excluded. Distances were measured or calculated for selected entries as in Figure S98b, including $d_{X–Cmin}$, d_{plane}, and r. Entries with to O–H/π interactions were restricted to structures where the bond length O–H was between 0.63 Å-1.04 Å, and the bond angle C–O–H was between 100°-140°. Similar to the "cylinder" restriction on entries containing S–H/π interactions, the entries containing O–H/π interactions were restricted H r ≤ 3.00 Å and $d_{H–plane}$ ≤ 3.63 Å; oxygen atoms were not restricted. Entries were manually parsed for criterion C (see above). Only divalent alcohol oxygen atoms were included in the original search parameters (criterion D was excluded using initial search restrictions). Only one O–H/π interaction was considered for each structure identified in the CSD; for structures containing multiple O–H/π interactions, only the interaction with the shortest $d_{H–Cmin}$ was considered in analyses.

A large number of entries were found in the CSD for alcohol groups located near a 6-membered aromatic ring. However, many of these structures may potentially have competing interactions with conventional hydrogen bonding groups (such as oxygen atoms or nitrogen atoms that can interact as O–H··O or O–H··N, respectively). In order to exclude competing interactions and identify only O–H/π interactions, entries identified with oxygen, nitrogen, or metal atoms within 2.50 Å of the alcohol hydrogen were excluded (determined via ConQuest). It was discovered that 84% of the entries contained a proximal atom that could potentially compete with the O–H/π interactions.
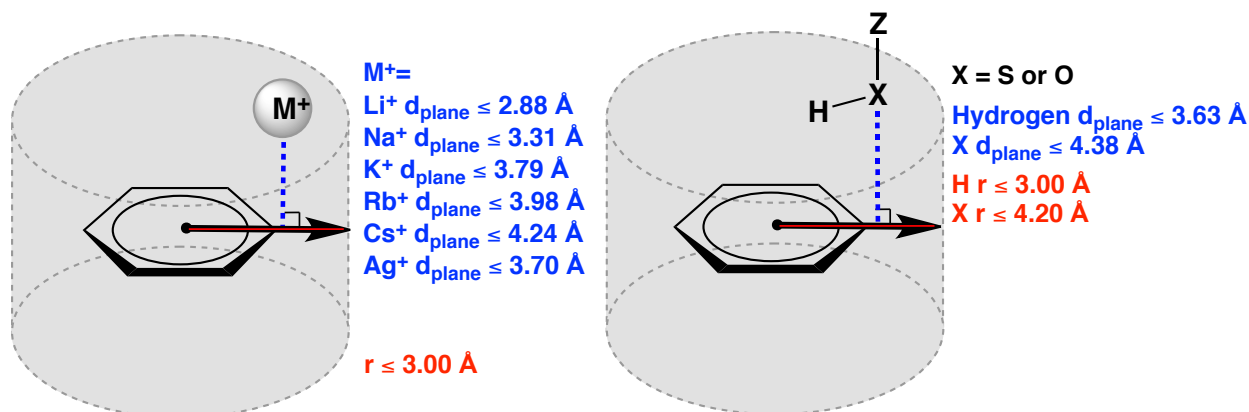
Figure S99. Identifying crystal structures obtained from the CSD with closely interacting cation/π or S–H/π aromatic interactions. A region of interaction was defined as a geometric cylinder for cations (left) and thiols (right) based on the plane of the aromatic ring. The cylinder restraints were established in order to identify potentially interacting groups, and to exclude non-interacting cations and thiols. The geometric restraints on the radius and distance d_{plane} are shown in the figure for cations (left) and thiols (right). The restrictions on the distance d_{plane} were defined as $1.25 \times \Sigma$(van der Waals radius of carbon and ionic radius for respective cations) for cations or $1.25 \times \Sigma$(van der Waals radii for carbon and hydrogen, sulfur, or oxygen) for thiols. The restriction on the distance r was set to twice the distance from the centroid to the edge of the aromatic ring (for sulfur and oxygen, an additional 1.20 Å were added to accommodate the S–H or O–H bond). Atomic coordinates that were located outside of the defined "cylinder" were excluded from this study.

Table S20. Summary of accumulated structures and entries in CSD database study, and the numbers of entries and structures remaining after each level of restriction. For thiol structures and entries, data were accumulated for the reported S-H bond and for normalizing all S–H bonds to be 1.338 Å (noted as "normalized" in the table). These entries were restricted based on a geometric "cylinder" that was defined based on the aromatic ring, and entries were retained for further study where the atom of interest (Li^+, Na^+, K^+, Rb^+, Cs^+, Ag^+, thiol H, or thiol S) was within the defined "cylinder." These entries were then manually examined and annotated with specific criteria (described above), and the "manual parsing" excludes entries fitting criteria A, B, C, D, E, and F (criteria A1 and G were included). In the O–H/π database manual parsing, duplicates and trivalent oxygen atoms were removed in the initial searches (criteria D and E) and only criterion C was removed manually (criteria A, A1, and G were included). The Ag^+ database was not manually parsed.

For the O–H/π interactions, an additional search was conducted to identify structures where a nitrogen, oxygen, or metal atom was found within 2.50 Å of the alcohol hydrogen atom ("nearby classical hydrogen bond acceptor").

	Initial Search		Cylinder Restriction		Manual Parsing	
	Structures	Entries	Structures	Entries	Structures	Entries
Li^+	82	198	37	87	19	43
Na^+	99	153	62	105	48	79
K^+	225	432	217	404	193	362
Rb^+	33	135	18	72	10	25
Cs^+	88	227	60	156	60	127
Ag^+	681	1120	437	664		
X-SH H reference	186	490	110	182	78	127
X-SH S reference	186	490	163	398	102	202
X-SH, normalized, H reference	186	490	111	178	79	122
X-SH, normalized, S reference	186	490	169	409	89	210
C-OH, all structures H reference	6743	11886	1725		1514	
C-OH, nearby classical hydrogen bond acceptor H reference	722	1176	290		270	

Table S21. Summary of comparisons between cation/π and S–H/π aromatic interactions in the CSD database study. Quantities of occurrences are shown where the $d_{X–Cmin}$ and $d_{X–centroid}$ distances were less than the $\Sigma vdWr$ for carbon and X, or where $d_{X–Cmin} < d_{X–centroid}$ (X = Li$^+$, Na$^+$, K$^+$, Rb$^+$, Cs$^+$, Ag$^+$, thiol S or thiol H). The relative percentage for each represented category is shown in parentheses. Quantities and statistics are shown after each level of parsing, where "cylinder restriction" indicates all structures where atom X was within a defined region of interaction (see description above, Figure S99), and where "manual parsing" indicates only structures that did not have unusual or potentially altered geometry due to external coordinating groups (see page S97). "H reference" and "S reference" refer to thiol structures where the hydrogen atom or sulfur atom was used for cylinder restrictions. "Normalized" refers to thiol structures where the S–H bond length was normalized to 1.338 Å, using ConQuest 1.17.

		Cylinder Restriction		Manual Parsing	
		Structures	**Entries**	**Structures**	**Entries**
$d_{Cmin} < \Sigma vdW$ radii	Li$^+$	14 (38%)	25 (29%)	7 (37%)	17 (40%)
	Na$^+$	5 (8%)	7 (7%)	4 (8%)	5 (6%)
	K$^+$	21 (10%)	35 (9%)	19 (10%)	32 (9%)
	Rb$^+$	4 (22%)	18 (25%)	2 (20%)	2 (8%)
	Cs$^+$	9 (15%)	25 (16%)	8 (13%)	16 (13%)
	Ag$^+$	47 (11%)	66 (10%)		
	X-SH H reference	58 (53%)	81 (45%)	45 (58%)	62 (49%)
	X-SH S reference	64 (39%)	89 (22%)	47 (46%)	65 (32%)
	X-SH, normalized, H reference	66 (59%)	98 (55%)	47 (60%)	71 (58%)
	X-SH, normalized, S reference	72 (43%)	106 (26%)	46 (52%)	62 (30%)
$d_{centroid} < \Sigma vdW$ radii	Li$^+$	8 (22%)	14 (16%)	2 (11%)	3 (7%)
	Na$^+$	7 (11%)	11 (10%)	5 (10%)	7 (9%)
	K$^+$	43 (20%)	92 (22%)	38 (20%)	84 (23%)
	Rb$^+$	5 (28%)	20 (28%)	2 (20%)	6 (24%)
	Cs$^+$	14 (23%)	26 (21%)	12 (20%)	18 (14%)
	Ag$^+$	5 (1%)	5 (8%)		
	X-SH H reference	18 (16%)	28 (15%)	18 (23%)	27 (21%)
	X-SH S reference	18 (11%)	28 (7%)	18 (18%)	27 (13%)
	X-SH, normalized, H reference	24 (22%)	35 (20%)	24 (29%)	35 (20%)
	X-SH, normalized, S reference	24 (14%)	35 (9%)	18 (20%)	23 (11%)
$d_{Cmin} < d_{centroid}$	Li$^+$	28 (76%)	72 (83%)	17 (89%)	40 (93%)
	Na$^+$	48 (77%)	79 (75%)	36 (75%)	61 (77%)
	K$^+$	124 (57%)	227 (56%)	110 (57%)	201 (56%)
	Rb$^+$	8 (44%)	44 (61%)	4 (40%)	10 (40%)
	Cs$^+$	43 (72%)	101 (65%)	37 (62%)	82 (65%)
	Ag$^+$	432 (99%)	649 (98%)		
	X-SH H reference	99 (90%)	164 (90%)	68 (87%)	111 (87%)
	X-SH S reference	152 (93%)	378 (95%)	92 (90%)	186 (92%)
	X-SH, normalized, H reference	98 (88%)	158 (89%)	66 (85%)	106 (87%)
	X-SH, normalized, S reference	155 (92%)	386 (94%)	81 (91%)	199 (95%)
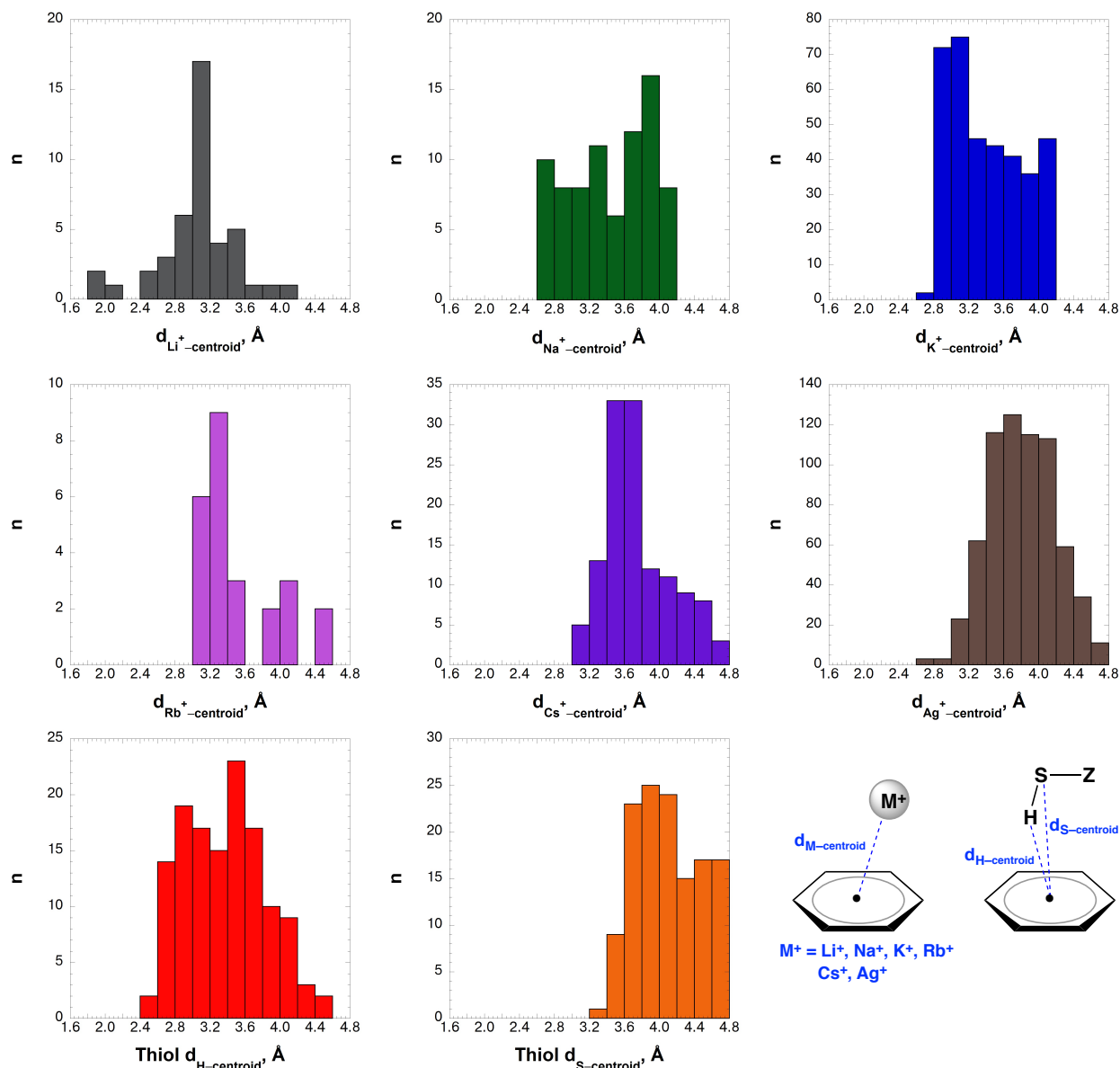
Figure S100. Distributions of the distance $d_{X-centroid}$, where X = Li$^+$, Na$^+$, K$^+$, Rb$^+$, Cs$^+$, Ag$^+$, thiol H, and thiol S. Histograms of the frequency of given distances from the aromatic centroid to the interacting atom X (X = Li$^+$, Na$^+$, K$^+$, Rb$^+$, Cs$^+$, Ag$^+$, thiol S, or thiol H). Measurements represented here include the atoms identified to be near to the aromatic ring, restricted by a "cylinder" with respect to the aromatic ring (Li$^+$ $d_{plane} \leq 2.88$ Å, Li$^+$ $r \leq 3.00$ Å; Na$^+$ $d_{plane} \leq 3.31$ Å, Na$^+$ $r \leq 3.00$ Å; K$^+$ $d_{plane} \leq 3.79$ Å, K$^+$ $r \leq 3.00$ Å; Rb$^+$ $d_{plane} \leq 3.98$ Å, Rb$^+$ $r \leq 3.00$ Å; Cs$^+$ $d_{plane} \leq 4.24$ Å, Cs$^+$ $r \leq 3.00$ Å; Ag$^+$ $d_{plane} \leq 3.70$ Å, Ag$^+$ $r \leq 3.00$ Å). Thiol hydrogen atoms are as reported in the CSD using the thiol hydrogen atom for reference in the cylinder restriction (Thiol H $d_{plane} \leq 3.63$ Å, Thiol H $r \leq 3.00$ Å), and no restrictions were placed on the thiol atoms. Represented data are within the criteria described above (excludes A, B, C, D, E, and F criteria), except for the Ag$^+$ database which was not manually parsed.

Figure S101. Distributions of the distance d_{X-Cmin}, where X = Li+, Na+, K+, Rb+, Cs+, Ag+, thiol H, and thiol S. Histograms of the frequency of given distances from the interacting atom X (X = Li+, Na+, K+, Rb+, Cs+, Ag+, thiol S, or thiol H) to the nearest aromatic ring carbon. Measurements represented here include the atoms identified to be near to the aromatic ring, restricted by a "cylinder" with respect to the aromatic ring (Li+ $d_{plane} \leq 2.88$ Å, Li+ r ≤ 3.00 Å; Na+ $d_{plane} \leq 3.31$ Å, Na+ r ≤ 3.00 Å; K+ $d_{plane} \leq 3.79$ Å, K+ r ≤ 3.00 Å; Rb+ $d_{plane} \leq 3.98$ Å, Rb+ r ≤ 3.00 Å; Cs+ $d_{plane} \leq 4.24$ Å, Cs+ r ≤ 3.00 Å; Ag+ $d_{plane} \leq 3.70$ Å, Ag+ r ≤ 3.00 Å). Thiol hydrogen atoms are as reported in the CSD using the thiol hydrogen atom for reference in the cylinder restriction (Thiol H $d_{plane} \leq 3.63$ Å, Thiol H r ≤ 3.00 Å), and no restrictions were placed on the thiol atoms. Represented data are within the criteria described above (excludes A, B, C, D, E, and F criteria), except for the Ag+ database which was not manually parsed.

Figure S102. Localization of interacting atoms Li^+, Na^+, K^+, Rb^+, Cs^+, Ag^+, thiol H, and thiol S atoms with respect to the plane of the aromatic ring. The atomic coordinates of the interacting atom, X, are indicated with reference to the plane of the aromatic ring for cation/π and S–H/π aromatic interactions. The distance $d_{X-plane}$ is correlated against the distance X r (radius), where X = Li^+, Na^+, K^+, Rb^+, Cs^+, Ag^+, thiol H, or thiol S. The X-axis represents the plane of the aromatic ring, and the origin represents the aromatic centroid. The origin (●) and edge (**C**) of the aromatic ring are indicated within the charts, where **C** is located at 1.40 Å from the origin. The black line indicates the sum of the van der Waals radii for carbon and the respective atoms or ions, where entries below the line are less than the sum of the van der Waals radii (Σ van der Waals radii for C and: Li^+ = 2.30 Å; Na^+ = 2.65 Å; K^+ = 3.03 Å; Rb^+ = 3.18 Å; Cs^+ = 3.39 Å; Ag^+ = 2.96 Å; thiol H = 2.90 Å; thiol S = 3.50 Å). Thiol hydrogen atoms are as reported in the CSD, and the thiol hydrogen atom was used for reference in the cylinder restriction (described above). The thiol sulfur atoms were not restricted to a defined geometric cylinder. Represented data are within the criteria described above (excludes A, B, C, D, E, and F criteria), except for the Ag^+ database which was not manually parsed.
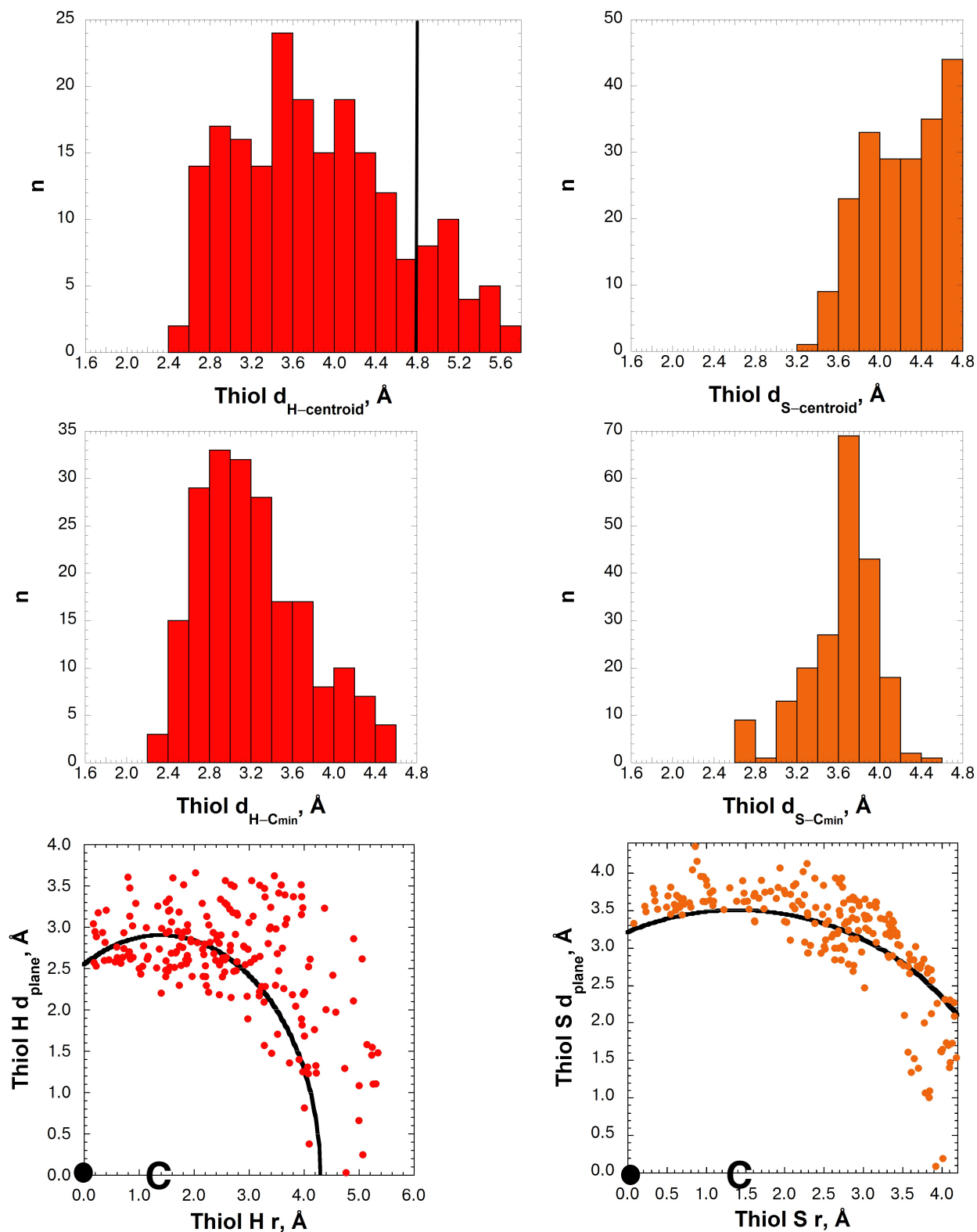
Figure S103. S–H/π interactions in the CSD using the reported S–H bond lengths and using the thiol sulfur atom as a reference for the cylinder restriction (thiol S $d_{plane} \leq 4.38$ Å, thiol S r ≤ 4.20 Å). Plots of $d_{X-centroid}$, d_{X-Cmin}, and atomic coordinates of X with respect to the plane of the

S104

aromatic ring, where X = thiol H or thiol S. Thiol hydrogen atoms are as reported in the CSD and were not restricted to a defined geometric cylinder. The black line indicates the sum of the van der Waals radii for carbon and the respective atoms or ions, where entries below the line are less than the sum of the van der Waals radii (Σ van der Waals radii for C and: Thiol H = 2.90 Å; Thiol S = 3.50 Å).
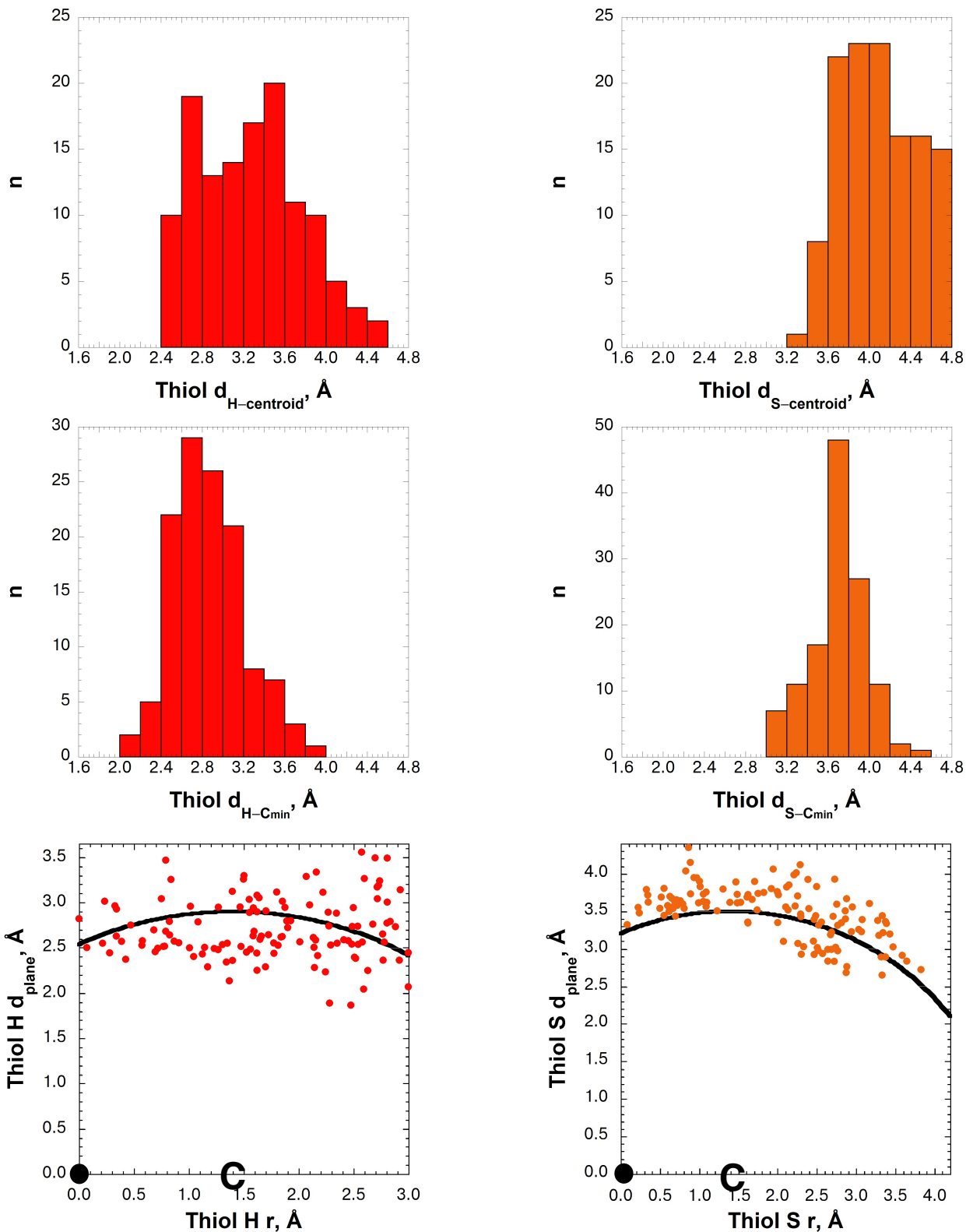
Figure S104. S–H/π interactions in the CSD using normalized S–H bond lengths and using the thiol hydrogen atom as a reference for cylinder restriction ($d_{H-plane} \leq 3.63$ Å, H r ≤ 3.00 Å). Plots of $d_{X-centroid}$, d_{X-Cmin}, and atomic coordinates of X with respect to the plane of the aromatic ring,

where X = thiol H or thiol S. The position of the thiol hydrogen was changed along the vector of the S–H bond to normalize the S–H bond lengths to 1.338 Å (ConQuest 1.17).[7] Thiol sulfur atoms were not restricted to a geometric cylinder. The black line indicates the sum of the van der Waals radii for carbon and the respective atoms or ions, where entries below the line are less than the sum of the van der Waals radii (Σ van der Waals radii for C and: Thiol H = 2.90 Å; Thiol S = 3.50 Å).

Figure S105. S–H/π interactions in the CSD using normalized S–H bond lengths and using the

thiol sulfur atom as a reference for cylinder restriction (thiol S $d_{plane} \leq 4.38$ Å, thiol S r ≤ 4.20 Å). Plots of $d_{X-centroid}$, d_{X-Cmin}, and atomic coordinates of X with respect to the plane of the aromatic ring, where X = thiol H or thiol S. The position of the thiol hydrogen was changed along the vector of the S–H bond to normalize the S–H bond lengths to 1.338 Å (ConQuest 1.17).[7] Thiol sulfur atoms were not restricted to a geometric cylinder. The black line indicates the sum of the van der Waals radii for carbon and the respective atoms or ions, where entries below the line are less than the sum of the van der Waals radii (Σ van der Waals radii for C and: Thiol H = 2.90 Å; Thiol S = 3.50 Å).

Figure S106. Direction of the thiol S–H bonds relative to the plane of the aromatic ring. The vector of the thiol S–H bond can approximate the location of the σ^* orbital in the context of the aromatic ring. The thiol S–H bond is represented as a vector, where the arrow points to the hydrogen atom location. The origin (●) and edge (**C**) of the aromatic ring are indicated within the plots, where **C** is located at 1.40 Å from the origin. The red line indicates the sum of the van der Waals radii for carbon and hydrogen (2.90 Å), where entries below the line are less than the sum of the van der Waals radii. Thiol hydrogen atoms are as reported in the CSD and the thiol hydrogen atom was used for reference in the cylinder restriction.

Left: All thiol data shown (excludes A, B, C, D, E, and F criteria)

Right: Only thiol data where $d_{\text{H–Cmin}}$ is less than the sum of the van der Waals radii for carbon and hydrogen atoms (excludes A, B, C, D, E, and F criteria).
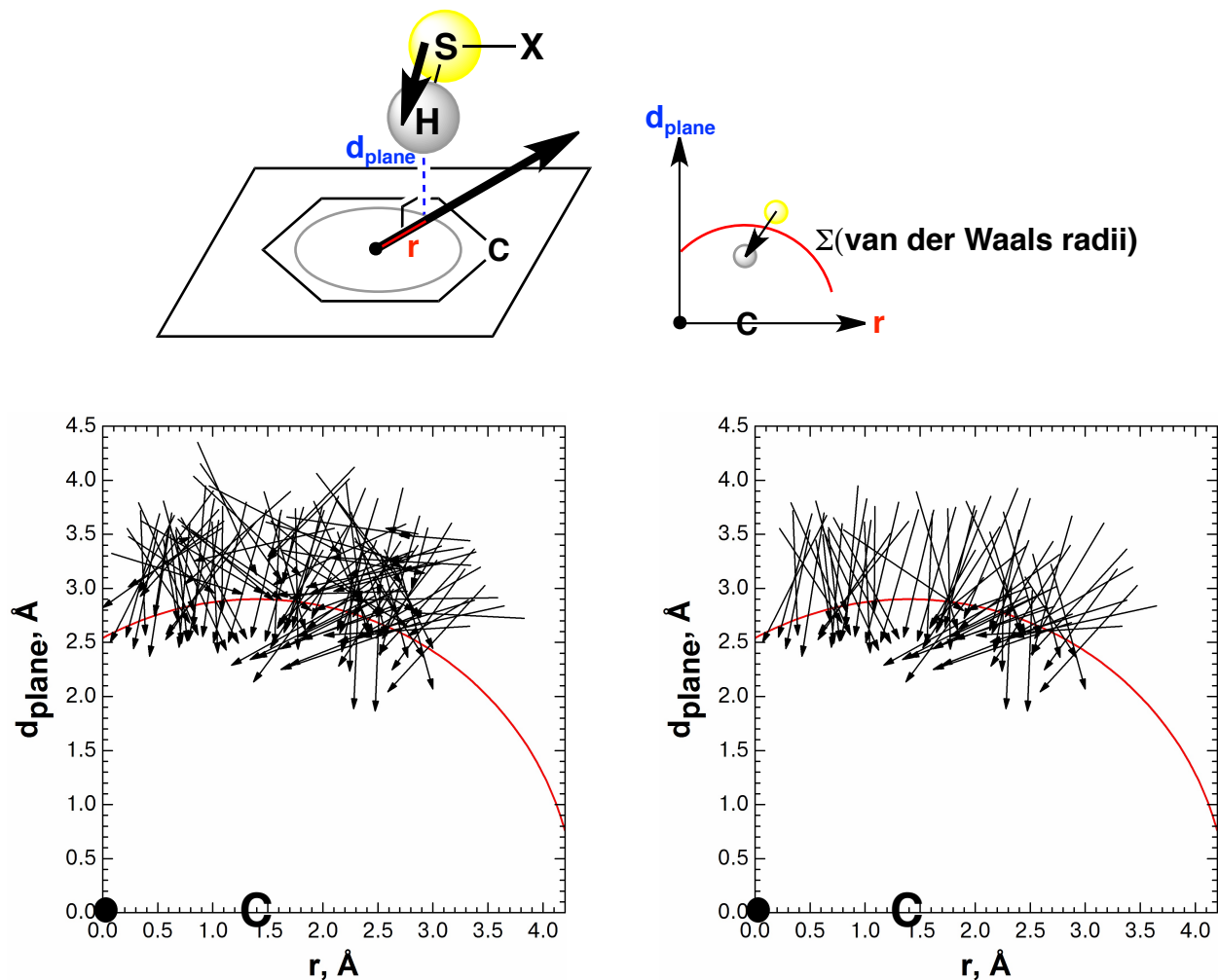
Figure S107. Direction of the thiol S–H bonds relative to the plane of the aromatic ring where the thiol bond length has been normalized to 1.338 Å, (ConQuest 1.17).[7] The vector of the thiol S–H bond can approximate the location of the σ^* orbital in the context of the aromatic ring. The thiol S–H bond is represented as a vector, where the arrow points to the hydrogen atom location. The origin (●) and edge (**C**) of the aromatic ring are indicated within the plots, where **C** is located at 1.40 Å from the origin. The red line indicates the sum of the van der Waals radii for carbon and hydrogen (2.90 Å), where entries below the line are less than the sum of the van der Waals radii. The cylinder restriction was applied to the thiol hydrogen atoms after the S–H bonds were normalized (thiol H $d_{plane} \leq 3.63$ Å, thiol H r ≤ 3.00 Å).
Left: All thiol data shown (excludes A, B, C, D, E, and F criteria)
Right: Only thiol data where $d_{H–Cmin}$ is less than the sum of the van der Waals radii for carbon and hydrogen atoms (excludes A, B, C, D, E, and F criteria)
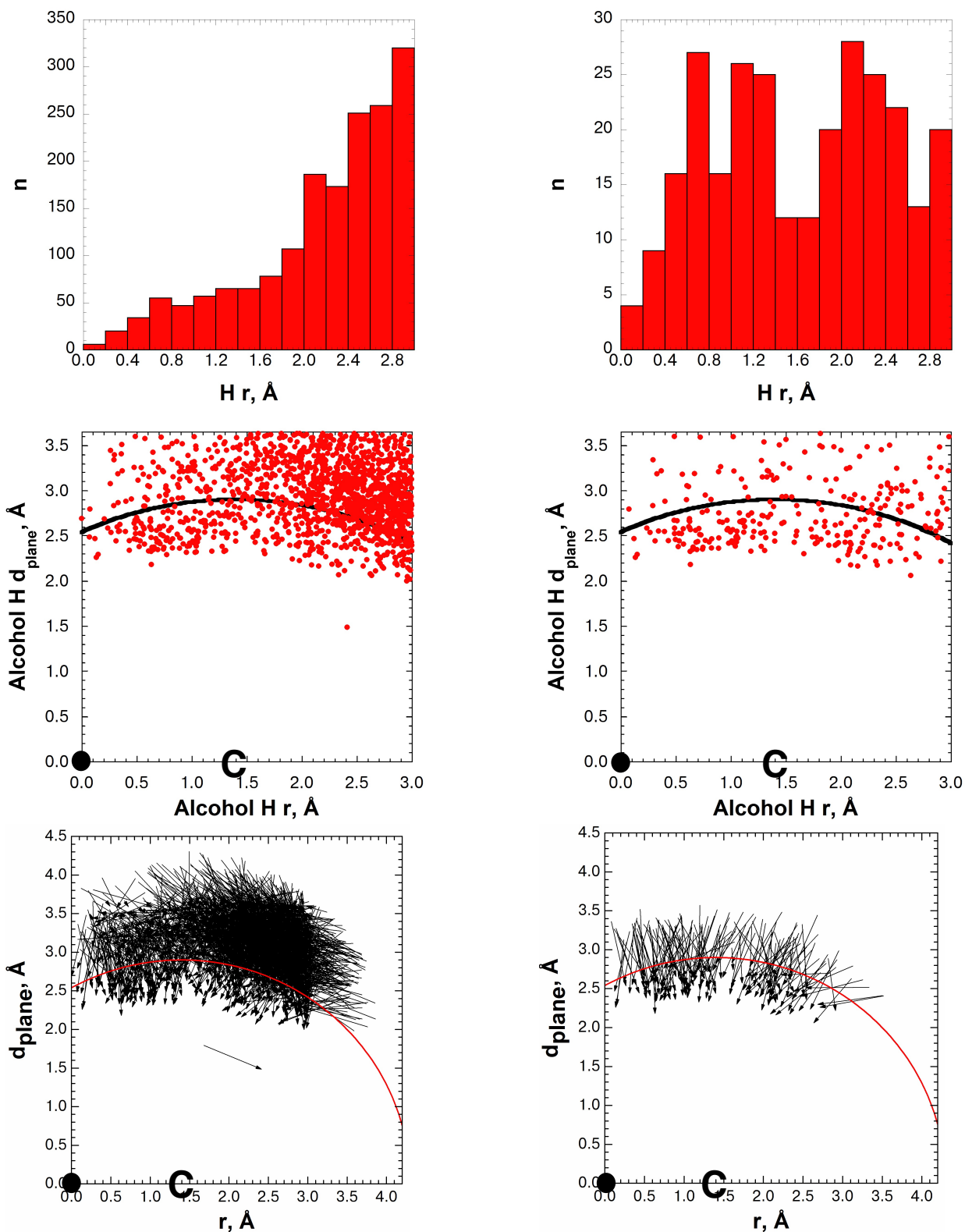
Figure S108. O–H/π interactions in the CSD using the reported O–H bond lengths and using the alcohol hydrogen atom as a reference for the cylinder restriction (alcohol H $d_{plane} \leq 3.63$ Å, alcohol H r ≤ 3.00 Å). Left: all entries identified in the CSD as C–O–H groups that are close to a

6-membered aromatic ring; right: entries identified after excluding potential competing classical hydrogen bonding interactions (where entries containing an oxygen, nitrogen, or metal atom within 2.50 Å of the alcohol hydrogen were removed). Top: histogram plots of H r; middle: atomic coordinates of H with respect to the plane of the aromatic ring (alcohol hydrogen atoms are as reported in the CSD. The black line indicates the sum of the van der Waals radii for carbon and hydrogen); bottom: direction of the alcohol O–H bonds relative to the plane of the aromatic ring. The alcohol O–H bond is represented as a vector, where the arrow points to the hydrogen atom location. The origin (●) and edge (**C**) of the aromatic ring are indicated within the plots, where **C** is located at 1.40 Å from the origin. The red line indicates the sum of the van der Waals radii for carbon and hydrogen (2.90 Å), where entries below the line are less than the sum of the van der Waals radii.

X-ray Crystallography

Orthorhombic, enantiopure crystals of **1** were obtained via slow evaporation at room temperature over one week of a solution of approximately 20 mg of **1** in 10 mL 25% ethyl acetate in hexanes.

Diffractable crystals of *p*-thiocresol were used directly from commercially available material (Sigma) without recrystallization.

The data crystals were selected and mounted on plastic mesh using oil flash-cooled to the data collection temperature. Data were collected on a Bruker-AXS APEX II Duo CCD diffractometer with graphite-monochromated Mo–Kα radiation (λ = 0.71073 Å) for **1** and *p*-thiocresol. Unit cell parameters were obtained from 60 data frames, 0.3° ω, from three different sections of the Ewald sphere, and refined with the entire diffraction data set. The systematic absences in the data and the unit cell parameters were uniquely consistent to the reported space groups. The data sets were treated with absorption corrections based on redundant multiscan data.[8] The structures were solved using direct methods and refined with full-matrix, least-squares procedures on F^2.[9] The absolute structure parameter for **1** refined to nil indicating the true hand of the data had been determined. The compound molecule of *p*-thiocresol resides on an inversion center and the full molecule was refined at half-occupancy with symmetry related atoms treated with equal atomic displacement parameters and with a minimal DAMP value for convergence. All non-hydrogen atoms were refined with anisotropic displacement parameters. All hydrogen atoms were treated as idealized contributions. Scattering factors and anomalous dispersion coefficients are contained in the SHELXTL program library.[9] Molecular graphics were obtained using Mercury CSD.[10] The crystallographic Information files for this paper have been deposited as CCDC 1416010 to 1416011. These data can be obtained free of charge via www.ccdc.cam.ac.uk/conts/retrieving.html (or from the CCDC, 12 Union Road, Cambridge CB2 1EZ, UK; fax: +44 1223 336033; email: deposit@ccdc.cam.ac.uk).

Crystal Structure of 1
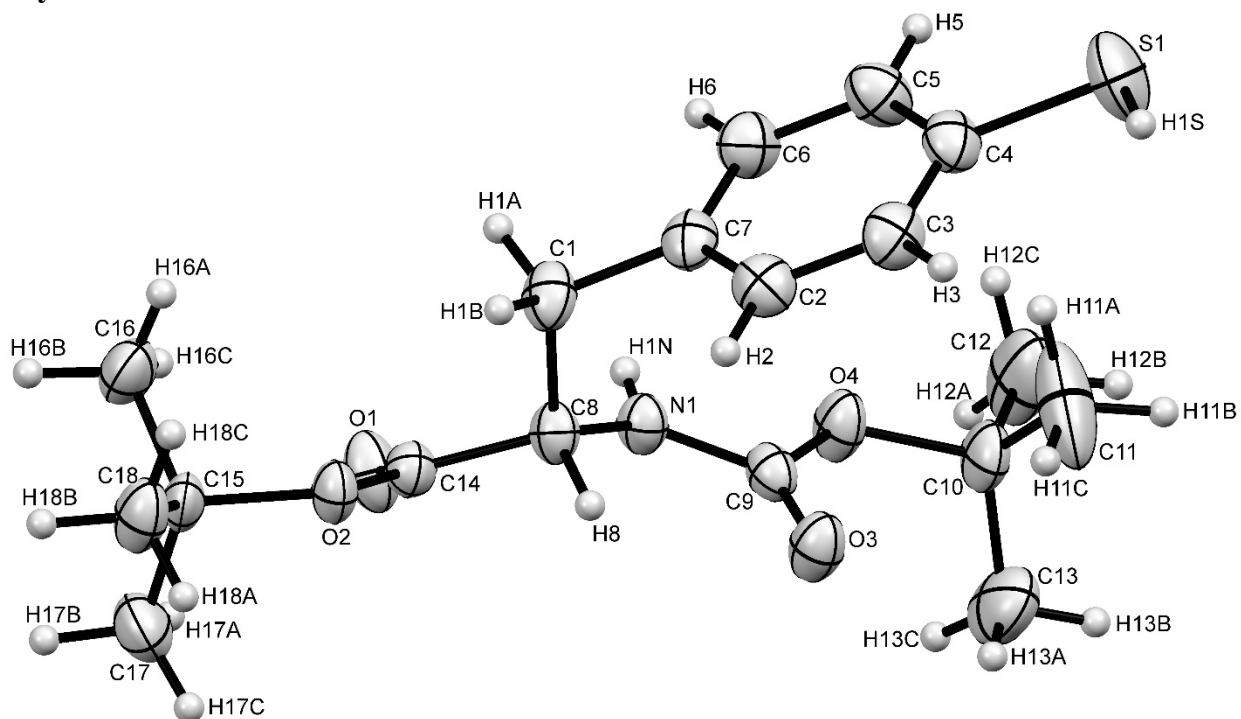
Figure S109. ORTEP diagram of **1**, with ellipsoids shown at 50% probability. Crystals were formed via slow evaporation from a solution of 25% ethyl acetate in hexanes (v/v) at room temperature over one week.
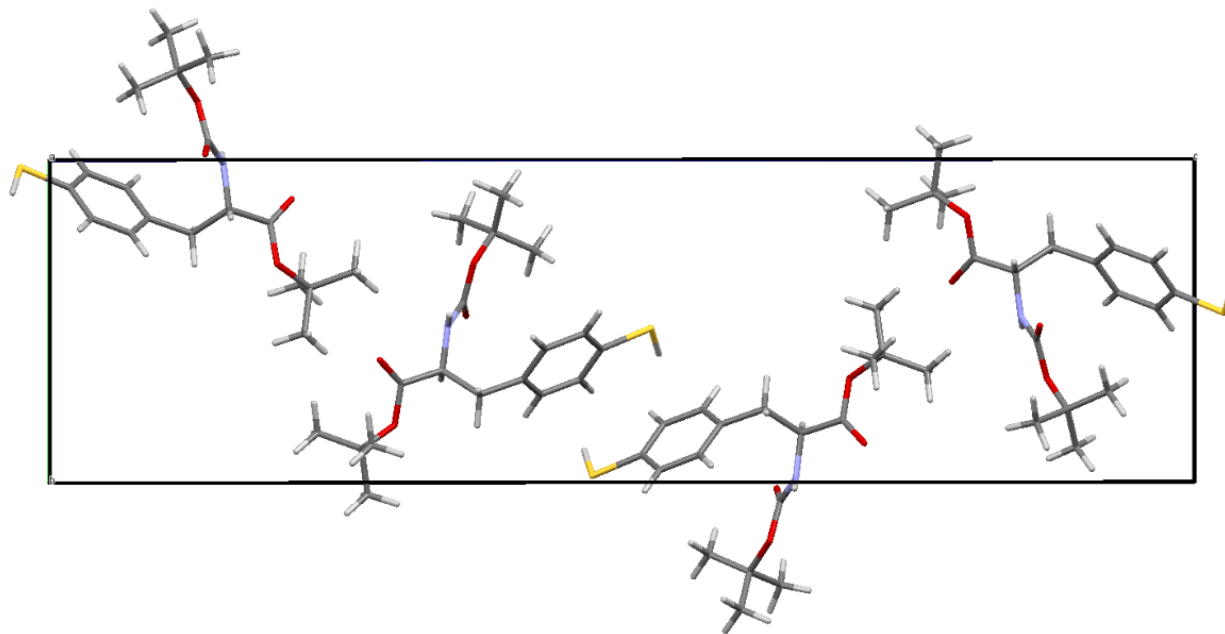
Figure S110. Unit cell for orthorhombic crystal structure of **1**. Crystals were formed via slow evaporation from a solution of 25% ethyl acetate in hexanes (v/v) at room temperature over one week.
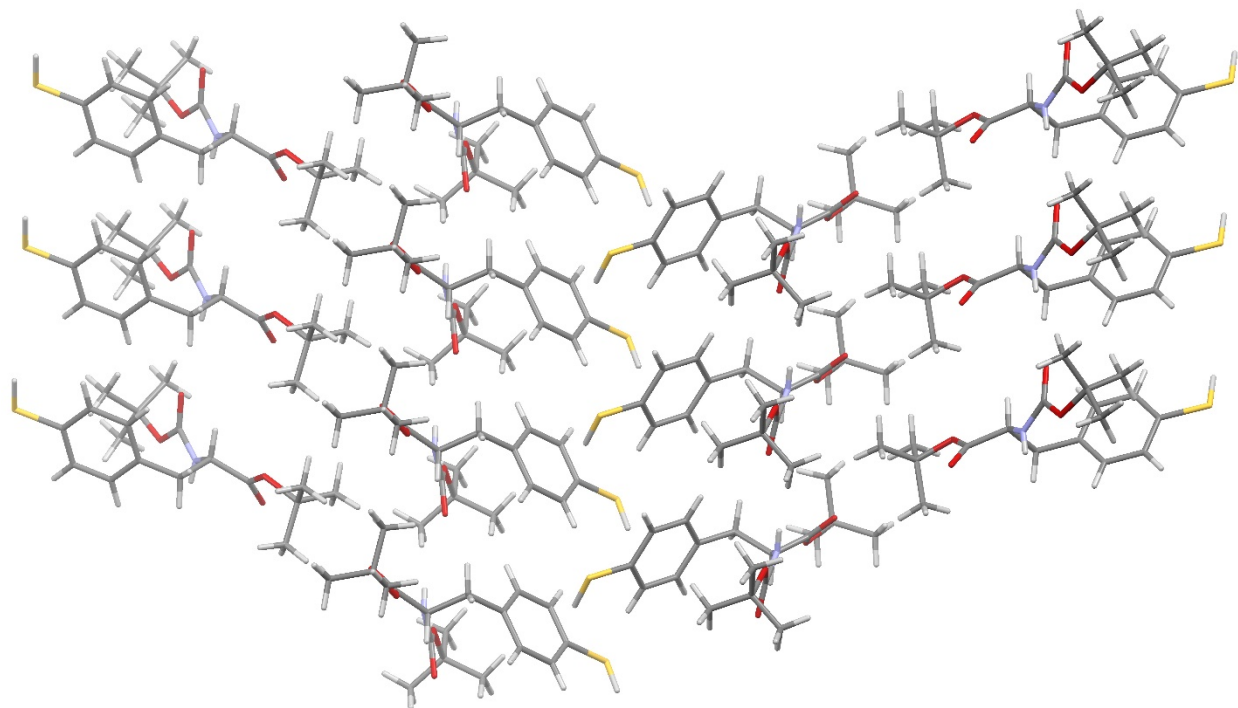
Figure S111. Overall crystal packing of **1**. Crystals were formed via slow evaporation from a solution of 25% ethyl acetate in hexanes (v/v) at room temperature over one week.

Table S22. Crystallographic data and refinement details for orthorhombic crystals of **1**.

empirical formula	$C_{18}H_{27}NO_4S$		
formula weight	353.46		
T (K)	200(2)		
wavelength (Å)	0.71073		
crystal system, space group	Orthorhombic, $P2_12_12_1$		
Unit cell dimensions (Å, °)	a = 5.4629(6)	$\alpha = 90$	
	b = 10.1217(11)	$\beta = 90$	
	c = 35.898(4)	$\gamma = 90$	
Volume (Å^3)	1984.9(4)		
Z, Z′, calcd density (g/cm^3)	4, 1, 1.183		
absorption coefficient (mm^{-1})	0.182		
F(000)	760		
crystal size (mm)	0.188 x 0.195 x 0.328		
θ range for data collection	2.09 to 27.47°		
Index ranges	$-6 \le h \le 7, -13 \le k \le 13, -46 \le l \le 46$		
Reflections collected/ unique	15122/4518 [R(int) = 0.0378]		
Coverage of independent reflections	100.0%		
Absorption correction	multi-scan		
Max. and min. transmission	0.7456 and 0.6789		
Structure solution technique	direct methods		
Refinement method	Full-matrix least-squares on F^2		
Function minimized	$\Sigma\, w(F_o^2 - F_c^2)^2$		
Data / restraints / parameters	4518 / 0 / 231		
Goodness-of-fit on F^2	1.015		
Final R indices	3579 data; I>2σ(I)	R1 = 0.0403, wR2 = 0.0870	
	all data	R1 = 0.0578, wR2 = 0.0962	
Weighting scheme	$w=1/[\sigma^2(F_o^2)+(0.0425P)^2+0.2479P]$ where $P=(F_o^2+2F_c^2)/3$		
Largest diff. peak and hole	0.161 and -0.232 eÅ^{-3}		
R.M.S. deviation from mean	0.034 eÅ^{-3}		

Table S23. Atomic coordinates ($\times 10^4$) and equivalent isotropic displacement parameters ($A^2 \times 10^3$) for orthorhombic crystals of **1**. U(eq) is defined as one third of the trace of the orthogonalized Uij tensor.

	x/a	y/b	z/c	U(eq)
S1	0.34521(19)	0.52173(9)	0.52548(2)	0.0622(3)
N1	0.5840(4)	0.5118(2)	0.34791(6)	0.0304(5)
O1	0.8164(4)	0.62103(16)	0.28823(5)	0.0436(5)
O2	0.6554(3)	0.82223(15)	0.30105(4)	0.0313(4)
O3	0.1861(3)	0.48255(17)	0.36414(5)	0.0403(4)
O4	0.4708(3)	0.31949(16)	0.37059(5)	0.0403(5)
C1	0.6943(5)	0.7273(2)	0.37559(7)	0.0393(6)
C2	0.3915(5)	0.7269(2)	0.42901(7)	0.0383(6)
C3	0.3109(5)	0.6810(3)	0.46314(7)	0.0397(6)
C4	0.4424(5)	0.5864(3)	0.48204(7)	0.0387(6)
C5	0.6586(5)	0.5389(3)	0.46688(7)	0.0427(6)
C6	0.7381(5)	0.5859(3)	0.43259(7)	0.0405(7)
C7	0.6071(5)	0.6801(2)	0.41336(7)	0.0346(6)
C8	0.5698(5)	0.6527(2)	0.34302(7)	0.0305(5)
C9	0.3936(5)	0.4416(2)	0.36141(6)	0.0309(6)
C10	0.3022(5)	0.2244(2)	0.38818(8)	0.0414(6)
C11	0.2005(10)	0.2795(3)	0.42364(10)	0.0920(15)
C12	0.4681(7)	0.1081(3)	0.39590(12)	0.0736(11)
C13	0.1084(7)	0.1843(3)	0.36078(10)	0.0678(10)
C14	0.6941(5)	0.6938(2)	0.30706(6)	0.0301(5)
C15	0.7963(5)	0.8954(2)	0.27215(7)	0.0320(5)
C16	0.0670(5)	0.8846(3)	0.28079(8)	0.0436(7)
C17	0.7318(6)	0.8458(3)	0.23376(7)	0.0483(8)
C18	0.7083(5)	0.0368(2)	0.27747(8)	0.0437(7)

Table S24. Bond lengths [Å] and angles [°] for orthorhombic crystals of **1**.

Bond lengths

S1-C4	1.773(3)	S1-H1S	1.26(4)
N1-C9	1.350(3)	N1-C8	1.439(3)
N1-H1N	0.75(3)	O1-C14	1.202(3)
O2-C14	1.335(3)	O2-C15	1.489(3)
O3-C9	1.211(3)	O4-C9	1.346(3)
O4-C10	1.474(3)	C1-C7	1.514(3)
C1-C8	1.549(3)	C1-H1A	0.99
C1-H1B	0.99	C2-C3	1.383(4)
C2-C7	1.388(4)	C2-H2	0.95
C3-C4	1.376(4)	C3-H3	0.95
C4-C5	1.386(4)	C5-C6	1.389(4)
C5-H5	0.95	C6-C7	1.378(4)
C6-H6	0.95	C8-C14	1.517(3)
C8-H8	1.0	C10-C11	1.497(4)
C10-C13	1.501(4)	C10-C12	1.511(4)
C11-H11A	0.98	C11-H11B	0.98
C11-H11C	0.98	C12-H12A	0.98
C12-H12B	0.98	C12-H12C	0.98
C13-H13A	0.98	C13-H13B	0.98
C13-H13C	0.98	C15-C17	1.509(4)
C15-C16	1.515(4)	C15-C18	1.522(4)
C16-H16A	0.98	C16-H16B	0.98
C16-H16C	0.98	C17-H17A	0.98
C17-H17B	0.98	C17-H17C	0.98
C18-H18A	0.98	C18-H18B	0.98
C18-H18C	0.98		

Bond angles

C4-S1-H1S	99.4(15)	C9-N1-C8	121.6(2)
C9-N1-H1N	118.(2)	C8-N1-H1N	117.(2)
C14-O2-C15	121.01(19)	C9-O4-C10	120.6(2)
C7-C1-C8	112.6(2)	C7-C1-H1A	109.1
C8-C1-H1A	109.1	C7-C1-H1B	109.1
C8-C1-H1B	109.1	H1A-C1-H1B	107.8
C3-C2-C7	120.9(3)	C3-C2-H2	119.5
C7-C2-H2	119.5	C4-C3-C2	120.3(3)

C4-C3-H3	119.8	C2-C3-H3	119.8
C3-C4-C5	119.5(2)	C3-C4-S1	122.3(2)
C5-C4-S1	118.2(2)	C4-C5-C6	119.7(3)
C4-C5-H5	120.1	C6-C5-H5	120.1
C7-C6-C5	121.2(2)	C7-C6-H6	119.4
C5-C6-H6	119.4	C6-C7-C2	118.3(2)
C6-C7-C1	120.2(2)	C2-C7-C1	121.4(2)
N1-C8-C14	110.54(19)	N1-C8-C1	111.6(2)
C14-C8-C1	108.2(2)	N1-C8-H8	108.8
C14-C8-H8	108.8	C1-C8-H8	108.8
O3-C9-O4	126.0(2)	O3-C9-N1	124.7(2)
O4-C9-N1	109.3(2)	O4-C10-C11	110.6(2)
O4-C10-C13	109.7(2)	C11-C10-C13	113.3(3)
O4-C10-C12	102.3(2)	C11-C10-C12	110.9(3)
C13-C10-C12	109.4(3)	C10-C11-H11A	109.5
C10-C11-H11B	109.5	H11A-C11-H11B	109.5
C10-C11-H11C	109.5	H11A-C11-H11C	109.5
H11B-C11-H11C	109.5	C10-C12-H12A	109.5
C10-C12-H12B	109.5	H12A-C12-H12B	109.5
C10-C12-H12C	109.5	H12A-C12-H12C	109.5
H12B-C12-H12C	109.5	C10-C13-H13A	109.5
C10-C13-H13B	109.5	H13A-C13-H13B	109.5
C10-C13-H13C	109.5	H13A-C13-H13C	109.5
H13B-C13-H13C	109.5	O1-C14-O2	126.4(2)
O1-C14-C8	124.0(2)	O2-C14-C8	109.46(19)
O2-C15-C17	110.5(2)	O2-C15-C16	109.0(2)
C17-C15-C16	113.0(2)	O2-C15-C18	102.55(19)
C17-C15-C18	110.7(2)	C16-C15-C18	110.5(2)
C15-C16-H16A	109.5	C15-C16-H16B	109.5
H16A-C16-H16B	109.5	C15-C16-H16C	109.5
H16A-C16-H16C	109.5	H16B-C16-H16C	109.5
C15-C17-H17A	109.5	C15-C17-H17B	109.5
H17A-C17-H17B	109.5	C15-C17-H17C	109.5
H17A-C17-H17C	109.5	H17B-C17-H17C	109.5
C15-C18-H18A	109.5	C15-C18-H18B	109.5
H18A-C18-H18B	109.5	C15-C18-H18C	109.5
H18A-C18-H18C	109.5	H18B-C18-H18C	109.5

Table S25. Anisotropic atomic displacement parameters (Å2) for orthorhombic crystals of **1**. The anisotropic atomic displacement factor exponent takes the form: -2π2[h2 a*2 U11 + ... + 2 h k a* b* U12]

	U_{11}	U_{22}	U_{33}	U_{23}	U_{13}	U_{12}
S1	0.0795(6)	0.0668(5)	0.0404(4)	0.0099(4)	0.0190(4)	0.0032(5)
N1	0.0320(12)	0.0243(10)	0.0349(11)	0.0032(9)	0.0036(10)	0.0016(10)
O1	0.0578(12)	0.0335(9)	0.0395(10)	0.0021(8)	0.0175(10)	0.0070(9)
O2	0.0321(9)	0.0254(7)	0.0365(9)	0.0080(7)	0.0065(8)	-0.0009(7)
O3	0.0353(10)	0.0314(9)	0.0542(11)	0.0077(8)	0.0049(9)	0.0006(8)
O4	0.0386(11)	0.0255(8)	0.0568(11)	0.0109(8)	0.0052(9)	-0.0013(8)
C1	0.0486(16)	0.0307(12)	0.0387(14)	-0.0031(11)	0.0077(13)	-0.0099(12)
C2	0.0447(16)	0.0321(13)	0.0380(14)	-0.0035(11)	-0.0004(12)	0.0013(12)
C3	0.0405(15)	0.0406(14)	0.0380(14)	-0.0077(12)	0.0074(13)	0.0022(13)
C4	0.0468(16)	0.0400(14)	0.0292(13)	-0.0035(11)	0.0033(12)	-0.0054(13)
C5	0.0454(16)	0.0431(14)	0.0398(14)	0.0018(12)	-0.0004(13)	0.0087(14)
C6	0.0378(16)	0.0448(15)	0.0389(14)	-0.0040(12)	0.0058(12)	0.0041(12)
C7	0.0410(15)	0.0315(12)	0.0314(13)	-0.0069(11)	0.0030(11)	-0.0088(12)
C8	0.0357(14)	0.0216(11)	0.0341(13)	0.0022(10)	0.0047(11)	0.0000(10)
C9	0.0413(16)	0.0234(11)	0.0280(12)	0.0019(10)	-0.0004(11)	-0.0026(10)
C10	0.0463(16)	0.0280(12)	0.0499(16)	0.0096(12)	0.0049(14)	-0.0100(12)
C11	0.166(4)	0.0501(19)	0.060(2)	0.0021(17)	0.054(3)	-0.022(3)
C12	0.063(2)	0.0437(18)	0.113(3)	0.038(2)	0.004(2)	-0.0029(16)
C13	0.062(2)	0.0511(18)	0.090(3)	0.0147(18)	-0.011(2)	-0.0226(17)
C14	0.0311(13)	0.0282(11)	0.0308(12)	0.0013(10)	0.0014(11)	-0.0024(11)
C15	0.0266(13)	0.0333(12)	0.0361(13)	0.0107(10)	0.0054(11)	-0.0057(11)
C16	0.0296(15)	0.0446(15)	0.0564(17)	0.0082(14)	0.0025(13)	-0.0044(13)
C17	0.059(2)	0.0519(17)	0.0345(14)	0.0085(13)	0.0024(13)	-0.0062(14)
C18	0.0398(16)	0.0316(13)	0.0595(17)	0.0125(13)	0.0065(14)	-0.0016(12)

Table S26. Hydrogen atomic coordinates and isotropic atomic displacement parameters (Å2) for orthorhombic crystals of **1**.

	x/a	y/b	z/c	U(eq)
H1S	0.173(7)	0.601(3)	0.5324(9)	0.083(11)
H1N	0.709(5)	0.482(3)	0.3493(7)	0.032(8)
H1A	0.8737	0.7150	0.3739	0.047
H1B	0.6597	0.8230	0.3732	0.047
H2	0.2980	0.7915	0.4161	0.046
H3	0.1640	0.7149	0.4736	0.048
H5	0.7519	0.4746	0.4799	0.051
H6	0.8856	0.5524	0.4222	0.049
H8	0.3936	0.6792	0.3419	0.037
H11A	0.3347	0.3130	0.4391	0.138
H11B	0.1129	0.2099	0.4371	0.138
H11C	0.0874	0.3518	0.4179	0.138
H12A	0.5273	0.0716	0.3723	0.11
H12B	0.3769	0.0401	0.4095	0.11
H12C	0.6078	0.1373	0.4109	0.11
H13A	-0.0109	0.2559	0.3581	0.102
H13B	0.0254	0.1046	0.3698	0.102
H13C	0.1843	0.1661	0.3366	0.102
H16A	1.0969	0.9134	0.3064	0.065
H16B	1.1597	0.9408	0.2636	0.065
H16C	1.1197	0.7926	0.2779	0.065
H17A	0.7926	0.7553	0.2307	0.072
H17B	0.8072	0.9030	0.2150	0.072
H17C	0.5536	0.8467	0.2306	0.072
H18A	0.5309	1.0408	0.2736	0.065
H18B	0.7900	1.0945	0.2594	0.065
H18C	0.7474	1.0663	0.3028	0.065

Table S27. Torsion angles (°) for orthorhombic crystals of **1**.

C7-C2-C3-C4	-0.8(4)	C2-C3-C4-C5	1.0(4)
C2-C3-C4-S1	-178.9(2)	C3-C4-C5-C6	-0.9(4)
S1-C4-C5-C6	179.0(2)	C4-C5-C6-C7	0.6(4)
C5-C6-C7-C2	-0.4(4)	C5-C6-C7-C1	-178.5(2)
C3-C2-C7-C6	0.5(4)	C3-C2-C7-C1	178.6(2)
C8-C1-C7-C6	95.4(3)	C8-C1-C7-C2	-82.6(3)
C9-N1-C8-C14	-140.0(2)	C9-N1-C8-C1	99.6(3)
C7-C1-C8-N1	-50.5(3)	C7-C1-C8-C14	-172.3(2)
C10-O4-C9-O3	-4.7(4)	C10-O4-C9-N1	176.4(2)
C8-N1-C9-O3	14.1(4)	C8-N1-C9-O4	-167.0(2)
C9-O4-C10-C11	-57.8(4)	C9-O4-C10-C13	68.0(3)
C9-O4-C10-C12	-176.0(3)	C15-O2-C14-O1	-9.5(4)
C15-O2-C14-C8	167.5(2)	N1-C8-C14-O1	-9.7(4)
C1-C8-C14-O1	112.7(3)	N1-C8-C14-O2	173.2(2)
C1-C8-C14-O2	-64.4(3)	C14-O2-C15-C17	66.5(3)
C14-O2-C15-C16	-58.3(3)	C14-O2-C15-C18	-175.4(2)

Crystal Structure of *p*-thiocresol
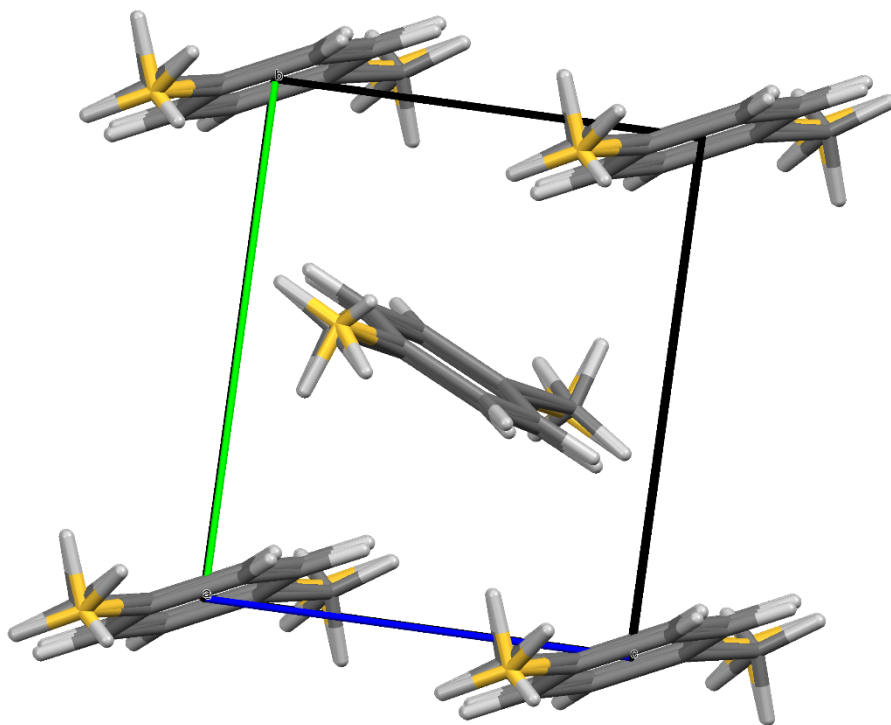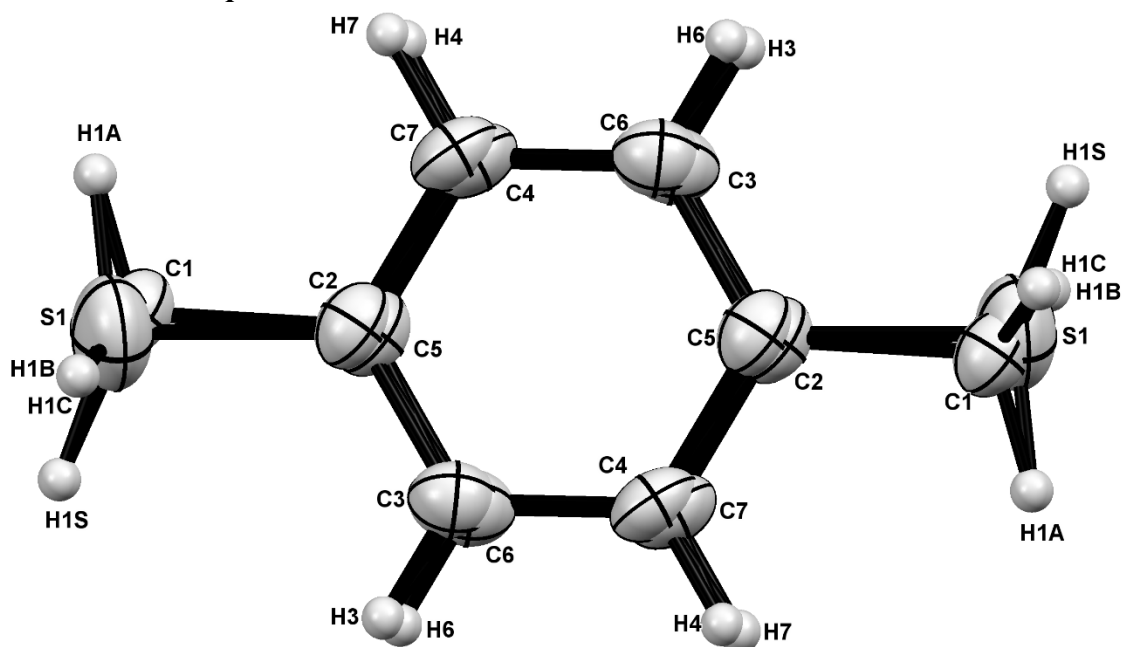
Figure S112. Crystal structure of *p*-thiocresol. Top: ORTEP diagram of the *p*-thiocresol monomer with ellipsoids shown at 50% probability; bottom: overall crystal packing. Diffractable crystals were used directly from commercially available material. Both disordered contributions are depicted and superimposed on one another.

Table S28. Crystallographic data and refinement details for *p*-thiocresol.

empirical formula	C_7H_8S
formula weight	124.19
T (K)	200(2)
wavelength (Å)	0.71073
crystal system, space group	Monoclinic, P1 2_1/c1
Unit cell dimensions (Å, °)	a = 7.742(3) α = 90
	b = 7.223(3) β = 92.953(6)
	c = 5.956(2) γ = 90
Volume (Å^3)	332.6(2)
Z, Z′, calcd density (g/cm^3)	2, 0.5, 1.240
absorption coefficient (mm^{-1})	0.371
F(000)	132
crystal size (mm)	0.141 x 0.204 x 0.230
θ range for data collection	2.63 to 27.68°
Index ranges	-10 ≤ h ≤ 10, -9 ≤ k ≤ 9, -7 ≤ l ≤ 7
Reflections collected/ unique	4782/774 [R(int) = 0.0501]
Coverage of independent reflections	99.7%
Absorption correction	multi-scan
Max. and min. transmission	0.7456 and 0.6534
Structure solution technique	direct methods
Refinement method	Full-matrix least-squares on F^2
Function minimized	$\Sigma\,w(F_o{}^2 - F_c{}^2)^2$
Data / restraints / parameters	774 / 1 / 41
Goodness-of-fit on *F^2*	1.077
Final *R* indices	560 data; I>2σ(I) R1 = 0.0575, wR2 = 0.1597
	all data R1 = 0.0809, wR2 = 0.1745
Weighting scheme	w=1/[σ^2(F$_o{}^2$)+(0.0974P)^2+0.0719P] where P=(F$_o{}^2$+2F$_c{}^2$)/3
Largest diff. peak and hole	0.368 and -0.186 eÅ^{-3}
R.M.S. deviation from mean	0.064 eÅ^{-3}

Table S29. Atomic coordinates ($\times\ 10^4$) and equivalent isotropic displacement parameters ($A^2 \times 10^3$) for *p*-thiocresol. U(eq) is defined as one third of the trace of the orthogonalized Uij tensor.

	x/a	y/b	z/c	U(eq)
S1	0.3507(3)	0.4458(6)	0.7745(6)	0.0533(10)
C1	0.6804(14)	0.5443(17)	0.2107(19)	0.0323(11)
C2	0.839(3)	0.533(4)	0.370(5)	0.0323(11)
C3	0.839(3)	0.450(4)	0.580(5)	0.0341(12)
C4	0.993(3)	0.424(4)	0.706(5)	0.0325(11)
C5	0.148(3)	0.482(4)	0.621(5)	0.0323(11)
C6	0.149(3)	0.565(4)	0.411(5)	0.0341(12)
C7	0.994(3)	0.591(4)	0.285(5)	0.0325(11)

Table S30. Bond lengths [Å] and angles [°] for *p*-thiocresol.

<u>Bond lengths</u>

S1-C5	1.793(12)	S1-H1S	1.07(7)
C1-C2	1.514(11)	C1-H1A	0.98
C1-H1B	0.98	C1-H1C	0.98
C2-C3	1.39	C2-C7	1.39
C3-C4	1.39	C3-H3	0.95
C4-C5	1.39	C4-H4	0.95
C5-C6	1.39	C6-C7	1.39
C6-H6	0.95	C7-H7	0.95

<u>Bond angles</u>

C5-S1-H1S	109.(4)	C2-C1-H1A	109.5
C2-C1-H1B	109.5	H1A-C1-H1B	109.5
C2-C1-H1C	109.5	H1A-C1-H1C	109.5
H1B-C1-H1C	109.5	C3-C2-C7	120.0
C3-C2-C1	123.1(17)	C7-C2-C1	116.4(17)
C4-C3-C2	120.0	C4-C3-H3	120.0
C2-C3-H3	120.0	C3-C4-C5	120.0
C3-C4-H4	120.0	C5-C4-H4	120.0
C4-C5-C6	120.0	C4-C5-S1	121.4(12)
C6-C5-S1	118.6(13)	C5-C6-C7	120.0
C5-C6-H6	120.0	C7-C6-H6	120.0
C6-C7-C2	120.0	C6-C7-H7	120.0
C2-C7-H7	120.0		

Table S31. Anisotropic atomic displacement parameters (Å2) for *p*-thiocresol. The anisotropic atomic displacement factor exponent takes the form: -2π2[h2 a*2 U11 + ... + 2 h k a* b* U12]

	U$_{11}$	U$_{22}$	U$_{33}$	U$_{23}$	U$_{13}$	U$_{12}$
S1	0.0358(12)	0.0682(15)	0.0550(14)	-0.0026(9)	-0.0068(9)	0.0079(10)
C1	0.038(3)	0.029(3)	0.0291(19)	-0.0008(19)	-0.0022(14)	0.0039(19)
C2	0.038(3)	0.029(3)	0.0291(19)	-0.0008(19)	-0.0022(14)	0.0039(19)
C3	0.037(3)	0.033(3)	0.033(2)	-0.001(2)	0.0075(15)	-0.001(2)
C4	0.045(3)	0.030(3)	0.022(2)	0.003(2)	0.0024(15)	0.002(2)
C5	0.038(3)	0.029(3)	0.0291(19)	-0.0008(19)	-0.0022(14)	0.0039(19)
C6	0.037(3)	0.033(3)	0.033(2)	-0.001(2)	0.0075(15)	-0.001(2)
C7	0.045(3)	0.030(3)	0.022(2)	0.003(2)		

Table S32. Hydrogen atomic coordinates and isotropic atomic displacement parameters (Å2) for *p*-thiocresol.

	x/a	y/b	z/c	U(eq)
H1S	1.448(9)	0.529(8)	0.702(11)	0.064
H1A	0.7074	0.6171	0.0781	0.048
H1B	0.5862	0.6041	0.2872	0.048
H1C	0.6450	0.4193	0.1640	0.048
H3	0.7325	0.4100	0.6378	0.041
H4	0.9925	0.3673	0.8496	0.039
H6	1.2547	0.6048	0.3531	0.041
H7	0.9947	0.6476	0.1413	0.039

Table S33. Torsion angles (°) for *p*-thiocresol.

C7-C2-C3-C4	0	C1-C2-C3-C4	172.3(17)
C2-C3-C4-C5	0	C3-C4-C5-C6	0
C3-C4-C5-S1	-178.2(12)	C4-C5-C6-C7	0
S1-C5-C6-C7	178.2(11)	C5-C6-C7-C2	0
C3-C2-C7-C6	0	C1-C2-C7-C6	-172.8(15)

References

1.   Forbes, C. R.; Pandey, A. K.; Ganguly, H. K.; Yap, G. P. A.; Zondlo, N. J., 4*R*- and 4*S*-iodophenyl hydroxyproline, 4*R*-pentynoyl hydroxyproline, and S-propargyl-4-thiolphenylalanine: conformationally biased and tunable amino acids for bioorthogonal reactions. *Org. Biomol. Chem.* **2016**, *14*, 2327-2346.

2.   van Rossum, B. J.; Forster, H.; de Groot, H. J. M., High-field and high-speed CP-MAS C-13 NMR heteronuclear dipolar-correlation spectroscopy of solids with frequency-switched Lee-Goldburg homonuclear decoupling. *J. Magn. Reson.* **1997**, *124*, 516-519.

3.   Frisch, M. J.; Trucks, G. W.; Schlegel, H. B.; Scuseria, G. E.; Robb, M. A.; Cheeseman, J. R.; Scalmani, G.; Barone, V.; Mennucci, B.; Petersson, G. A.; Nakatsuji, H.; Caricato, M.; Li, X.; Hratchian, H. P.; Izmaylov, A. F.; Bloino, J.; Zheng, G.; Sonnenberg, J. L.; Hada, M.; Ehara, M.; Toyota, K.; Fukuda, R.; Hasegawa, J.; Ishida, M.; Nakajima, T.; Honda, Y.; Kitao, O.; Nakai, H.; Vreven, T.; Montgomery, J. A., Jr.; Peralta, J. E.; Ogliaro, F.; Bearpark, M.; Heyd, J. J.; Brothers, E.; Kudin, K. N.; Staroverov, V. N.; Kobayashi, R.; Normand, J.; Raghavachari, K.; Rendell, A.; Burant, J. C.; Iyengar, S. S.; Tomasi, J.; Cossi, M.; Rega, N.; Millam, J. M.; Klene, M.; Knox, J. E.; Cross, J. B.; Bakken, V.; Adamo, C.; Jaramillo, J.; Gomperts, R.; Stratmann, R. E.; Yazyev, O.; Austin, A. J.; Cammi, R.; Pomelli, C.; Ochterski, J. W.; Martin, R. L.; Morokuma, K.; Zakrzewski, V. G.; Voth, G. A.; Salvador, P.; Dannenberg, J. J.; Dapprich, S.; Daniels, A. D.; Farkas, Ö.; Foresman, J. B.; Ortiz, J. V.; Cioslowski, J.; Fox, D. J. *GAUSSIAN 09*, Revision B.01; Gaussian, Inc.: Wallingford, CT, 2009.

4.   Glendening, E. D.; Reed, A. E.; Carpenter, J. E.; Weinhold, F. *NBO*, Version 3.1.

5.   Breneman, C. M.; Wiberg, K. B., Determining atom-centered monopoles from molecular electrostatic potentials. The need for high sampling density in formamide conformational analysis. *J. Comput. Chem.* **1990**, *11*, 361-373.

6.   Gadre, S. R.; Sen, K. D., Radii of monopositive atomic ions. *J. Phys. Chem.* **1993**, *99*, 3149-3150.

7.   Gilli, G.; Gilli, P., *The Nature of the Hydrogen Bond: Outline of a Comprehensive Hydrogen Bond Theory*. Oxford University Press: New York, 2009; Vol. 23.

8.   Bruker *Apex2*, Bruker AXS, Inc.: Madison, WI, 2007.

9.   Sheldrick, G. M., A short history of SHELX. *Acta Crystallogr., Sect. A* **2008**, *64*, 112-122.

10.   Macrae, C. F.; Bruno, I. J.; Chisholm, J. A.; Edgington, P. R.; McCabe, P.; Pidcock, E.; Rodriguez-Monge, L.; Taylor, R.; van de Streek, J.; Wood, P. A., *Mercury CSD 2.0* - new features for the visualization and investigation of crystal structures. *J. Appl. Crystallogr.* **2008**, *41*, 466-470.